DISSERTATION

# DEVELOPMENT OF LOW-COST CAPILLARY DRIVEN IMMUNOASSAYS FOR IMPROVED MEDICAL DIAGNOSTICS

Submitted by:

Jeremy S. Link

Department of Chemistry

In partial fulfilment of the requirements

For the Degree of Doctor of Philosophy

Colorado State University

Fort Collins, Colorado

Summer 2023

Doctoral Committee:

Advisor: Charles S. Henry

Alan Van Orden
Christopher J. Ackerson
Matt J. Kipper

# ABSTRACT

## DEVELOPMENT OF LOW-COST CAPILLARY DRIVEN IMMUNOASSAYS FOR IMPROVED MEDICAL DIAGNOSTICS

Rapid medical diagnostics are a crucial part of an effective healthcare system. While traditional laboratory diagnostic methods are well established and sensitive, they are also time consuming and expensive. Point of care (POC) diagnostics offer an attractive alternative to traditional testing for more affordable, fast results. Their simplicity allows for POC devices to be run quickly by untrained personnel, but the simplicity often limits their detection range and sensitivity. In this dissertation I discuss affordable, capillary-driven immunoassay devices that are capable of passively delivering reagents associated with a traditional well-plate enzyme linked immunosorbent assay (ELISA) to test strips. These devices are made of patterned and laser cut double-sided adhesive. When stacked and laminated together, the patterns cut from the layers form hollow microfluidic channels that can passively transport fluids through capillary action. The devices in this dissertation require only a single end-user step to perform a sandwich immunoassay, and signal from the enzyme/substrate reaction is detectable in under 30 min.

Chapter 2 discusses the first application for visual detection of SARS-CoV-2 in these affordable capillary-driven immunoassay devices. The device in this chapter uses the enzyme horseradish peroxidase (HRP) and the substrate 3,3',5,5'-tetramethylbenzydine (TMB) to produce signal at the test line. Upon sample addition, the device channels fill, rehydrating the detection antibody and substrate dried on conjugate release pads that are stored in the channels of the device. Within 20 min, target, reagents, and washing steps are passively delivered to a nitrocellulose test

strip containing a capture antibody test line. The device performance was compared to a well-plate ELISA, and the detection limits for inactivated SASR-CoV-2 were 86 PFU/mL and 8 PFU/mL for the device and ELISA respectively. A dose response curve was also generated for spiked nasal swab samples with a detection limit of 222 PFU/mL, demonstrating the device's use with complex biological samples.

Chapter 3 expands on the work in Chapter 2 by demonstrating an alternative detection method. Chemiluminescent immunoassays are highly sensitive assays that rely on the energy provided by a chemical reaction to excite electrons. When the electrons move back to the ground state, they produce light that can be detected with an imager. In Chapter 3, I demonstrate the first example of a one-step, capillary driven immunoassay for chemiluminescent detection. The device is similar to that in Chapter 2, but the detection system relies on the reaction between HRP and a luminol based substrate to detect SARS-CoV-2 antigen. This work was done in collaboration with Burst Diagnostics Inc. and will be published when the appropriate patents and protections are in place.

Chapter 4 introduces the first capillary driven enzyme-linked immunoassay for the simultaneous detection of multiple biomarkers. This multiplexed device is made of the same inexpensive materials as the previous chapters, but the microfluidic channels are designed in such a way that reagents are delivered to two, spatially separated test strips. This separation allows for simultaneous detection of two targets without cross-reactivity between reagents, reducing the chance of false positives. To demonstrate the purpose of this device, they were used to detect SARS-CoV-2 antigen on one test strip, and influenza antigen on the other. The illnesses caused by these two viruses lead to very similar symptoms, so distinguishing between the two illnesses from a single device would be beneficial. Dose response curves were gathered for both antigens, and

the device was able to detect both diseases visually without false positives on the other test strip. Another form of multiplexed detection is simultaneous detection of two targets. To demonstrate this, SARS-CoV-2 and influenza antigen were detected simultaneously. Additionally, SARS-CoV-2 virus and c-reactive protein (CRP), a biomarker that can be used to determine the severity of COVID-19 cases, were detected simultaneously. This multiplexed assay has the potential to tell a healthcare provider 1) if an infection is or is not SARS-CoV-2, and 2) what level of care might be needed.

This dissertation introduces three capillary driven immunoassay devices primarily for the use of detecting communicable diseases. The devices all run from a single end-user step, and fully automate the steps required for a more time consuming and expensive ELISA. Although the focus of this dissertation was on detecting communicable diseases, these devices can (and are) being further developed for chronic illnesses. In the future, by swapping the antibodies used in the immunoassay, the applications of these devices are innumerable. Additionally, different detection methods, such as fluorescent, electrochemical, and further chemiluminescent work could continue to push the detection limit down, widening the application of these devices even further.

# ACKNOWLEDGEMENTS

I need to first thank my academic advisor and mentor, Dr. Chuck Henry. His passion for his work and his compassion for the students in his group are unrivaled and have created a welcoming and high functioning group dynamic. His optimism and encouragement have helped me through multiple difficult moments in my time at CSU. Along with academic growth, Chuck provided opportunities for me to present my research, conduct industry internships, and to continue to grow professionally and personally. I am, and will always be, grateful for his help and mentorship.

Many other scientists have pushed me to where I am. My committee members, Dr. Alan Van Orden, Dr. Christopher Ackerson, and Dr. Matt Kipper have provided excellent feedback and challenging questions along my path through graduate school. Their advice and influence have helped me think broadly about my projects and focus on every detail of understanding the chemistry behind them. Dr. Rose Nash, helped (and continues to help) me develop as a scientist and a professional. During my time working as an intern for Burst Diagnostics, she has changed the way I think about solving complex problems. Her zeal for her work, her breadth of knowledge, and her passion for her people make her an amazing person to work for and with. My undergraduate advisor, Dr. Kristen Skogerboe, allowed me to learn, teach, and eventually conduct my own research in analytical chemistry at Seattle University. Without her advice and encouragement, I likely would not be in graduate school, let alone graduating. She is a role model for me, and a strong woman in science teaching and growing the next generations of chemists.

My fellow Henry Group members have been a constant source of support and friendship during my PhD. Throughout my time at CSU, I've always had group members I felt comfortable

relying on for academic, professional, and personal advice. In particular, I'd like to thank Dr. Cody Carrell for showing me the ropes. He helped me develop the immunoassays systems in this dissertation, and was also a good volleyball player that's sorely missed by team Cooper. Dr. Isabelle Samper and Dr. Kaylee Clark were a constant source of advice and friendship, and I'm glad I had the opportunity to work with them. I'd also like to thank some of my undergraduate assistants who helped with my research. Rae Bellows and John O'donnell-Sloan, both now graduate students themselves, are excellent scientists, reliable help, and interesting conversationalists. Along with Elijah Barstis, the amount of fun and frustration we had working on the device in Chapter 2 can't be quantified.

Lastly, I need to thank my family. My parents, Ken and Beth Link, have always encouraged me to push myself. Their constant support while growing up, in undergrad, and now is the reason for any success I may have. When I was growing up, my mom homeschooled me and my 4 siblings. We would attend weekly science classes at the Oregon Museum of Science and Industry (OMSI), where I think I really started to consider natural sciences as a career instead of just a class. I'd like to thank everyone involved in that program at OMSI for continuing to develop and teach young scientists. I'd like to thank my brother, Josh, for being a role model and friend my whole life. I'd like to thank my sisters, Ginny, Mary, and Sarah, all of whom are now strong women in science and industry. They're an inspiration to me, and I'm sure an inspiration to others. Lastly, I need to thank my wife, Alia Zieg-Link. Her unrelenting love and support is truly why I'm here. I cannot overstate how much any success I have in life is directly a result of her. She is my best friend, and my greatest supporter.

For Chapter 2, I would specifically like to acknowledge Dr. Cody Carrell and Dr. Ilhoon Jang for their contributions to this chapter. Dr. Jang is one of the primary inventors of the device

used in this chapter, and Dr. Carrell provided much of the groundwork that lead to its success. As such, they and I are coauthors on the paper that was submitted based on this work. I would also like to thank Elijah Barstis for gathering the ELISA data and the visual LOD data used in this chapter. Financial support for this work was provided by a grant from the National Institute of Health through the SPARK-REACH program (UO1-HL152405) and through R01AI132668 and R01EB031510 Additional support was provided by the National Science Foundation (NSF STTR 2032222).

For Chapter 3, I would like to express special thanks to Dr. Rose Nash, Dr. Zachary Call, and Allison Dolence from BurstDx Inc for their help on this project. Their knowledge and insight was paramount to the success of these experiments.

In Chapter 4, I again have to thank John O'Donnell-Sloan and Sierra Curdts, two undergraduate research assistants, for their help in collecting the data above. I would also like to thank Elijah Barstis for his contributions to the H1N1 ELISA development.

For Appendix 1, I would like to thank Rae Bellows, a fellow graduate research assistant for her work on the antibody selection. Her work in collecting the data in A1.2 was crucial to the success of the assay in Chapter 2 of this dissertation.

TABLE OF CONTENTS

# CHAPTER 1: INTRODUCTION

## 1.1 Point of Care/Need Diagnostics

Traditional medical care is notoriously time consuming, expensive, and, as is human biology, complicated. In the United States, the average health care cost is >$12,000 per person each year.[1] Modern medical science has led to the eradication of some diseases, new treatments for chronic illnesses, and life-saving procedures for otherwise terminal conditions. However, an area of research and development that has consistently been overlooked is the roll of diagnostics in the treatment process. It has been estimated only 5% of medical spending goes to diagnostics despite the fact that the results influence 60-70% of further treatment decisions.[2] The underrepresentation of diagnostics can lead to misdiagnosis and mistreatment.[3-4] A meta-analysis of medical malpractice claims published in 2013 found that the leading cause of permanent injury or death in these claims was diagnostic errors.[4] Many safeguards have been suggested in response to these issues, but improved diagnostics would undoubtedly decrease the incidence of misdiagnosis.[5]

Improved diagnostics should be highly selective and sensitive to the intended biomarker, but higher sensitivity can often come at the cost of time and resources. Most instrumentation for medical testing and diagnosis already relies on a regular power source, temperature-controlled settings, and trained personnel to operate, restricting them to well-established medical facilities. While much of the world has access to these types of facilities, they are much fewer and at greater distances in developing countries and rural areas.[6-8] Although the accuracy and reliability of medical diagnostics may improve, if patients in need cannot access them, these improvements will not be realized. Therefore, improvements in diagnostic accessibility are also required.

Since the early 1990s, a push for portable, durable medical diagnosis and care was spearheaded by militaries.[9] For obvious reasons, being able to diagnose and treat patients quickly and in austere environments can mean the difference between life and death. Similarly, delay in diagnosis and treatment for patients with deadly illnesses can also be life threatening. Much of the developed world has at least some access to healthcare, although not perfect, but much of the need for POC medicine was aimed to assist in developing countries. In 2004, a study showed that the mean distance between patients and the nearest health clinic ranged from 4.7 km in Uganda to as far as 26.9 miles in Niger.[8, 10] This distance, although not too far by car, puts a heavy strain on people who do not have access to regular transportation. The same study indicated that distance and cost are two of the most important factors when it comes to access to treatment and patient outcomes. Because of this, lowering the cost and improving the accessibility of medical care was, and still is, a vital area of interest.

In the early 2000s, in light of the AIDS crisis, medical care professionals evaluated the most effective use of medical resources and the impact they have on medical outcomes.[11-13] One thing that seemed to be simultaneously crucial and overlooked was the use of effective diagnostic techniques. Laboratory methods were (and continue to be) expensive and inaccessible to many, while portable alternatives did not yet exist in significant numbers. The concept of point of care testing to reduce these barriers had been present before the 2000s;[14-16] however, the World Health Organization (WHO) developed a set of criteria to guide researchers as they develop a more ideal and accessible diagnostics for sexually transmitted infections.[17-18] The ASSURED criteria (**A**ffordable, **S**ensitive, **S**pecific, **U**ser-friendly, **R**apid & Robust, **E**quipment-free, **D**elivered), highlights aspects of a diagnostic device that would make it more accessible. Meeting these criteria would remove the need for many of the barriers that prevent effective diagnosis in low-income

and rural areas. It would allow medical professionals to travel to patients, bringing diagnosis and healthcare to the point of need (PON) or point of care (POC). Although these ASSURED criteria were initially developed to improve STI diagnostics, it was almost immediately recognized for its application to all PON/POC diagnostic devices.

### 1.2 Microfluidic Devices and Paper-Based Microfluidic Devices

In the decades following the onset of the ASSURED criteria, POC diagnostic devices have taken innumerable forms for an equally large number of diseases and conditions. On of the most effective ways to reduce the cost and increase the accessibility of a diagnostic device is to incorporate some sort of miniaturization.[9, 19-22] Reducing the materials needed to make a device and the volume of solutions required to operate it will increase manufacturability and reduce overall cost. Microfluidic devices are perhaps one of the best methods for miniaturization of diagnostic devices. Microfluidic devices, defined as fluid handling devices with channel dimensions <1 mm, can be manufactured in a variety of ways.[9, 23-24] More traditional microfluidic devices were originally designed and manufactured using photolithography methods, first introduced in 1998.[25] Typically, a light sensitive polymer is coated on a surface. A photomask with the desired channel dimensions and patterns cut out is placed over the coated surface. The surface is exposed to light, and only the unmasked sections. The remaining, soluble section of the polymer coating are washed away before a siloxane layer (typically polydimethylsiloxane, PDMS) is placed over the remining channel casts. Lastly, the PDMS layer now containing the channels is adhered to another flat surface to enclose the channels.[24, 26] Using this method, complex microchannels can be obtained that can perform impressive fluid manipulation, making low sample volume, high throughput methods realizable.[27-30]

While traditional microfluidics are impressive for their throughput and liquid handling capabilities, they often rely on syringe pumps and other instrumentation to operate. Efforts have been made to minimize or remove these limitations, but some sort of power source is still required. To remove these pumps and power sources, researchers have used large reservoirs and gravity,[31-32] air pressure,[33] or capillary pressure to drive flow.[34-37] However, the most popular way to passively drive flow in microfluidics is through capillary action and paper-based microfluidic devices.

In 2007, Martinez et. al. introduced paper microchannels as an alternative to hollow microfluidic channels.[38] Rather than using a hollow channel, the pores of the hydrophilic cellulose membrane act as channels in which solution can flow. Using a similar photolithography technique to traditional microfluidic device fabrication described above, they were able to create hydrophobic barriers on cellulose filter paper to define channels. The remaining hydrophilic areas of the filter paper were used for glucose and total protein detection and quantification.[38] While this was certainly not the first example of fibrous membranes being used as a method of fluid transport, it is commonly referenced as the seminal example of what are now called microfluidic paper-based analytical devices (μPAD). Paper has been used as a tool in chemical analysis as far back as the 1300s with the invention of litmus paper.[39] Although one of the earliest known examples, litmus paper is a prime example of paper's most appealing qualities for portable chemical assays. Reagents can be dried and stored on paper to be rehydrated and used later. Paper is affordable, ubiquitous, and easily disposable. Perhaps most importantly for μPAD, papers hydrophilic and porous structure allows for passive flow to occur via capillary force, negating the need for bulky external pumps or instrumentation.[40-41] These benefits have been harnessed in a myriad of μPADs in creative ways for decades. Electrochemical and fluorescent μPAD devices have been

extensively investigated over the years; however, they typically still require some instrumentation for excitation or signal readout.[42-46] While this instrumentation continues to miniaturize through the use of portable electrochemical systems and smartphones, colorimetric detection remains the simplest option for point of care testing.

Colorimetric detection in μPADs is attractive for yes/no readouts; if color is present after running the device, target is present in the sample. This type of analysis can be used for determining if someone has an infectious disease,[47-48] if water is contaminated with bacteria,[49-51] or any other case where any amount or target present is deleterious. Other methods have been developed to create quantitative devices without the use of external equipment. For example, radial or and distance-based detection methods have been used to quantify heavy metals.[52-54] In these cases, the metal present in sample is the limiting reagent. As the sample flows through the paper, a chelating ligand in the paper binds the target metal, and the distance of the colored product can be corelated to the amount of metal that was present in the sample (**Figure 1. something**). Counting based methods work on a similar concept where the number of colored areas or spots corresponds to the amount of target present.[55] Further, with the ubiquity of smartphones, simple image processing apps can be created and used to quantify the intensity of a colored product at a test line or spot.[46, 56-57]

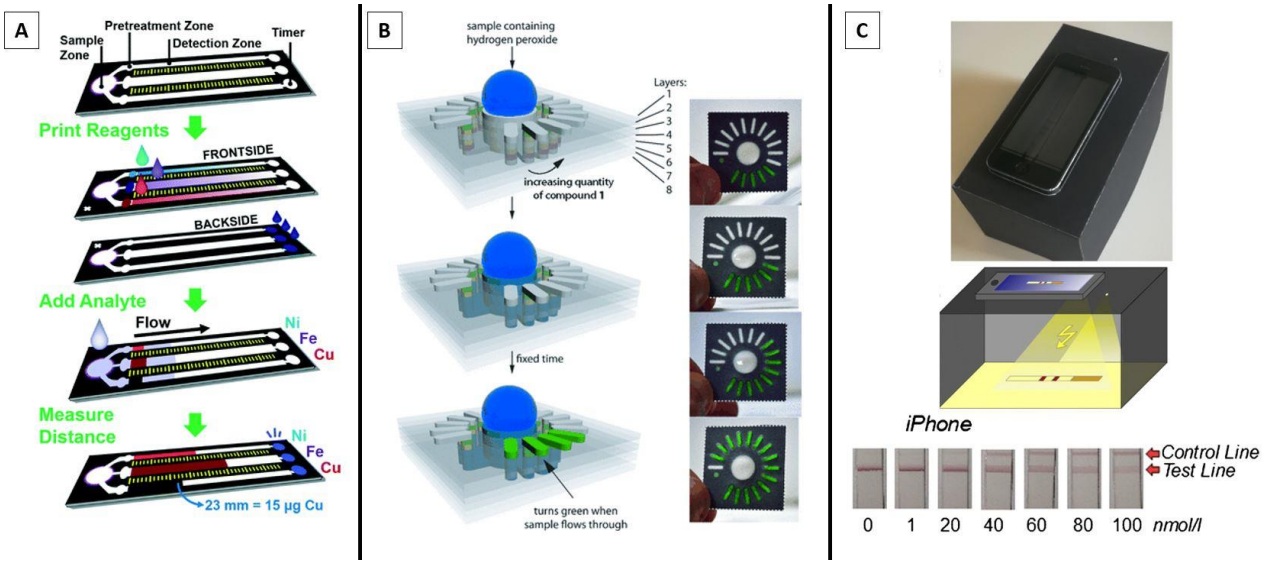


**Figure 1.1** Examples of different colorimetric detection methods on paper-based devices. A) Distance based detection of heavy metals, adapted from work by *Cate, D. et. al* with permission from *Lab on a Chip*.[52] B) Detection based on counting where the number of colored detection zones corresponds to the amount of $H_2O_2$ present in a given sample. This figure was adapted from work by *Lewis, G. et. al.* with permission from *Angewandte Chemi*.[55] C) An example of smartphone detection from *Ruppert, C. et. al.* uses a free software package from R to create an app that can automatically quantify LFA signal intensity for digoxin.[58] This figure was adapted with permission from *Microchimica Acta*.

Color generation also varies widely in µPADs based on the target of interest. Chelating ligands can be used for heavy metal detection.[52, 54, 59-60] Enzymes present in lysed bacteria of interest can react with an added substrate to produce a colorimetric reaction.[61-63] Enzyme substrate pairs can be used in immunoassays. Paper-based devices using antibodies to capture and/or detect the target of interest are known as immunoassays. Recent developments in paper-based immunoassays use enzyme labeled signal antibodies to enhance signal when target it present.[64-66] However, the most common detection motif for paper-based immunoassays is through the use of signal antibody conjugated to nanoparticles in lateral flow assays (LFAs).[67-69]

## 1.3 Immunoassays

The first immunoassay was developed in the late 1950s, where radiolabeled insulin was used in a competitive assay to determine the concentration of free insulin in a patient's serum.[70-71] In this type of competitive immunoassay, the more free insulin present in the sample, the less labeled insulin can bind to the capture antibody, reducing the detectable signal. Competitive assays are one of many types of immunoassays (examples shown in **Figure 1.2**), but the aspect all have in common is their use of antibodies for target capture and/or recognition.[72] While signal antibodies can be conjugated to fluorophores or radiolabels, one of the most common ways to generate signal is through the use of an enzyme/substrate pair. Relying on an enzyme and substrate, the signal produced for every target present can be amplified if the reaction is left longer in the presence of excess substrate. This method, known as an enzyme-linked immunosorbent assay (ELISA), is commonly used but required multiple washing steps to prevent false positives. Therefore, in every case described below in **Figure 1.2**, the most typical layout is in a 96 well plate where reagent addition and washing steps can be performed in each well. While multiple conditions can be analyzed and spatially separated by well, the procedures for well-plate ELISAs are complicated and take either expensive automated equipment or trained personnel to perform. Automation instrumentation and trained personnel are both costly, and ELISAs are still time consuming, requiring multiple long incubation steps.

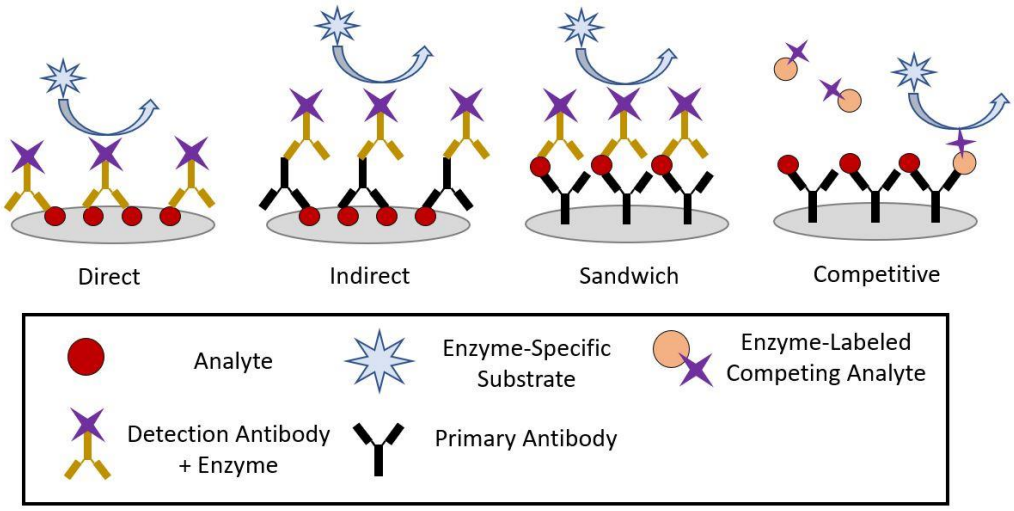


**Figure 1.2** In direct immunoassays, sample is used to coat the well plate, and a detection antibody is used to bind any target present in the sample. Indirect immunoassays are similar, but a primary antibody is used before the detection antibody with a wash step in between to improve specificity. In sandwich immunoassays, the plate is coated with primary antibody, target is added, and a detection antibody specific to the target is used to generate signal. Competitive immunoassays use an enzyme-labeled competing analyte to generate signal; if more analyte is present in a sample, less competing analyte will bind, reducing the signal produced.

A popular alternative to laboratory immunoassays is the lateral flow assay, or lateral flow immunoassay (FLA or LFIA) described briefly above.[67, 69] This type of paper-based assay relies on a series of porous membranes, that contain capture or signal antibody. When sample is added, it flows through a sample pad, followed by a conjugate release pad containing dried detection antibody. The detection antibody is rehydrated, and is the intended target is present, it will bind to the detection antibody. The bound analyte/detection antibody continues to flow past a test strip where capture antibody is bound to the surface. As mentioned above, detection antibodies in LFAs have traditionally been bound to gold nanoparticles, and the aggregation of these particles at a test line produces a deep red color. A generic example of a LFA is shown in **Figure 1.3**. Although the concept of lateral flow assays had been around long before, the first commercially available LFA for home diagnostics was a pregnancy test released in 1988.[69] Recognizing the impact of this tool

for home diagnostics, researchers have spent the following decades developing LFAs for communicable diseases,[73-75] bacterial infections,[74, 76-77] pesticides,[78-80] chronic illness biomarkers,[81-83] and innumerable other examples. The original concept of the LFA is ideal for qualitative results where only a yes/no answer is necessary. For example, there are only two outcomes of a pregnancy test, pregnant or not pregnant. However, for more quantitative applications, LFAs have been paired with smartphones and imaging software to measure the intensity of the test line.[46, 57-58]

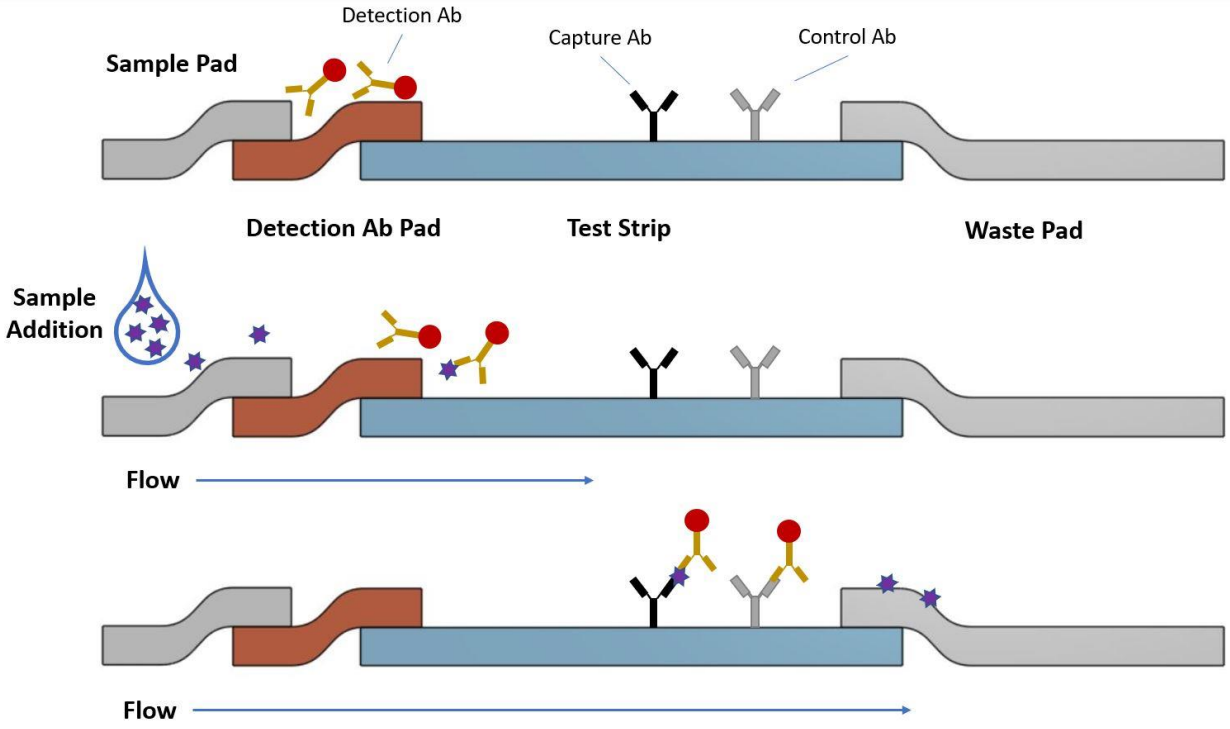


**Figure 1.3** A generic lateral flow assays is shown above with the locations of the sample pad, detection antibody pad, capture antibody test strip, and waste pad.

Unfortunately, signal intensity in nanoparticle LFAs is solely dependent on the binding affinity of the antibodies selected and the nanoparticle characteristics. Some research has been done to improve upon the nanoparticle characteristics or use different materials, but signal is still

limited to antibody binding and nanoparticles.[84-87] As is the case with ELISAs, enzymes could also be conjugated to the detection antibody in an LFA. While this would theoretically provide an option for signal enhancement via an enzyme/substrate reaction, ELISAs contain crucial washing steps to remove any unbound, excess enzyme from the well before substrate is added. Without this step, unbound enzyme would remain in the well and provide false positive results. Unfortunately, the simplicity and linear arrangement of LFAs does not allow for additional washing steps or reagent addition steps without further interaction from an end user.

Many attempts have been made to adjust the geometry of μPADs to provide reagent delivery and washing steps to create a POC/PON ELISA. For example, Virma M. et. al. developed a device containing a series of stacked and folded paper channels.[66] A test strip can be pulled under different reagent pads, and buffer can be added to vertically flow the reagents to the test strip. While this method simplifies a traditional ELISA significantly, it still requires an end user to correctly manipulate the device in timed steps as well as multiple buffer addition steps.[66] A rotary manifold has been developed by Carrell et. al. to similarly ease the steps of a traditional ELISA.[88] This example removes error that may come from the end user misaligning the paper channels, it still requires multiple timed steps from the user.[88] A fully automated, user-friendly ELISA would be greatly beneficial to improve POC testing and diagnostics, but is still yet to be actualized in the literature.

### 1.4 Fast Flow, Capillary Driven Devices and Flow Control

Capillary action has been used to induce passive flow in microfluidic devices since the early 2000s.[36] These devices use capillary pumps that rely on adhesion and cohesion of water/sample to drive flow through the channels of the devices.[37] Since their initial inception, capillary driven devices have been used for complex liquid handling, valving, sample preparation,

and miniaturization of complex biological assays.[37, 89-91] However, these devices still require complex fabrication, like photolithography techniques, or multiple end-user steps to perform an assay.[36, 90-91]

In 2018, the Henry group published work demonstrating rapid and sustained flow in multilayered paper-based microfluidic devices.[92] These devices were simply fabricated with double-sided tape and wax-printed paper to form flow channels. The flow rate in the channels was over two orders of magnitude greater than flow rates in paper alone, and the flow rates did not correspond to mathematical modeling for traditional paper-based flow (**Figure 1.3A**). Further work was conducted to model the flow in these channels, and the power of this new method of fluid transport and manipulation is a continued area of research.[93] It was also found that similar flow characteristics and can be obtained in hollow channels containing no paper, but fabricated with polyester transparency film and double-sided adhesive.[94-95] Using CAD software and laser cutting channel dimensions, complex valving, mixing, and velocity control can be obtained on miniature, affordable devices without the need for syringe pumps or other external instrumentation (**Figure 1.3B and C**).[95]

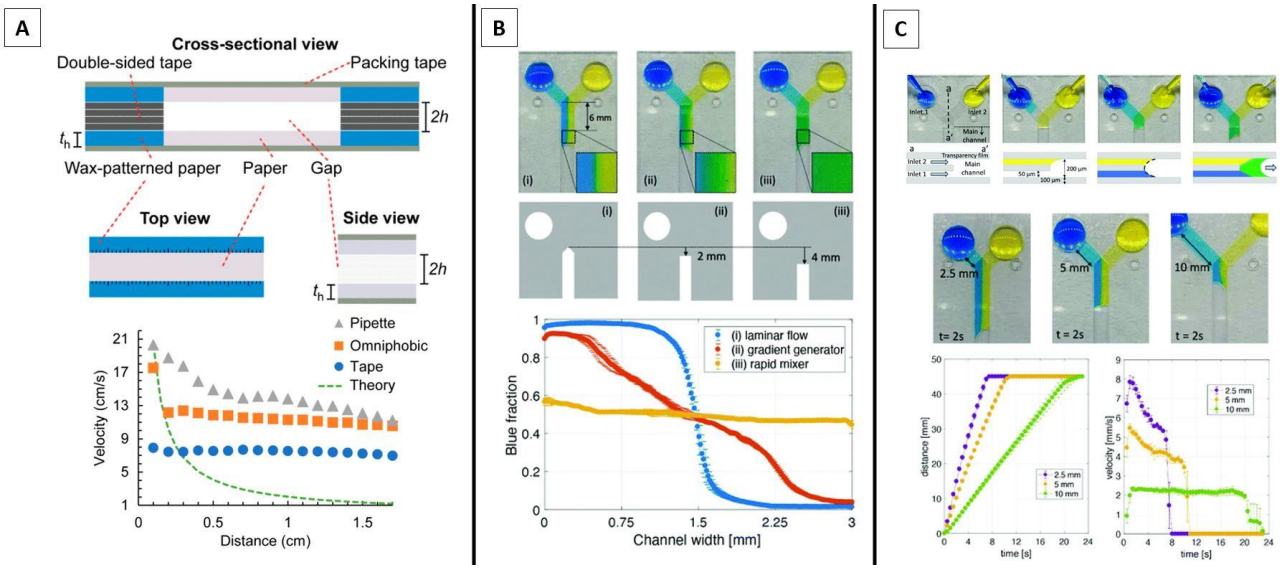

**Figure 1.3** A) the first example of this type of simple, capillary driven device was made with stacked layers of patterned paper and double-sided adhesive. This work showed rapid, sustained flow that did not match the mathematical modeling for traditional paper channels. This figure was adapted from work by *Channon, R. et. al.* with permission from the journal, *Analytical Chemistry*.[93] Making hollow channels for capillary flow with transparency film and double-sided adhesive, fluid control and manipulation like passive mixing and gradient generation (B); valving; and flow rate control (C). These figures were adapted from work by *Jang, I. et. al.* wither permission from the journal *Analyst*.[95]

The investigation of these concepts coincided with the onset of the COVID-19 pandemic caused by the SARS-CoV-2 virus in early late 2019. Accordingly, we intended to use the benefits of these capillary driven devices to create user friendly diagnostic tools to investigate SARS-CoV-2 biomarkers.

## 1.5 Capillary Driven Immunoassays for SARS-CoV-2 Biomarker Detection

SARS-CoV-2, the virus responsible for the COVID-19 pandemic, spread rapidly in late 2019. By the start of 2023, there had been >600 million reported cases, and >6 million deaths associated with the new disease.[96] Although social distancing, isolation, and mask-wearing, and other preventative measures were implemented, viral shed and transmission of the disease occur up to 3 days before the onset of symptoms.[97-99] This means that a person not yet experiencing symptoms for the disease could already be spreading the virus before they are aware of the infection. Because of this, a heavy emphasis was placed on rapid, and affordable testing for regular diagnosis. However, the techniques mainly used at testing sites, polymerase chain reaction (PCR) or less commonly, ELISAs, are notoriously time consuming, and the infrastructure put in place was incapable of handling such high volume.[100-101] LFAs for SARS-CoV-2 antigen became widely available to the public. However, many of the emergency use authorized tests had poor reliability.

When independently tested, many LFA devices performed far worse than claimed by the manufacturer in nasal swab samples, having detection limits well above the FDA's suggestion of 500 PFU/mL.[102]

In this dissertation, three separate capillary driven immunoassays were developed for enhanced POC diagnostic testing of SARS-CoV-2. Chapter two describes a colorimetric assay using a capillary driven device that automates the steps associated with a traditional well-plate ELISA from a single end-user sample addition step. The microfluidic front end of the device controls the sequence of flow following sample addition, allowing target, detection antibody, washing steps, and reagent delivery to be passively delivered to a nitrocellulose test strip containing capture antibody and control line. The device was developed using antibodies against SARS-CoV-2 nucleocapsid protein and was used to detect inactivated virus samples. The device was tested with virus in buffer, and a filtering step was implemented to detect virus on spiked nasal swab samples. On spiked samples, images of the test strips following assay completion were captured, and image processing was performed to determine a quantitative detection limit of 222 PFU/mL. A detection limit of 100 PFU/mL was determined following the FDA's emergency use authorization protocol by polling 20 untrained end users, asking them on which devices they could see a test line. This work has been submitted and is under review for the journal *Lab on a Chip*.

Chapter 3 expands on the device in chapter 2. The device design and function remain similar, but the detection motif used was chemiluminescent. Luminescent assays are popular for their increased sensitivity over absorbance-based methods. Additionally, because they require no external excitation or light source, chemiluminescent assays are particularly attractive for more portable, POC applications.[103] Chemiluminescent assays for SARS-CoV-2 IgM and IgG antibody detection exist, primarily for drug and vaccine screening tools.[104-106] However, this chapter

presents the first example of a rapid, capillary-driven chemiluminescent immunoassay for SARS-CoV-2 antigen. Additionally, this chapter shows data from a single channel device that was used in the assay development and optimization. This simplified device can help to rapidly screen assay conditions, accelerating proof of concept experiments and the assay development process. Using the capillary driven immunoassay device and a benchtop chemiluminescent imager, the analytical detection for SARS-CoV-2 nucleocapsid protein was 865 pg/mL. Some data has shown that circulating nucleocapsid protein concentration can range from 3-4000 ng/mL in the serum of an infected patient; the results in this study are well within that range.[107] We believe with further optimization and alternative imagers, this limit of detection can continue to improve. This work was done in collaboration with Burst Dx Inc. and will be part of a publication they submit when proper intellectual property and patents has been secured.

Chapter 2 and 3 demonstrate novel methods to passively perform the steps from an ELISA, but both were only performed for a single analyte. One benefit to laboratory based ELISAs is their ability to test for or distinguish between multiple targets simultaneously in spatially separated wells. Multiplexed analysis is also the ideal outcome from POC devices as well. Being able to monitor multiple biomarkers in a single test would greatly increase the diagnostic value of the results. Some LFA designs have been developed to multiplex by either adding more test lines to a single test strip or radially placing multiple LFAs surrounding the same sample inlet.[108-110] However, increasing the length of the test membrane too much will slow the assay time, and increasing the number of test strips will increase sample volume, both undesirable outcomes. Additionally, although some effort to develop more user friendly ELISAs has been discussed above, no publication has demonstrated a single-step, multiplexed ELISA.

In chapter 4, I present the first example of a single step, spatially separated ELISA that can simultaneously detect or distinguish between two targets in a sample using a capillary flow microfluidic device. The device was originally designed to distinguish between SARS-CoV-2 and H1N1 in patients presenting with symptoms indicative of both diseases. The device is designed with a capillary driven microfluidic device that branches off into two sections from the sample inlet. Each section has its own nitrocellulose test strip with capture antibody against either SARS-CoV-2 nucleocapsid protein or H1N1 hemagglutinin. Each section also houses dried signal antibody and substrate required for a colorimetric ELISA to take place at the test strips. Upon sample addition, either or both target protein present in the sample flow through both test strips, and the reagents and subsequent washes required for each ELISA are delivered to their respective test strip via capillary action. By design, the geometry of the device channels prevent reagents from one section from combining or cross reacting with reagents from the other. Using this device, I was able to detect nucleocapsid protein independently with a LOD of 133 pg/mL and hemagglutinin independently with a LOD of 840 pg/mL. To demonstrate the devices capabilities of detection two targets simultaneously, both nucleocapsid protein and hemagglutinin were spiked into the same sample and run in the device. At varying concentrations, signal was present on both sides of the device when both targets were present. However, a patient infected with both diseases is unlikely. To demonstrate another assay type, nucleocapsid protein was run concurrently with C-reactive protein, a biomarker associated with inflammation. Again, both targets were detected simultaneously. This work will be submitted to *Analytical Chemistry* in April 2023.

In this dissertation, I demonstrate the application of simple microfluidic systems for automated ELISAs with point of care diagnostics in mind. These capillary driven immunoassay devices reduce the complexity of a traditional ELISA to a single end-user step. The immunoassays

presented in this work have detection limits in biologically relevant ranges, and some were performed in complex biological samples. I also demonstrate the ability to sensitively detect multiple biomarkers simultaneously in under 15 min. The immunoassays in this dissertation and the technologies they're developed on represent a significant step forward in affordable, reliable diagnostics.

## CHAPTER 1 CITATIONS


1. National Health Expenditure Data. https://www.cms.gov/research-statistics-data-and-systems/statistics-trends-and-reports/nationalhealthexpenddata (accessed 2/10/2023).

2. Clifford Goodman, E. F., Ciara Gould, Erin Karnes, Ashley Smith, Christine Aguiar, Cameron Nelson, Atul Grover, Amy Berlin, Richard Phillips, Alison Horan *The Value of Diagnostics Innovation, Adoption and Diffusion into Health Care*; The Lewin Group, Inc.: July, 2005, 2005.

3. Petti, C. A.; Polage, C. R.; Quinn, T. C.; Ronald, A. R.; Sande, M. A., Laboratory Medicine in Africa: A Barrier to Effective Health Care. *Clinical Infectious Diseases* **2006,** *42* (3), 377-382.

4. Saber Tehrani, A. S.; Lee, H.; Mathews, S. C.; Shore, A.; Makary, M. A.; Pronovost, P. J.; Newman-Toker, D. E., 25-Year summary of US malpractice claims for diagnostic errors 1986–2010: an analysis from the National Practitioner Data Bank. *BMJ Quality & Safety* **2013,** *22* (8), 672-680.

5. Graber, M. L., The incidence of diagnostic error in medicine. *BMJ Quality & Safety* **2013,** *22* (Suppl 2), ii21-ii27.

6. Herd, G. C. E.; Musaad, S. M. A., Point-of-Care Testing in Rural and Remote Settings to Improve Access and Improve Outcomes: A Snapshot of the New Zealand Experience. *Archives of Pathology & Laboratory Medicine* **2020,** *145* (3), 327-335.

7. Jordan, H.; Roderick, P.; Martin, D.; Barnett, S., Distance, rurality and the need for care: access to health services in South West England. *International Journal of Health Geographics* **2004,** *3* (1), 21.

8. Devarajan, S. R., R.; Ahmad, J.; Commins, S.; Filmer, D.; Hammer, J.; Pritchett, L.; Shah, S.; Soucat, A.; Chaudhury, N. *Making Services Work for Poor People*; The International Bank for Reconstruction and Development/The World Bank: 2004.

9. Yager, P.; Edwards, T.; Fu, E.; Helton, K.; Nelson, K.; Tam, M. R.; Weigl, B. H., Microfluidic diagnostic technologies for global public health. *Nature* **2006,** *442* (7101), 412-418.

10. Peeling, R. W.; Holmes, K. K.; Mabey, D.; Ronald, A., Rapid tests for sexually transmitted infections (STIs): the way forward. *Sexually Transmitted Infections* **2006,** *82* (suppl 5), v1-v6.

11. Clinton, W. J., Turning the Tide on the AIDS Pandemic. *New England Journal of Medicine* **2003,** *348* (18), 1800-1802.

12. Gayle, H. D., Curbing the Global AIDS Epidemic. *New England Journal of Medicine* **2003,** *348* (18), 1802-1805.

13. Benatar, S. R., Health Care Reform and the Crisis of HIV and AIDS in South Africa. *New England Journal of Medicine* **2004,** *351* (1), 81-92.

14. Price, C. P., Point of care testing. *Bmj* **2001,** *322* (7297), 1285-8.

15. Sachdeva, S.; Davis, R. W.; Saha, A. K., Microfluidic Point-of-Care Testing: Commercial Landscape and Future Directions. *Frontiers in Bioengineering and Biotechnology* **2021,** *8*.

16. Gessler, F.; Pagel-Wieder, S.; Avondet, M.-A.; Böhnel, H., Evaluation of lateral flow assays for the detection of botulinum neurotoxin type A and their application in laboratory diagnosis of botulism. *Diagnostic Microbiology and Infectious Disease* **2007,** *57* (3), 243-249.

17. Kettler, H.; White, K.; Hawkes, S. J.; Research, U. N. W. B. W. S. P. f.; Training in Tropical, D., Mapping the landscape of diagnostics for sexually transmitted infections : key

findings and recommendations / Hannah Kettler, Karen White, Sarah Hawkes. World Health Organization: Geneva, 2004.

18. Mabey, D.; Peeling, R. W.; Ustianowski, A.; Perkins, M. D., Diagnostics for the developing world. *Nature Reviews Microbiology* **2004,** *2* (3), 231-240.

19. Racine, T.; Kobinger, G. P., Challenges and perspectives on the use of mobile laboratories during outbreaks and their use for vaccine evaluation. *Human vaccines & immunotherapeutics* **2019,** *15* (10), 2264-2268.

20. Bingham, D.; Kendall, J.; Clancy, M., The Portable Laboratory: An Evaluation of the Accuracy and Reproducibility of i-STAT©. *Annals of Clinical Biochemistry* **1999,** *36* (1), 66-71.

21. Dias, D.; Paulo Silva Cunha, J., Wearable Health Devices-Vital Sign Monitoring, Systems and Technologies. *Sensors (Basel)* **2018,** *18* (8), 2414.

22. Convery, N.; Gadegaard, N., 30 years of microfluidics. *Micro and Nano Engineering* **2019,** *2*, 76-91.

23. Bragheri, F.; Martínez Vázquez, R.; Osellame, R., Chapter 12.3 - Microfluidics. In *Three-Dimensional Microfabrication Using Two-Photon Polymerization (Second Edition)*, Baldacchini, T., Ed. William Andrew Publishing: 2020; pp 493-526.

24. Stroock, A. D., Chapter 17 - MICROFLUIDICS. In *Optical Biosensors (Second Edition)*, Ligler, F. S.; Taitt, C. R., Eds. Elsevier: Amsterdam, 2008; pp 659-681.

25. Duffy, D. C.; McDonald, J. C.; Schueller, O. J. A.; Whitesides, G. M., Rapid Prototyping of Microfluidic Systems in Poly(dimethylsiloxane). *Analytical Chemistry* **1998,** *70* (23), 4974-4984.

26. Scott, S. M.; Ali, Z., Fabrication Methods for Microfluidic Devices: An Overview. *Micromachines* **2021,** *12* (3), 319.

27. Alrifaiy, A.; Lindahl, O. A.; Ramser, K., Polymer-Based Microfluidic Devices for Pharmacy, Biology and Tissue Engineering. *Polymers* **2012,** *4* (3), 1349-1398.

28. Wheeler, A. R.; Throndset, W. R.; Whelan, R. J.; Leach, A. M.; Zare, R. N.; Liao, Y. H.; Farrell, K.; Manger, I. D.; Daridon, A., Microfluidic Device for Single-Cell Analysis. *Analytical Chemistry* **2003,** *75* (14), 3581-3586.

29. Kuswandi, B.; Nuriman; Huskens, J.; Verboom, W., Optical sensing systems for microfluidic devices: A review. *Analytica Chimica Acta* **2007,** *601* (2), 141-155.

30. Yang, T.; Stavrakis, S.; deMello, A., A High-Sensitivity, Integrated Absorbance and Fluorescence Detection Scheme for Probing Picoliter-Volume Droplets in Segmented Flows. *Analytical Chemistry* **2017,** *89* (23), 12880-12887.

31. Yang, Y.; Fathi, P.; Holland, G.; Pan, D.; Wang, N. S.; Esch, M. B., Pumpless microfluidic devices for generating healthy and diseased endothelia. *Lab Chip* **2019,** *19* (19), 3212-3219.

32. Komeya, M.; Hayashi, K.; Nakamura, H.; Yamanaka, H.; Sanjo, H.; Kojima, K.; Sato, T.; Yao, M.; Kimura, H.; Fujii, T.; Ogawa, T., Pumpless microfluidic system driven by hydrostatic pressure induces and maintains mouse spermatogenesis in vitro. *Scientific Reports* **2017,** *7* (1), 15459.

33. Lee, E. J.; Kim, B.-k.; Lee, K. K., Finger-powered, capillary-driven blood diagnostic chip for point-of-care technology. *Sensors and Actuators A: Physical* **2020,** *312*, 112153.

34. Hassan, S. U.; Zhang, X., Design and Fabrication of Capillary-Driven Flow Device for Point-Of-Care Diagnostics. *Biosensors (Basel)* **2020,** *10* (4).

35. Iakovlev, A. P.; Erofeev, A. S.; Gorelkin, P. V., Novel Pumping Methods for Microfluidic Devices: A Comprehensive Review. *Biosensors (Basel)* **2022,** *12* (11), 956.

36. Juncker, D.; Schmid, H.; Drechsler, U.; Wolf, H.; Wolf, M.; Michel, B.; de Rooij, N.; Delamarche, E., Autonomous Microfluidic Capillary System. *Analytical Chemistry* **2002,** *74* (24), 6139-6144.

37. Zimmermann, M.; Hunziker, P.; Delamarche, E., Valves for autonomous capillary systems. *Microfluidics and Nanofluidics* **2008,** *5* (3), 395-402.

38. Martinez, A. W.; Phillips, S. T.; Butte, M. J.; Whitesides, G. M., Patterned Paper as a Platform for Inexpensive, Low-Volume, Portable Bioassays. *Angewandte Chemie International Edition* **2007,** *46* (8), 1318-1320.

39. Coleman, W. F., Molecular Models of Indicators. *Journal of Chemical Education* **2008,** *85* (8), 1152.

40. Martinez, A. W.; Phillips, S. T.; Whitesides, G. M.; Carrilho, E., Diagnostics for the Developing World: Microfluidic Paper-Based Analytical Devices. *Analytical Chemistry* **2010,** *82* (1), 3-10.

41. Noviana, E.; Ozer, T.; Carrell, C. S.; Link, J. S.; McMahon, C.; Jang, I.; Henry, C. S., Microfluidic Paper-Based Analytical Devices: From Design to Applications. *Chemical Reviews* **2021,** *121* (19), 11835-11885.

42. Ataide, V. N.; Mendes, L. F.; Gama, L. I. L. M.; de Araujo, W. R.; Paixão, T. R. L. C., Electrochemical paper-based analytical devices: ten years of development. *Analytical Methods* **2020,** *12* (8), 1030-1054.

43. Dungchai, W.; Chailapakul, O.; Henry, C. S., Electrochemical Detection for Paper-Based Microfluidics. *Analytical Chemistry* **2009,** *81* (14), 5821-5826.

44. Solhi, E.; Hasanzadeh, M.; Babaie, P., Electrochemical paper-based analytical devices (ePADs) toward biosensing: recent advances and challenges in bioanalysis. *Analytical Methods* **2020,** *12* (11), 1398-1414.

45. Arai, M. S.; de Camargo, A. S. S.; Carrilho, E., Chapter 8 - Fluorescent paper-based analytical devices. In *Paper-based Analytical Devices for Chemical Analysis and Diagnostics*, de Araujo, W. R.; Paixão, T. R. L. C., Eds. Elsevier: 2022; pp 183-212.

46. Ulep, T. H.; Yoon, J. Y., Challenges in paper-based fluorogenic optical sensing with smartphones. *Nano convergence* **2018,** *5* (1), 14.

47. Rozand, C., Paper-based analytical devices for point-of-care infectious disease testing. *European Journal of Clinical Microbiology & Infectious Diseases* **2014,** *33* (2), 147-156.

48. Pandey, M.; Srivastava, M.; Shahare, K.; Bhattacharya, S., Paper Microfluidic-Based Devices for Infectious Disease Diagnostics. In *Paper Microfluidics: Theory and Applications*, Bhattacharya, S.; Kumar, S.; Agarwal, A. K., Eds. Springer Singapore: Singapore, 2019; pp 209-225.

49. Kim, H. J.; Kwon, C.; Noh, H., Paper-Based Diagnostic System Facilitating Escherichia coli Assessments by Duplex Coloration. *ACS Sensors* **2019,** *4* (9), 2435-2441.

50. Kim, H. J.; Kwon, C.; Lee, B. S.; Noh, H., One-step sensing of foodborne pathogenic bacteria using a 3D paper-based device. *Analyst* **2019,** *144* (7), 2248-2255.

51. Kim, D.-M.; Yoo, S.-M., Colorimetric Systems for the Detection of Bacterial Contamination: Strategy and Applications. *Biosensors (Basel)* **2022,** *12* (7), 532.

52. Cate, D. M.; Noblitt, S. D.; Volckens, J.; Henry, C. S., Multiplexed paper analytical device for quantification of metals using distance-based detection. *Lab on a Chip* **2015,** *15* (13), 2808-2818.

53. Hofstetter, J. C.; Wydallis, J. B.; Neymark, G.; Reilly Iii, T. H.; Harrington, J.; Henry, C. S., Quantitative colorimetric paper analytical devices based on radial distance measurements for aqueous metal determination. *Analyst* **2018,** *143* (13), 3085-3090.

54. Cate, D. M.; Dungchai, W.; Cunningham, J. C.; Volckens, J.; Henry, C. S., Simple, distance-based measurement for paper analytical devices. *Lab on a Chip* **2013,** *13* (12), 2397-2404.

55. Lewis, G. G.; DiTucci, M. J.; Phillips, S. T., Quantifying Analytes in Paper-Based Microfluidic Devices Without Using External Electronic Readers. *Angewandte Chemie International Edition* **2012,** *51* (51), 12707-12710.

56. Wu, D.; Zhang, J.; Xu, F.; Wen, X.; Li, P.; Zhang, X.; Qiao, S.; Ge, S.; Xia, N.; Qian, S.; Qiu, X., A paper-based microfluidic Dot-ELISA system with smartphone for the detection of influenza A. *Microfluidics and Nanofluidics* **2017,** *21* (3), 43.

57. Dong, M.; Wu, J.; Ma, Z.; Peretz-Soroka, H.; Zhang, M.; Komenda, P.; Tangri, N.; Liu, Y.; Rigatto, C.; Lin, F., Rapid and Low-Cost CRP Measurement by Integrating a Paper-Based Microfluidic Immunoassay with Smartphone (CRP-Chip). *Sensors (Basel)* **2017,** *17* (4), 684.

58. Ruppert, C.; Phogat, N.; Laufer, S.; Kohl, M.; Deigner, H.-P., A smartphone readout system for gold nanoparticle-based lateral flow assays: application to monitoring of digoxigenin. *Microchimica Acta* **2019,** *186* (2), 119.

59. Cate, D. M.; Nanthasurasak, P.; Riwkulkajorn, P.; L'Orange, C.; Henry, C. S.; Volckens, J., Rapid Detection of Transition Metals in Welding Fumes Using Paper-Based Analytical Devices. *The Annals of Occupational Hygiene* **2014,** *58* (4), 413-423.

60. Mentele, M. M.; Cunningham, J.; Koehler, K.; Volckens, J.; Henry, C. S., Microfluidic Paper-Based Analytical Device for Particulate Metals. *Analytical Chemistry* **2012,** *84* (10), 4474-4480.

61. Asif, M.; Awan, F. R.; Khan, Q. M.; Ngamsom, B.; Pamme, N., Paper-based analytical devices for colorimetric detection of S. aureus and E. coli and their antibiotic resistant strains in milk. *Analyst* **2020,** *145* (22), 7320-7329.

62. Jokerst, J. C.; Adkins, J. A.; Bisha, B.; Mentele, M. M.; Goodridge, L. D.; Henry, C. S., Development of a Paper-Based Analytical Device for Colorimetric Detection of Select Foodborne Pathogens. *Analytical Chemistry* **2012,** *84* (6), 2900-2907.

63. Boehle, K. E.; Gilliand, J.; Wheeldon, C. R.; Holder, A.; Adkins, J. A.; Geiss, B. J.; Ryan, E. P.; Henry, C. S., Utilizing Paper-Based Devices for Antimicrobial-Resistant Bacteria Detection. *Angewandte Chemie International Edition* **2017,** *56* (24), 6886-6890.

64. Cheng, C.-M.; Martinez, A. W.; Gong, J.; Mace, C. R.; Phillips, S. T.; Carrilho, E.; Mirica, K. A.; Whitesides, G. M., Paper-Based ELISA. *Angewandte Chemie International Edition* **2010,** *49* (28), 4771-4774.

65. Shih, C.-M.; Chang, C.-L.; Hsu, M.-Y.; Lin, J.-Y.; Kuan, C.-M.; Wang, H.-K.; Huang, C.-T.; Chung, M.-C.; Huang, K.-C.; Hsu, C.-E.; Wang, C.-Y.; Shen, Y.-C.; Cheng, C.-M., Paper-based ELISA to rapidly detect Escherichia coli. *Talanta* **2015,** *145*, 2-5.

66. Verma, M. S.; Tsaloglou, M.-N.; Sisley, T.; Christodouleas, D.; Chen, A.; Milette, J.; Whitesides, G. M., Sliding-strip microfluidic device enables ELISA on paper. *Biosensors and Bioelectronics* **2018,** *99*, 77-84.

67. Koczula, K. M.; Gallotta, A., Lateral flow assays. *Essays Biochem* **2016,** *60* (1), 111-120.

68. Jiang, N.; Ahmed, R.; Damayantharan, M.; Ünal, B.; Butt, H.; Yetisen, A. K., Lateral and Vertical Flow Assays for Point-of-Care Diagnostics. *Advanced Healthcare Materials* **2019,** *8* (14), 1900244.

69. van Amerongen, A.; Veen, J.; Arends, H. A.; Koets, M., Chapter 7 - Lateral Flow Immunoassays. In *Handbook of Immunoassay Technologies*, Vashist, S. K.; Luong, J. H. T., Eds. Academic Press: 2018; pp 157-182.

70. Yalow, R. S.; Berson, S. A., Assay of Plasma Insulin in Human Subjects by Immunological Methods. *Nature* **1959,** *184* (4699), 1648-1649.

71. Yalow, R. S.; Berson, S. A., Immunoassay of endogenous plasma insulin in man. *J Clin Invest* **1960,** *39* (7), 1157-75.

72. Darwish, I. A., Immunoassay Methods and their Applications in Pharmaceutical Analysis: Basic Methodology and Recent Advances. *International journal of biomedical science : IJBS* **2006,** *2* (3), 217-35.

73. Boehringer, H. R.; O'Farrell, B. J., Lateral Flow Assays in Infectious Disease Diagnosis. *Clin Chem* **2021,** *68* (1), 52-58.

74. Kim, H.; Chung, D.-R.; Kang, M., A new point-of-care test for the diagnosis of infectious diseases based on multiplex lateral flow immunoassays. *Analyst* **2019,** *144* (8), 2460-2466.

75. Patil, A. A.; Kaushik, P.; Jain, R. D.; Dandekar, P. P., Assessment of Urinary Biomarkers for Infectious Diseases Using Lateral Flow Assays: A Comprehensive Overview. *ACS Infectious Diseases* **2023,** *9* (1), 9-22.

76. Sohrabi, H.; Majidi, M. R.; Fakhraei, M.; Jahanban-Esfahlan, A.; Hejazi, M.; Oroojalian, F.; Baradaran, B.; Tohidast, M.; Guardia, M. d. l.; Mokhtarzadeh, A., Lateral flow assays (LFA)

for detection of pathogenic bacteria: A small point-of-care platform for diagnosis of human infectious diseases. *Talanta* **2022,** *243*, 123330.

77. Tominaga, T., Rapid detection of coliform bacteria using a lateral flow test strip assay. *Journal of Microbiological Methods* **2019,** *160*, 29-35.

78. Jara, M. D. L.; Alvarez, L. A. C.; Guimarães, M. C. C.; Antunes, P. W. P.; de Oliveira, J. P., Lateral flow assay applied to pesticides detection: recent trends and progress. *Environmental science and pollution research international* **2022,** *29* (31), 46487-46508.

79. Kim, Y. A.; Lee, E.-H.; Kim, K.-O.; Lee, Y. T.; Hammock, B. D.; Lee, H.-S., Competitive immunochromatographic assay for the detection of the organophosphorus pesticide chlorpyrifos. *Analytica Chimica Acta* **2011,** *693* (1), 106-113.

80. Luo, P.; Chen, X.; Xiao, J.; Zhao, Y.; Wang, Z., Rapid detection of iprodione in cucumber and apple using an immunochromatographic strip test. *Food and Agricultural Immunology* **2019,** *30* (1), 701-712.

81. Yin, M.; Nie, Y.; Liu, H.; Liu, L.; Tang, L.; Dong, Y.; Hu, C.; Wang, H., Development of a europium nanoparticles lateral flow immunoassay for NGAL detection in urine and diagnosis of acute kidney injury. *BMC Nephrology* **2022,** *23* (1), 30.

82. Gong, Y.; Hu, J.; Choi, J. R.; You, M.; Zheng, Y.; Xu, B.; Wen, T.; Xu, F., Improved LFIAs for highly sensitive detection of BNP at point-of-care. *International journal of nanomedicine* **2017,** *12*, 4455-4466.

83. Bayoumy, S.; Martiskainen, I.; Heikkilä, T.; Rautanen, C.; Hedberg, P.; Hyytiä, H.; Wittfooth, S.; Pettersson, K., Sensitive and quantitative detection of cardiac troponin I with upconverting nanoparticle lateral flow test with minimized interference. *Scientific Reports* **2021,** *11* (1), 18698.

84. Bishop, J. D.; Hsieh, H. V.; Gasperino, D. J.; Weigl, B. H., Sensitivity enhancement in lateral flow assays: a systems perspective. *Lab on a Chip* **2019,** *19* (15), 2486-2499.

85. Qin, Z.; Chan, W. C. W.; Boulware, D. R.; Akkin, T.; Butler, E. K.; Bischof, J. C., Significantly Improved Analytical Sensitivity of Lateral Flow Immunoassays by Using Thermal Contrast. *Angewandte Chemie International Edition* **2012,** *51* (18), 4358-4361.

86. Shen, G.; Xu, H.; Gurung, A. S.; Yang, Y.; Liu, G., Lateral flow immunoassay with the signal enhanced by gold nanoparticle aggregates based on polyamidoamine dendrimer. *Analytical sciences : the international journal of the Japan Society for Analytical Chemistry* **2013,** *29* (8), 799-804.

87. Yang, Y.; Ozsoz, M.; Liu, G., Gold nanocage-based lateral flow immunoassay for immunoglobulin G. *Microchimica Acta* **2017,** *184* (7), 2023-2029.

88. Carrell, C. S.; Wydallis, R. M.; Bontha, M.; Boehle, K. E.; Beveridge, J. R.; Geiss, B. J.; Henry, C. S., Rotary manifold for automating a paper-based Salmonella immunoassay. *RSC Advances* **2019,** *9* (50), 29078-29086.

89. Delamarche, E.; Juncker, D.; Schmid, H., Microfluidics for Processing Surfaces and Miniaturizing Biological Assays. *Advanced Materials* **2005,** *17* (24), 2911-2933.

90. Olanrewaju, A.; Beaugrand, M.; Yafia, M.; Juncker, D., Capillary microfluidics in microchannels: from microfluidic networks to capillaric circuits. *Lab on a Chip* **2018,** *18* (16), 2323-2347.

91. Parandakh, A.; Ymbern, O.; Jogia, W.; Renault, J.; Ng, A.; Juncker, D., 3D-printed capillaric ELISA-on-a-chip with aliquoting. *Lab on a Chip* **2023**.

92. Channon, R. B.; Nguyen, M. P.; Scorzelli, A. G.; Henry, E. M.; Volckens, J.; Dandy, D. S.; Henry, C. S., Rapid flow in multilayer microfluidic paper-based analytical devices. *Lab on a Chip* **2018,** *18* (5), 793-802.

93. Channon, R. B.; Nguyen, M. P.; Henry, C. S.; Dandy, D. S., Multilayered Microfluidic Paper-Based Devices: Characterization, Modeling, and Perspectives. *Analytical Chemistry* **2019,** *91* (14), 8966-8972.

94. Jang, I.; Carrão, D. B.; Menger, R. F.; Moraes de Oliveira, A. R.; Henry, C. S., Pump-Free Microfluidic Rapid Mixer Combined with a Paper-Based Channel. *ACS Sensors* **2020,** *5* (7), 2230-2238.

95. Ilhoon, J.; David S., D.; Brian J., G.; Charles, H.; Hyunwoong, K.; Simon, S., *Flow Control in a Laminate Capillary-Driven Microfluidic Device*. 2020.

96. COVID-19 Dashboard. https://coronavirus.jhu.edu/map.html (accessed 1/27/2023).

97. Cevik, M.; Tate, M.; Lloyd, O.; Maraolo, A. E.; Schafers, J.; Ho, A., SARS-CoV-2, SARS-CoV, and MERS-CoV viral load dynamics, duration of viral shedding, and infectiousness: a systematic review and meta-analysis. *The Lancet Microbe* **2021,** *2* (1), e13-e22.

98. He, X.; Lau, E. H. Y.; Wu, P.; Deng, X.; Wang, J.; Hao, X.; Lau, Y. C.; Wong, J. Y.; Guan, Y.; Tan, X.; Mo, X.; Chen, Y.; Liao, B.; Chen, W.; Hu, F.; Zhang, Q.; Zhong, M.; Wu, Y.; Zhao, L.; Zhang, F.; Cowling, B. J.; Li, F.; Leung, G. M., Temporal dynamics in viral shedding and transmissibility of COVID-19. *Nature Medicine* **2020,** *26* (5), 672-675.

99. Wölfel, R.; Corman, V. M.; Guggemos, W.; Seilmaier, M.; Zange, S.; Müller, M. A.; Niemeyer, D.; Jones, T. C.; Vollmar, P.; Rothe, C.; Hoelscher, M.; Bleicker, T.; Brünink, S.; Schneider, J.; Ehmann, R.; Zwirglmaier, K.; Drosten, C.; Wendtner, C., Virological assessment of hospitalized patients with COVID-2019. *Nature* **2020,** *581* (7809), 465-469.

100. Peeling, R. W.; Heymann, D. L.; Teo, Y. Y.; Garcia, P. J., Diagnostics for COVID-19: moving from pandemic response to control. *Lancet* **2022,** *399* (10326), 757-768.

101. Rethinking diagnostics for pandemic readiness. *Nature Biomedical Engineering* **2022,** *6* (3), 221-222.

102. Cubas-Atienzar, A. I.; Kontogianni, K.; Edwards, T.; Wooding, D.; Buist, K.; Thompson, C. R.; Williams, C. T.; Patterson, E. I.; Hughes, G. L.; Baldwin, L.; Escadafal, C.; Sacks, J. A.; Adams, E. R., Limit of detection in different matrices of 19 commercially available rapid antigen tests for the detection of SARS-CoV-2. *Scientific Reports* **2021,** *11* (1), 18313.

103. Dodeigne, C.; Thunus, L.; Lejeune, R., Chemiluminescence as diagnostic tool. A review. *Talanta* **2000,** *51* (3), 415-439.

104. Weber, M. C.; Risch, M.; Thiel, S. L.; Grossmann, K.; Nigg, S.; Wohlwend, N.; Lung, T.; Hillmann, D.; Ritzler, M.; Ferrara, F.; Bigler, S.; Egli, K.; Bodmer, T.; Imperiali, M.; Salimi, Y.; Fleisch, F.; Cusini, A.; Heer, S.; Renz, H.; Paprotny, M.; Kohler, P.; Vernazza, P.; Risch, L.; Kahlert, C. R., Characteristics of Three Different Chemiluminescence Assays for Testing for SARS-CoV-2 Antibodies. *Disease Markers* **2021,** *2021*, 8810196.

105. Matsuzaki, N.; Orihara, Y.; Kodana, M.; Kitagawa, Y.; Matsuoka, M.; Kawamura, R.; Takeuchi, S.; Imai, K.; Tarumoto, N.; Maesaki, S.; Maeda, T., Evaluation of a chemiluminescent enzyme immunoassay-based high-throughput SARS-CoV-2 antigen assay for the diagnosis of COVID-19: The VITROS® SARS-CoV-2 Antigen Test. *Journal of Medical Virology* **2021,** *93* (12), 6778-6781.

106. Liu, B.; Su, X.; Yu, G.; Yang, S.; Wang, F.; Huang, T.; Zhou, L.; Hui, Z.; Liao, Y.; Qiu, Y.; Huang, J.; Gao, H.; Liu, J.; Zhong, Y., An automated chemiluminescent immunoassay

(CLIA) detects SARS-CoV-2 neutralizing antibody levels in COVID-19 patients and vaccinees. *International Journal of Infectious Diseases* **2022,** *115*, 116-125.

107. Zhang, Y.; Ong, C. M.; Yun, C.; Mo, W.; Whitman, J. D.; Lynch, K. L.; Wu, A. H. B., Diagnostic Value of Nucleocapsid Protein in Blood for SARS-CoV-2 Infection. *Clin Chem* **2021,** *68* (1), 240-248.

108. Peng, J.; Wang, Y.; Liu, L.; Kuang, H.; Li, A.; Xu, C., Multiplex lateral flow immunoassay for five antibiotics detection based on gold nanoparticle aggregations. *RSC Advances* **2016,** *6* (10), 7798-7805.

109. Chen, Y.; Chen, Q.; Han, M.; Zhou, J.; Gong, L.; Niu, Y.; Zhang, Y.; He, L.; Zhang, L., Development and optimization of a multiplex lateral flow immunoassay for the simultaneous determination of three mycotoxins in corn, rice and peanut. *Food Chemistry* **2016,** *213*, 478-484.

110. Zhao, Y.; Wang, H.; Zhang, P.; Sun, C.; Wang, X.; Wang, X.; Yang, R.; Wang, C.; Zhou, L., Rapid multiplex detection of 10 foodborne pathogens with an up-converting phosphor technology-based 10-channel lateral flow assay. *Scientific Reports* **2016,** *6* (1), 21342.

# CHAPTER 2: CAPILLARY-DRIVEN IMMUNOASSAY PLATFORM FOR RAPID COVID-19 ANTIGEN DIAGNOSTICS

## 2.1 Chapter Overview:

The SARS-CoV-2 pandemic has made the need for rapid, affordable diagnostics more compelling than ever. While traditional laboratory diagnostics like PCR and ELISA are sensitive and specific, they can take multiple days to return results to a patient. At-home diagnostics like lateral flow assays (LFAs) are a simple, rapid alternative, but many commercially available LFAs have been criticized for their poor analytical sensitivity. The Capillary-Driven Immunoassay (CaDI) device described in this work uses microfluidic channels and capillary action to passively automate the steps of a traditional well-plate ELISA. On adding sample, an enzyme-conjugated secondary antibody, wash steps, and substrate are sequentially delivered to test and control lines consisting of a capture antibody and recombinant analyte, respectively on a nitrocellulose test strip. The end user can visually detect SARS-CoV-2 in 15-20 min, or results can be quantified using a smartphone and ImageJ. Analytical limits of detection of 83 PFU/mL for SARS-CoV-2 was determined for virus in buffer, and 222 PFU/mL for virus spiked into nasal swabs. Additionally, a visual limit of detection of 100 PFU/mL was determined in contrived nasal swab samples by polling 20 untrained end-users. While the CaDI device was used for detecting clinically relevant levels of SARS-CoV-2 in this study, the CaDI device can be easily adapted to other applications by changing the reagents and antibodies.

For this chapter, my contributions included overall project management, data generation/analysis for the CaDI device optimization, data generation/analysis for the CaDI dose response curves, initial draft writing for the manuscript, and editing for the manuscript. At the time

this chapter was written, the corresponding manuscript was under review in the Royal Society of Chemistry journal, *Lab on a Chip*.

## 2.2 Introduction:

SARS-CoV-2, the causative agent of COVID-19, is most infectious directly before and after the onset of symptoms.[1] Studies have shown that viral load in the respiratory tract of patients peaks within the first week of symptom onset;[2] however, because viral shedding can occur before symptom onset, it has been argued that symptomatic and *pre*-symptomatic spread are large contributors to rapid pathogen transmission.[3] For this reason, one of the most important tools to quell the spread of COVID-19 (and other contagious diseases), is readily available, affordable, and rapid testing.[4] The ideal diagnostic would be operational outside the laboratory, have high clinical specificity and sensitivity (i.e., high positive and negative predictive values), be simple enough for average untrained users to operate, and fast enough to screen large numbers of people (<15 min).

Quantitative polymerase chain reaction (qPCR) is the most common method used to detect SARS-CoV-2. qPCR methods have been shown to detect both genomic and subgenomic RNA. While genomic RNA would be a good indication that viable, transmittable virus is still present in a patient, subgenomic RNA may be remnants of dead or inactive virus that remain in the nose or pharynx after a patient is no longer contagious.[2, 5] Consequently, work by Alexandersen et al. have shown that qPCR can return a positive result up to 17 days after symptom onset when an individual is no longer infectious, arguing that PCR targeting subgenomic RNA may have some crucial faults as a diagnostic method.[5] Furthermore, qPCR requires expensive instruments, trained technicians, and several hours to run *after* the time it takes to transport sample to a laboratory. For these reasons, frequent, affordable, testing has been advocated for over infrequent but sensitive qPCR.[6-9] Rapid testing offering qualitative, yes/no results in less than 30 min would dramatically increase the

number of tests performed while providing actionable results. Assays that target antigen detection rather than RNA amplification offer a compromise between sensitivity and practicality and are available in several formats including laboratory-based enzyme linked immunosorbent assays (ELISA) and lateral flow assays (LFAs).

Laboratory ELISA offers higher sensitivity and specificity than LFAs, but like qPCR requires expensive instrumentation and trained technicians, making rapid, point-of-need testing extremely difficult.[10] LFAs offer an easy-to-use, affordable alternative to laboratory-based testing. LFAs are made of inexpensive materials, are user-friendly, and are performed in ~15 min. Most LFAs are comprised of a sequence of porous membranes containing dried secondary antibody conjugated to gold nanoparticles. When concentrated at a test line the aggregation of gold nanoparticles is visible by the naked eye, indicating a positive result. However, the improvements in ease-of-use relative to laboratory tests come at the cost of performance. Rapid antigen LFAs for SARS-CoV-2 have shown decent performance in controlled settings and much poorer in actual clinical validations.[11-14] For example, Cubas-Atienzar et al. found that only 4/19 rapid antigen tests maintained a limit of detection below the World Health Organization's suggestion of 500 PFU/mL when using dry nasal swabs.[13] Additionally, many tests meet the sensitivity requirements only when a patient has a high viral load, but struggle to maintain their sensitivity otherwise.[15-17] Therefore, an urgent need still exists for a diagnostic with the analytical performance of a laboratory-based ELISA and the ease-of-use of an LFA.

ELISAs outperform LFAs for several reasons, but their superior sensitivity stems from the ability to use an enzyme/substrate reaction as a label instead of a gold nanoparticle.[18] LFAs cannot use enzyme labels because they lack the ability to sequentially add and wash reagents from the test zone.[19] The ability to wash excess target, enzyme, and substrate from a well plate also helps

improve specificity in ELISAs. Implementing reagent addition and washing steps into an LFA would improve their performance but would come at the cost of ease-of-use, affordability, and portability, which are the properties that make LFAs one of the most popular diagnostic tools. Devices designed to automate the reagent delivery and washing steps associated with an ELISA exist, but often require multiple steps, lack simplicity and portability, or are too complicated for minimally trained end-users. Table A1 in Appendix 1 highlights several of these technologies.[20-25] Included are devices that perform enzyme-labeled sandwich immunoassays without the support of a powered instrument, although some still require complicated designs and manufacturing techniques.[26-27] Sequential steps in capillary driven devices have been previously demonstrated, but often fail to demonstrate efficient washing between reagent addition steps.[28-32] Instead, they use gold-enhancement reagents to improve the signal of traditional nanoparticle-based assays instead of enzyme/substrate amplification, which requires much more stringent washing to avoid background noise.[28-32]

In this work, we describe a microfluidic device that fully automates the reagent delivery and washing steps of an ELISA while retaining the simplicity of an LFA. Using fast-flowing, capillary-driven microfluidics discussed in previous works,[33-36] the capillary-driven immunoassay (CaDI) device sequentially delivers sample, reagents, and wash buffer to a nitrocellulose test zone to perform an enzymatic sandwich immunoassay. The CaDI device is created by stacking alternating layers of patterned hydrophilic polyethylene film and double-sided adhesive to create hollow channels for flow (Figs. S1 and S2). Conjugate release pads embedded in the channels contain the reagents needed for each binding step of the assay. A nitrocellulose test strip is connected to the outlet of the device for readout, and a waste pad is used to draw buffer and reagents through the nitrocellulose. The point-of-care ELISA systems outlined in Table A1 all use

cellulose-based channels to transport reagents to the detection zone. Although inexpensive and easy to fabricate, paper channels present several problems for immunoassays, including very low flow rates, loss of reagent and sample to adsorption/absorption, and the inability to handle large sample volumes.[33, 37-38] The channels in the CaDI device supply the same power-free capillary flow and solve these problems, resulting in more efficient washing of the test zone, increased reagent delivery, and 15-20 min assay times. After adding sample to the CaDI device, all remaining reagent addition and washing steps occur automatically, and the assay is complete in 15-20 min. Results can be read by eye for a positive/negative answer, or a smart phone image can be analyzed for quantitative results.

We previously demonstrated a similar concept to the CaDI device used to detect SARs-CoV-2 antibodies from whole human blood as well as the tuberculosis marker, LAM.[39-40] While antibody detection gives information on a person's level of immunity, it does not necessarily diagnose active infections. Here, we demonstrate the CaDI device's ability to detect SARS-CoV-2 nucleocapsid protein (N-protein) from inactivated SARS-CoV-2 virus in buffer and in contrived clinical samples. Unlike the previous devices, the CaDI device used in this study was improved in terms of the manufacturing process as well as uniform reagent delivery to the detection zone. Since the CaDI device for this work was designed without overlapping channel geometry, the device could be fabricated with fewer steps and layers compared to the CaDI device for detecting SARs-CoV-2 antibodies. This feature allows the cost of the device manufacturing to be further reduced. Also, new design factors were considered to enhance the uniformity of reagent delivery. With this device, a detection limit of 83 PFU/mL was obtained for inactivated SARS-CoV-2 spiked into buffer run in the CaDI device, only one order of magnitude above the limit of detection (LOD) for a traditional ELISA run with the same reagents. Nasal swabs were collected and spiked with

inactivated virus; for these contrived samples, an analytical detection limit of 222 PFU/mL was determined. In addition to the analytical limits of detection, a visual LOD of 100 PFU/mL from contrived nasal swab samples was obtained by polling 20 untrained end-users. Beyond the SARs-CoV-2 assays demonstrated in this and previous work, the CaDI device can be used for a multitude of point-of-care immunoassays. The device represents a major step forward in providing high quality diagnostics in at-home and resource limited settings. The CaDI device bridges the gap between the easy-to-operate LFA and the high-performing laboratory standard ELISA.

### 2.3 Materials and Methods:

*Device assembly*:

The CaDI is made of alternating layers of transparency film (3M$^{TM}$ 9984, Saint Paul, MN, USA) and double-sided adhesive (3M$^{TM}$ 467MP, Saint Paul, MN, USA). The channels in each layer are cut under a flow of nitrogen gas with a $CO_2$ laser cutter (Epilog Zing, Golden, CO, USA) and laminated together using a temperature controlled TruLam laminator at room temperature. The channel designs and dimensions are shown in Figure A1.1. The first four layers are stacked and laminated. The reagent pads are then added to the channels, followed by the final layer of patterned 9984 film. Finally, the nitrocellulose test strip (FF80HP Plus, Cytiva, Marlborough, MA, USA) was inserted to the outlet of the device and an absorbent material (CFSP223000, MilliporeSigma Burlington, MA, USA) was placed on the end of the nitrocellulose and secured with adhesive (3M$^{TM}$ 468MP, Saint Paul, MN, USA). To demonstrate sequential delivery and washing in the device (Figure 2.2A), tartrazine (yellow dye, 1870 μM) and erioglaucine (blue dye, 800 μM) were dried onto reagent pads.[34]

*Reagent pad preparation:*

The reagent pads were made from a glass fiber conjugate release pad (GFDX203000, MilliporeSigma Burlington, MA, USA) pretreated by immersing in a blocking solution of 10 mM PBS (Thermo Scientific, Rockford, IL, USA), 3% sucrose, 0.5% Tween-20, and 0.1% thimerosal (MilliporeSigma) for 15 min. The pads were removed from the blocking solution, dried overnight at 37 °C, and cut into 3×5 $mm^2$ rectangles by hand with a razor blade. The reagent pads containing the enzyme-conjugated secondary antibody were further blocked with 15 µL of 0.57% casein (MilliporeSigma) dissolved in 50 mM borate buffer per pad and dried for 30-45 min at 37 °C. After drying, 5 µL of detection antibody labeled with horseradish peroxidase (2°Ab-HRP) was pipetted onto the casein-blocked pad (40143-MM05-H, Sino Biological, Beijing, China) and dried for 30 min at 37°C. The 2°Ab-HRP was diluted in a stabilizing, long-term storage buffer consisting of 0.01 M ethylenediaminetetraacetic acid, 0.01 M $FeSO_4$, 4% trehalose, and 0.1% BSA in PBS, before adding to the pad.[41] 3,3',5,5'-tetramethylbenzidine solution (TMBM-0100-01, Surmodics Inc., Eden Prairie, MN, USA) was pipetted onto the second reagent pad in 3, 7.5 µL aliquots, allowing the pad to dry for 5-7 min at 37 °C between additions. After the final TMB addition both reagent pads were dried for 120 min at 37 °C before added to the CaDI device.

*Nitrocellulose preparation:*

The nitrocellulose test strip (FF80HP Plus, Cytiva, Marlborough, MA, USA) was striped with a control and test line using a BioSpot reagent printer (BioFluidix, Breisgau, Germany). The control line was striped with a SARS-CoV-2 N-protein at 0.25 mg/mL (40143-V08B, Sino Biological) in a solution of 20 mM Tris, 500 mM NaCl, 10% glycerol, pH 7.4, 5% - 8% trehalose, mannitol and 0.01% Tween80. The test line was striped with a monoclonal anti-SARS-CoV-2 N-protein at 0.88 mg/mL (40143-MM08, Sino Biological). The test line striping solution contained

trehalose (Calbiochem, San Diego, CA USA) and glycerol (Mallinckrodt, Dublin, Ireland) with final concentration of 45 mM and 4.5% respectively to increase stability of the protein during drying. After striping, the nitrocellulose was dried overnight in a desiccator and blocked with Stabilguard™ (SG01-1000, Surmodics Inc.) by allowing it to wick through the membrane from bottom to top until the membrane was fully saturated. The nitrocellulose was then dried again for 5 h at 37 °C before cutting into 3×15 $mm^2$ strips with the laser cutter and stored at 4°C with desiccant pouches until use.

*Assay operation:*

The extraction/running buffer was made of a 1.5X stable peroxide buffer (Thermo Fisher, 34062) buffered to pH 6.5 with sodium hydroxide. 150 mM sodium chloride and 0.1% Igepal CA630 were added for viral lysis and inactivation (Fisher Scientific), and 0.1% Tween-20 was added to reduce non-specific adsorption. Inactivated SARS-CoV-2 virus (USA-WA1/2020) was prepared and quantified by plaque assay as previously described.[42] Inactivated virus was spiked into extraction buffer at the desired concentration before 100 µL of sample is added to the sample inlet on the CaDI device to begin the assay. For experiments requiring nasal swab samples, an anterior nares swab (FoamTec Medical, MP1301AST) was collected under approval of the IRB board of Colorado State University by swabbing the inside of the nostril, three rotations of the swab in each nostril. For spiked swab samples, 50 µL of inactivated virus sample was added to the swab after collection. The swabs were submerged in 300 µL of extraction buffer, swirled for 15 s, filtered with a 0.2 µm PTFE syringe filter (Fisher, 13-1001-14), and 100 µL of the filtered sample was added to the device to begin the assay. The workflow for nasal swab samples can be seen in Figure 2.1.

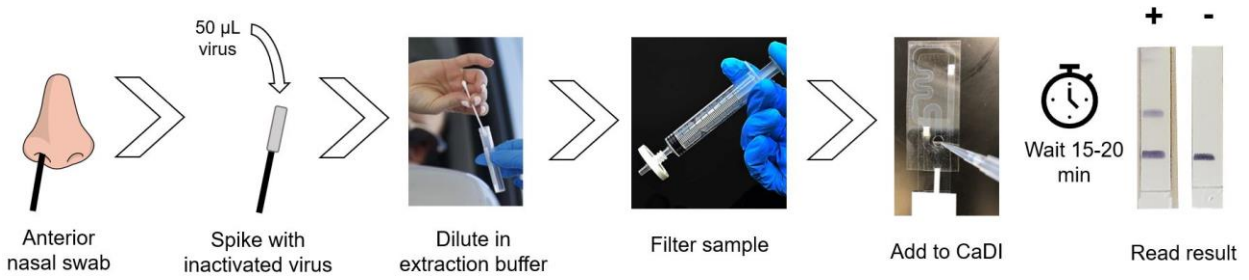


**Figure 2.1** The workflow for nasal swab samples is shown above. After a swab is collected, it is submerged in extraction buffer to lyse any virus present. The buffer/sample is then pushed through a syringe filter before adding to the device.

The 100 µL of extraction buffer provides the washing buffer and target analyte, while the CaDI device supplies all other reagents, so no further end user input is required. The assay is finished once the channel above the substrate reagent pad is emptied, which takes 15-20 min. The nitrocellulose strip is then allowed to dry at room temperature for 5 min before imaging for analysis.

*Image/Data Analysis:*

After an assay was complete, the nitrocellulose was removed, dried, and placed on a white background in a light box containing 16 LEDs for consistent lighting.[20, 43] Images were captured using a Motorola One smartphone. NIH ImageJ software was used for analysis. Images were inverted, converted to 8-bit greyscale, and the area around the test line was surrounded using the polygon tool. The mean gray value was taken for the selected area at the test line and directly below the test line. The ratio of the two values (test line/background) is the "mean gray ratio," and helps account for slight differences in lighting/background between images. The mean gray ratio was used as the signal to quantify the color change at the test line.

*Visual LOD:*

For the visual limit of detection, a variation of methods from FDA emergency use authorization approved devices was used.[44] CaDI devices were run (n=1) at varying concentrations (0, 50, 100, 200, 300, 400, 500 PFU/mL) of inactivated virus following the nasal swab assay operation as previously described. First, an anterior nasal swab was collected by swabbing inside both nostrils, 3 rotations in each. 50 µL of inactivated virus sample was then added to the swab after collection. The swabs were submerged in 300 µL of extraction buffer, swirled for 15 s, filtered with a 0.2 mm PTFE syringe filter (Fisher, 13-1001-14), and 100 µL of the filtered sample was added to the device to begin the assay. The nitrocellulose test strip was removed from the device, placed into a small petri dish, and randomly assigned a letter between A and G.

Twenty untrained volunteers were recruited and informed that two lines present on the nitrocellulose membrane indicate a positive test, while a single line indicates a negative test. They were instructed to look at each of seven nitrocellulose test strips and to identify each strip as a positive or negative test. Responses for each nitrocellulose test strip were recorded.

*Well-Plate ELISA:*

50 mL of 40143-MM08 (1 mg/mL diluted in 10 mM PBS, pH 7.2, along with 45 mM trehalose and 4.5% glycerol) was added to each well in a Corning™ Costar® 96-well assay plate and allowed to adsorb overnight at 4 °C while shaking. Each well in the plate was then washed three times with 200 mL of wash buffer (10 mM PBS containing 0.1% Tween-20). After washing, wells were blocked with 200 mL StabilGuard™ Immunoassay Stabilizer for 1 h at 37 °C while shaking. After an additional 3 washes, 50 mL of varying concentrations of inactivated SARS-CoV-

2 virus (diluted in extraction buffer with varying conditions described in the supplemental section) was added to the wells and allowed to incubate for 1 h at ambient temperature while shaking. Each well was washed three times, and 50 mL of 40143-MM05 (0.5 µg/mL diluted in drying buffer described above) was then added to each well and incubated for 1 h at ambient temperature while shaking. After a final three washes, 50 mL of TMB substrate (1-Step™ Ultra TMB-ELISA, Thermo Fisher Scientific) was added to each well and allowed to react for 2.5 min. This reaction was then stopped by adding 50 mL of 1 M $H_2SO_4$ to each well and read at OD 450 nm with a Perkin Elmer VICTOR™ X5 2030 Multilabel plate reader.

**2.4 Results and Discussion:**

*Sequential delivery and washing:*

Sandwich immunoassays are a popular format for LFAs and ELISAs and use two antibodies that bind to different epitopes of the target antigen for signal production.[45] To visualize the steps of the sandwich assay used in the CaDI device, yellow dye was used to simulate the HRP-conjugated secondary antibody, and blue dye was used to simulate the TMB substrate (Figure 2.2A and 2.2B). After adding sample diluted in extraction buffer, the CaDI device channels fill, and sample reaches the nitrocellulose. The grey arrows in Figure 2.2B show the direction in which the channels fill from the sample inlet. As the channels fill, air escapes from the channels via vents above the two conjugate release pads. Once the channel is filled and the nitrocellulose is wetted by the sample, all fluid in the CaDI device flow into the waste pad through the nitrocellulose, because the capillary force at the waste pad is the only driving force after this point. However, the order of flow is determined depending on the channel geometry such as the channel height and length between the waste pad and sample inlet working as an inlet for the air.

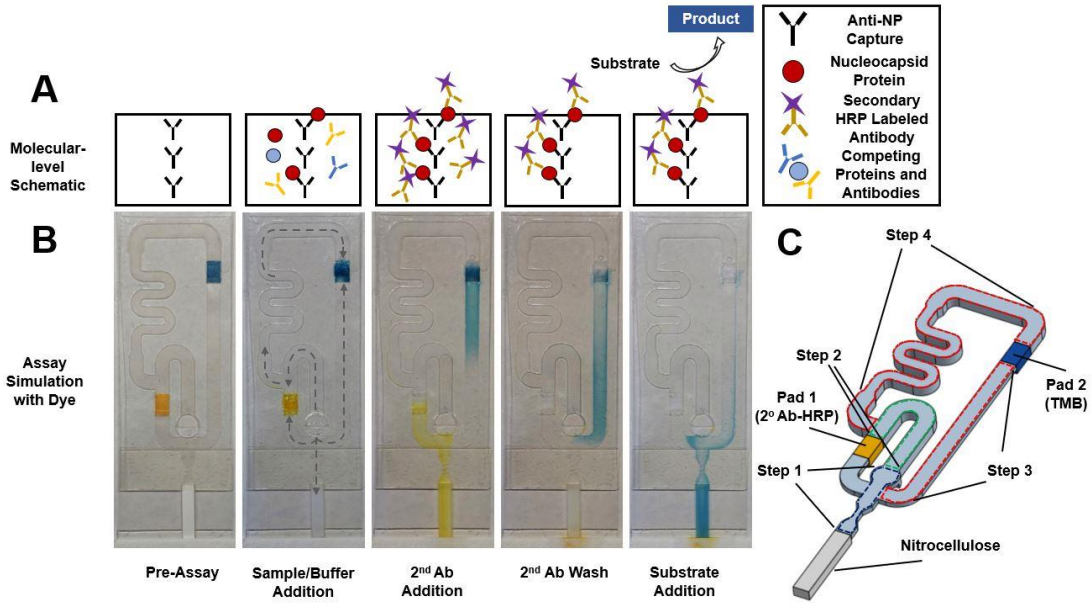


**Figure 2.2** (A) Molecular level representation of the immunoassay steps using an HRP-labeled antibody. The steps show here occur at the test line on the nitrocellulose. (B) Simulation of reagent addition and washing steps using yellow food dye to represent the HRP-antibody and blue food dye to represent the TMB substrate. (C) 3D rendering of the CaDI device channels that show how each plug of buffer in the channels is used in the assay.

In step 1 (Figure 2.2C), N-protein conjugates to a capture antibody at the test line of the nitrocellulose. The channel area of step 1 has the shortest length between the waste pad and the sample inlet, so the remaining sample after filling the channel area flows through the nitrocellulose first. As the solution flows through the nitrocellulose, the dried reagents (represented by blue and yellow dye in Figure 2.2B) are rehydrated and sequentially flow through the nitrocellulose and across the test and control lines. During step 2, the buffer in the channel between pad 1 and the inlet is used to rehydrate and transport 2°Ab-HRP (represented by the yellow dye in Figure 2.2B) to the test line where it binds to the target. Although two channels are connected to the sample inlet, air only comes into the channel on the top half of the inlet because the height of this channel is larger (see Fig. A1 and A2 in Appendix 1 for channel dimensions and layers). There is N-protein

in the buffer that will bind to 2°Ab-HRP in the conjugate release pad; however, in this study this did not lead to a noticeable hook effect.

In traditional ELISAs, washing by rinsing the well several times with 200-500 µL of wash buffer is required before adding the substrate to prevent high background and/or false positives. These washing steps help improve sensitivity and specificity but add time and complexity.[46-47] Thorough washing is difficult in LFAs due to the fact that the buffer flows linearly through the LFA without any separation of steps by flow. The washing step in a CaDI device is performed using the buffer occupying the channel between pad 2 and the nitrocellulose membrane (Step 3). This wash step is critical for removing any excess 2°Ab-HRP from the test line, preventing false positives. After efficiently washing excess 2°Ab-HRP from the channels, rehydrated TMB substrate (represented by the blue dye in Figure 2.2B) is rinsed through the nitrocellulose (Step 4). The dye simulations of reagent delivery and washing like those shown in Figure 2.2B were used to optimize channel dimensions to ensure proper washing before running an immunoassay. For example, because the channel on the right has a shorter height, buffer fills that channel slower at the sample loading step. The serpentine pattern in the left-most channel was added to ensure that the buffer from both channels meet at the TMB pad at similar times, preventing air bubbles from stopping flow. The pinched channel near the nitrocellulose was implemented in an attempt to induce passive mixing,[48] ensuring that the 2°Ab-HRP and TMB cover the nitrocellulose evenly as they flow through.

*Enzyme-substrate system:*

The next consideration for the CaDI antigen assay was the choice of enzyme and substrate. With a single sample addition step, all washing, binding, and enzymatic reaction steps must occur

under the same conditions. Each of these steps has its own optimal operating conditions, so determining assay parameters that can work for the entire assay was critical. Horseradish peroxidase (HRP) was chosen for this application because it is stable and active at physiological pH and has several colorimetric substrates that can be used for naked-eye detection. Of these substrates, 3,3',5,5'-tetramethylbenzidine (TMB) was chosen. Oxidized TMB is soluble and would be washed through the nitrocellulose after reacting with HRP and $H_2O_2$ under normal conditions. However, the commercially available TMB blotting solution used contains additives that form an insoluble product, leaving a dark blue precipitate.

*Immunoassay optimization:*

Immunoassays are highly dependent on the specificity and binding efficiency of the antibodies. An extensive report on commercially available antibodies for SARS-CoV-2 N-protein detection was published in 2021, and the results from that study were used to guide the antibody selection in this work.[49] Five Sino Biological antibodies were chosen for screening in the CaDI devices (Figure A1.3 and A1.4), and 40413-MM05 and 40413-MM08 were chosen as the detection and capture antibodies respectively as a result. To determine optimal buffer conditions, a traditional well-plate ELISA was performed under different buffer conditions as described in the methods section (Figure A1.5). The extraction buffer at pH 6.5 and 150 mM NaCl was comparable to buffer at pH 7.4 and 225 mM NaCl. However, the optimal pH for antibody binding is ~7.2, and the optimal pH for HRP activity is ~5.5.[50] Since it lies in between that pH range, buffer containing 150 mM NaCl at pH 6.5 was chosen as the extraction buffer. The surfactants in the extraction buffer, Igepal and Tween-20, serve to both lyse the virus if any is present and help reduce non-specific binding of proteins and secondary antibodies to the test line. The volume of

TMB dried on the conjugate release pads was determined by holding all other conditions constant and adjusting the TMB volume. Volume was used for optimization instead of concentration as the concentration is proprietary information from the supplier. The buffer conditions described above were used, and the MM05-HRP concentration was 20 µg/mL. Devices were then run at 0 and 550 PFU/mL for each TMB volume. A volume of 22.5 µL was chosen as the condition that gave the greatest signal before increasing signal in the blanks (Figure 2.3A). The concentration of MM05-HRP was determined in a similar fashion. All other conditions were held constant, and the concentration of the 2°Ab-HRP was varied. For the 2°Ab-HRP, 5 µL of 20 µg/mL was chosen similar reasons as the TMB optimization. Despite the error in the positives, 20 µg/mL MM05-HRP is the concentration that had the greatest average signal before increasing the error in the blank (Figure 2.3A and B).

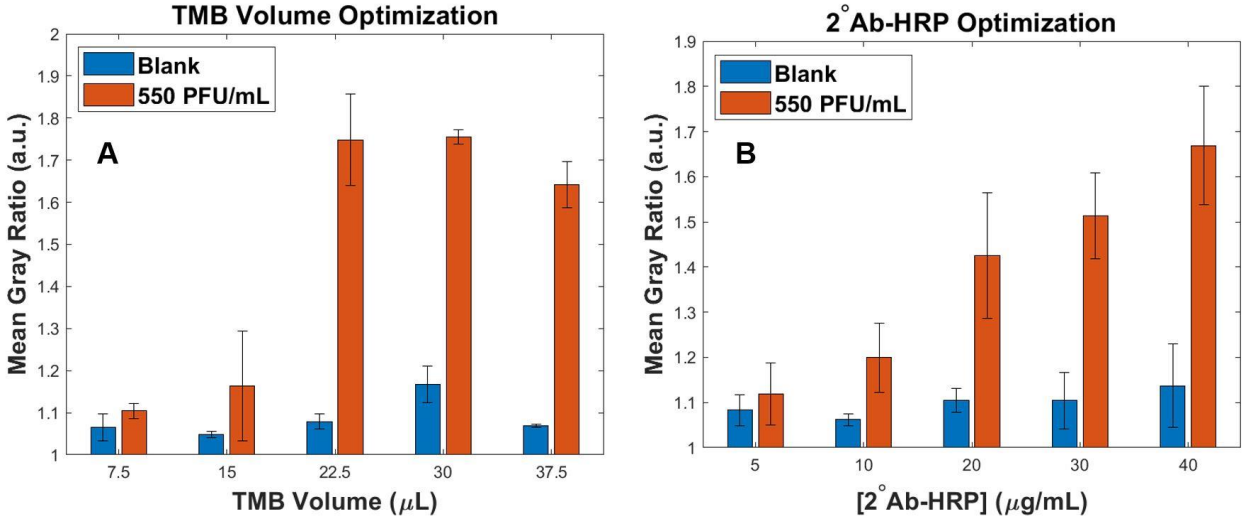


**Figure 2.3** (A) Buffer conditions (described above) and 2°Ab-HRP concentrations were held constant (20 µg/mL) while the volume of TMB dried on the conjugate release pad was varied. (B) Buffer conditions (described above) and TMB volume were held constant (22.5 µL) while the concentration of 2°Ab-HRP was varied. Each condition was run with 0 and 550 PFU/mL of inactivated virus to determine the condition that would give the greatest signal without increasing the signal of the blank.

*Assay performance:*

Figure 2.4 shows the comparison between the CaDI device and a well plate ELISA using inactivated SARS-CoV-2 spiked into extraction buffer. Varying concentrations of inactivated virus was spiked into buffer and run in either a well plate ELISA or the CaDI device. After completion of the CaDI devices, the nitrocellulose was removed from the device and images were captured with a Motorola 1 smartphone under a light box lined with 16 LEDs. The images were opened in ImageJ, converted to 8-bit gray scale, and the color was inverted. The "mean gray ratio" (eq 2.1) was gathered by taking ratio of the mean grayscale value of the test line, divided by the same area just below the test line.

$$mean\ gray\ ratio = \frac{test\ line\ mean\ gray\ value}{background\ mean\ gray\ value} \tag{2.1}$$

For the dose response curves, the data was fit to a four-parameter logistic regression (eq 2.2), where *y* is the mean gray ratio, *x* is concentration, $a$ is the theoretical response with no target present, $b$ is the slope factor, $c$ is the inflection point, and $d$ is the theoretical response with infinite target present.

$$y = d + \frac{a - d}{\left[1 + \left(\frac{x}{c}\right)^{b}\right]} \tag{2.2}$$

Solving eq 2.2 for x, the limit of detection (LOD) was determined as the concentration when *y* is equal to the signal of the blank, $S_b$, plus three times its standard deviation, $\sigma_b$ (eq 2.3).

$$LOD = c\left[\left(\frac{a - d}{(S_b + 3 * \sigma_b) - d}\right) - 1\right]^{\frac{1}{b}} \tag{2.3}$$

Using equations A1.1-A1.3, an analytical detection limit of 8 and 84 PFU/mL for the ELISA and CaDI device respectively. Although this is a 10-fold difference in LOD, the four parameter logistic fits for these curves align closely, but the biggest contribution affecting the difference in LOD is the standard deviation of the blank in the CaDI device. The higher LOD and greater standard deviation is due in part to the difference in the instrumentation used for quantification: A UV-Vis spectrophotometer with a 0.5 cm path length for the ELISA versus a cell phone image inside a homemade light box for the CaDI. Additionally, the TMB solution used here is supposed to make an insoluble product that will remain at the test line; however, some oxidized TMB can still be seen flowing into the waste pad. In the well-plate ELISA, all the product is contained in the well, ensuring all colored product is detected by the plate reader. Importantly, the CaDI device achieved similar performance to the ELISA in a much simpler format. The ELISA requires 18 pipetting steps, over 5 h of analysis time, and an expensive instrument (~$5,000-15,000) for quantification. The CaDI only requires one pipetting step, 15 min from sample addition to result, and results can be quantified from smartphone images. The results in Figure 2.4 demonstrate the CaDI device's ability to provide the performance of a complex, laboratory-based ELISA with the simplicity of a standard LFA.

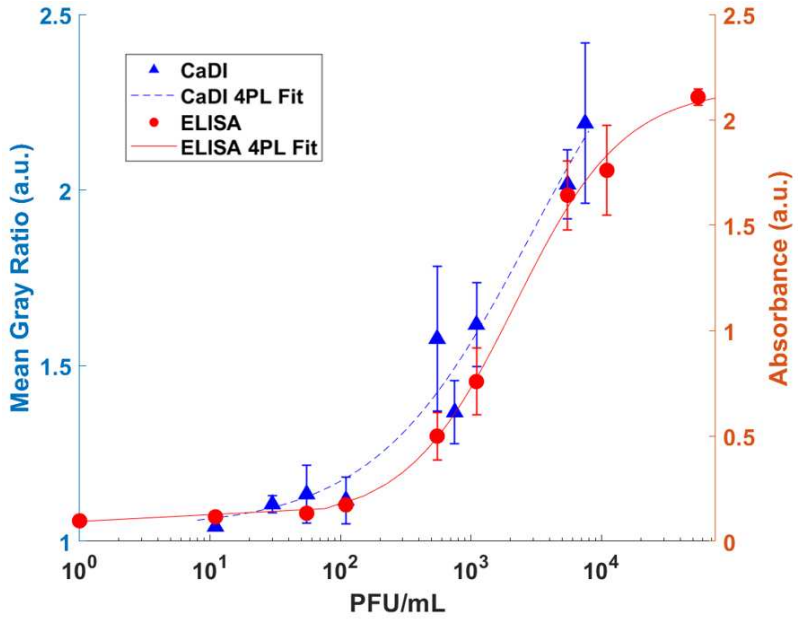


**Figure 2.4** Inactivated virus diluted in extraction buffer comparing the CaDI devices (blue triangles and dashed trace) to a well plate ELISA (red circles and solid trace). The limits of detection were 86 PFU/mL and 8 PFU/mL for the CaDI and ELISA respectively. Each point for the ELISA and CaDI devices were run as n=3 for standard deviation, except for the blank in the CaDI devices which was run as n=5.

*Nasal Swab Samples:*

To demonstrate the CaDI device's ability to perform in complex sample matrices, spiked nasal swab samples were also run in the device. Unfortunately, due to cellular debris and mucins from nasal samples, the pores of the nitrocellulose clog in the current design of the device, so a filtering step was implemented for nasal swab samples. This filtering step is necessary for the current device format, but future will be performed to incorporate on-device filtering to maintain simplicity for POC testing. Anterior nares nasal swab samples were collected from individuals who had recently tested negative for SARS-CoV-2 by swirling 3-5 times in each nostril, and 50 µL of varying inactivated virus concentrations was added to the swab. Each swab was then submerged in 300 µL of extraction buffer and swirled for 15-20 s at a frequency of 1-3 Hz.[51] The

sample was then pushed through a syringe filter before 100 µL of the filtered sample was added to the inlet of the CaDI device. After filtering, the nasal sample assays completed in a similar amount of time as the assays run with buffer (15-20 min). From this experiment, an LOD of 222 PFU/mL of the solution spiked on the nasal swab was determined (Figure 2.5).

Our LOD is slightly more than double that of the virus diluted in extraction buffer. This makes sense considering that 50 µL of virus-containing solution is diluted in 300 µL of buffer after being added to the swab. It's possible that the complexity of the sample matrix and loss to the swab and filter also contributed to the higher LOD. Additionally, there was minor background signal in the blanks, which affects how the LOD is calculated in eq 2.3. Although these issues were minimal, we believe that further optimization and blocking of the NC would improve this LOD further.

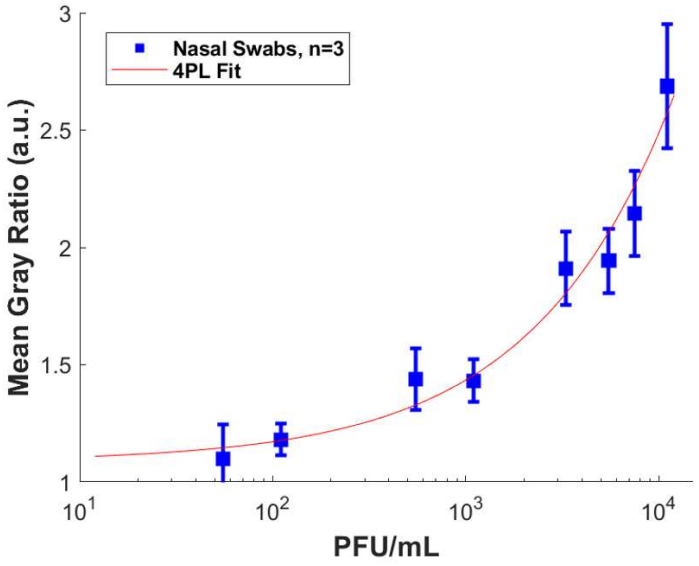


**Figure 2.5** 50 µL of varying virus concentrations was added to nasal swabs after collected (n=3 for each concentration). The swabs were submerged in extraction buffer, filtered, and added to the device. The LOD from this study was 222 PFU/mL.

In addition to the analytical LOD described above, anterior nares swab samples were collected and spiked with 50 µL of six varying inactivated virus concentrations. The swabs samples were filtered and ran on CaDI devices as described above, and the resulting randomized nitrocellulose strips were shown to 20 untrained end-users who were blinded to the virus concentration. Individuals were asked to identify which strips were positive, e.g., which strips showed both test and control lines. Of the individuals polled, 100% identified 100 PFU/mL as positive, and 0% identified the blank as positive (Table 1). The FDA suggests that a visual LOD is the concentration at which 19/20 untrained end users can correctly identify a positive result (95% sensitivity),[44] meaning the visual LOD for the CaDI is 100 PFU/mL from this study. This LOD is significantly below commercial tests on the market today.[13]

**Table 2.1** Visual limit of detection study. Twenty individuals were asked to identify positive results on nitrocellulose that was run from nasal swabs with the virus concentrations listed below.

| **Virus Concentration (PFU/mL)** | **0** | **50** | **100*** | **200** | **300** | **400** | **500** |
|---|---|---|---|---|---|---|---|
| Individuals who marked "positive" | 0 | 7 | 20 | 20 | 20 | 20 | 20 |
| Total individuals polled | 20 | 20 | 20 | 20 | 20 | 20 | 20 |
| Percent correctly identified | 100% | 35% | 100% | 100% | 100% | 100% | 100% |

*Visual LOD

## 2.5 Conclusion:

Current antigen LFA devices, while easy to use and relatively cost effective, are limited in specificity and sensitivity due to the lack of signal amplification and washing steps. An ideal replacement would maintain the operational simplicity of LFAs while adding these functions found in more sophisticated ELISA assays. We have described a method here that addresses shortcomings with current LFA technologies by adding a microfluidic front end to provide

complicated fluid handling in line with a nitrocellulose membrane. The resulting CaDI device can be fabricated without utilizing an overlapped channels and perform sample delivery, washing, and signal amplification steps from a single sample addition. Using the CaDI device, we were able to detect clinically relevant levels of SARS-CoV-2 N-protein from nasal swabs in under 20 min. Because of the device's unique design, the sample addition, reagent delivery, and washing steps associated with a traditional well-plate ELISA can be performed from a single end-user step with the resulting quantitative data having the same general concentration trend as an optical instrument. Furthermore, we were able to show detection limits of 100 PFU/mL for contrived nasal swab samples using naked eye detection by untrained users. This represents a significant improvement over existing COVID-19 LFA systems. Finally, while the CaDI device has been used to detect SARS-CoV-2, by changing the antibodies and antigens used in the device, we can detect any biomarker(s) associated with other disease states. Due to its low cost and ease of use, we believe the CaDI device will be a valuable platform for rapid diagnostics in the future.

## CHAPTER 2 CITATIONS


1. He, X.; Lau, E. H. Y.; Wu, P.; Deng, X.; Wang, J.; Hao, X.; Lau, Y. C.; Wong, J. Y.; Guan, Y.; Tan, X.; Mo, X.; Chen, Y.; Liao, B.; Chen, W.; Hu, F.; Zhang, Q.; Zhong, M.; Wu, Y.; Zhao, L.; Zhang, F.; Cowling, B. J.; Li, F.; Leung, G. M., Temporal dynamics in viral shedding and transmissibility of COVID-19. *Nature Medicine* **2020,** *26* (5), 672-675.

2. Cevik, M.; Tate, M.; Lloyd, O.; Maraolo, A. E.; Schafers, J.; Ho, A., SARS-CoV-2, SARS-CoV, and MERS-CoV viral load dynamics, duration of viral shedding, and infectiousness: a systematic review and meta-analysis. *The Lancet Microbe* **2021,** *2* (1), e13-e22.

3. Cevik, M.; Kuppalli, K.; Kindrachuk, J.; Peiris, M., Virology, transmission, and pathogenesis of SARS-CoV-2. *BMJ* **2020,** *371*, m3862.

4. Kretzschmar, M. E.; Rozhnova, G.; Bootsma, M. C. J.; van Boven, M.; van de Wijgert, J. H. H. M.; Bonten, M. J. M., Impact of delays on effectiveness of contact tracing strategies for COVID-19: a modelling study. *The Lancet Public Health* **2020,** *5* (8), e452-e459.

5. Alexandersen, S.; Chamings, A.; Bhatta, T. R., SARS-CoV-2 genomic and subgenomic RNAs in diagnostic samples are not an indicator of active replication. *medRxiv* **2020**, 2020.06.01.20119750.

6. Larremore, D. B.; Wilder, B.; Lester, E.; Shehata, S.; Burke, J. M.; Hay, J. A.; Tambe, M.; Mina, M. J.; Parker, R., Test sensitivity is secondary to frequency and turnaround time for COVID-19 surveillance. *medRxiv* **2020**, 2020.06.22.20136309.

7. Mina, M. J.; Parker, R.; Larremore, D. B., Rethinking Covid-19 Test Sensitivity — A Strategy for Containment. *New England Journal of Medicine* **2020**.

8. Chin, E. T.; Huynh, B. Q.; Chapman, L. A.; Murrill, M.; Basu, S.; Lo, N. C., Frequency of routine testing for COVID-19 in high-risk environments to reduce workplace outbreaks. *medRxiv* **2020**, 2020.04.30.20087015.

9. Paltiel, A. D.; Zheng, A.; Walensky, R. P., Assessment of SARS-CoV-2 Screening Strategies to Permit the Safe Reopening of College Campuses in the United States. *JAMA Network Open* **2020,** *3* (7), e2016818-e2016818.

10. St John, A.; Price, C. P., Existing and Emerging Technologies for Point-of-Care Testing. *Clin Biochem Rev* **2014,** *35* (3), 155-167.

11. Igloi, Z.; Velzing, J.; van Beek, J.; van de Vijver, D.; Aron, G.; Ensing, R.; Benschop, K.; Han, W.; Boelsums, T.; Koopmans, M.; Geurtsvankessel, C.; Molenkamp, R., Clinical Evaluation of Roche SD Biosensor Rapid Antigen Test for SARS-CoV-2 in Municipal Health Service Testing Site, the Netherlands. *Emerging Infectious Disease journal* **2021,** *27* (5), 1323.

12. Fernandez-Montero, A.; Argemi, J.; Rodríguez, J. A.; Ariño, A. H.; Moreno-Galarraga, L., Validation of a rapid antigen test as a screening tool for SARS-CoV-2 infection in asymptomatic populations. Sensitivity, specificity and predictive values. *eClinicalMedicine* **2021,** *37*.

13. Cubas-Atienzar, A. I.; Kontogianni, K.; Edwards, T.; Wooding, D.; Buist, K.; Thompson, C. R.; Williams, C. T.; Patterson, E. I.; Hughes, G. L.; Baldwin, L.; Escadafal, C.; Sacks, J. A.; Adams, E. R., Limit of detection in different matrices of 19 commercially available rapid antigen tests for the detection of SARS-CoV-2. *Scientific Reports* **2021,** *11* (1), 18313.

14. Jegerlehner, S.; Suter-Riniker, F.; Jent, P.; Bittel, P.; Nagler, M., Diagnostic accuracy of a SARS-CoV-2 rapid antigen test in real-life clinical settings. *International Journal of Infectious Diseases* **2021,** *109*, 118-122.

15. Jeewandara, C.; Guruge, D.; Pushpakumara, P. D.; Madhusanka, D.; Jayadas, T. T.; Chaturanga, I. P.; Aberathna, I. S.; Danasekara, S.; Pathmanathan, T.; Jayathilaka, D.; Somathilaka, G.; Kuruppu, H.; Gomes, L.; Gunasekara, V.; Wijayamuni, R.; Ogg, G. S.; Malavige, G. N., Sensitivity and specificity of two WHO approved SARS-CoV2 antigen assays in detecting patients with SARS-CoV2 infection. *BMC Infectious Diseases* **2022,** *22* (1), 276.

16. Dinnes, J.; Deeks, J. J.; Adriano, A.; Berhane, S.; Davenport, C.; Dittrich, S.; Emperador, D.; Takwoingi, Y.; Cunningham, J.; Beese, S.; Dretzke, J.; Ferrante di Ruffano, L.; Harris, I. M.; Price, M. J.; Taylor-Phillips, S.; Hooft, L.; Leeflang, M. M.; Spijker, R.; Van den Bruel, A., Rapid, point-of-care antigen and molecular-based tests for diagnosis of SARS-CoV-2 infection. *The Cochrane database of systematic reviews* **2020,** *8* (8), Cd013705.

17. Organization, W. H., Antigen-detection in the diagnosis of SARS-CoV-2 infection. *Interim Guide* **2021**.

18. Davies, C., Chapter 2.1 - Principles of Competitive and Immunometric Assays (Including ELISA)1. In *The Immunoassay Handbook (Fourth Edition)*, Wild, D., Ed. Elsevier: Oxford, 2013; pp 29-59.

19. van Amerongen, A.; Veen, J.; Arends, H. A.; Koets, M., Chapter 7 - Lateral Flow Immunoassays. In *Handbook of Immunoassay Technologies*, Vashist, S. K.; Luong, J. H. T., Eds. Academic Press: 2018; pp 157-182.

20. Henry, C. S.; Feeny, R.; Franklin, A. B.; Carrell, C., Rotary manifold for paper-based immunoassays. Google Patents: 2020.

21. Verma, M. S.; Tsaloglou, M.-N.; Sisley, T.; Christodouleas, D.; Chen, A.; Milette, J.; Whitesides, G. M., Sliding-strip microfluidic device enables ELISA on paper. *Biosensors and Bioelectronics* **2018,** *99*, 77-84.

22. Chen, C.-A.; Yeh, W.-S.; Tsai, T.-T.; Chen, C.-F., Three-dimensional origami paper-based device for portable immunoassay applications. *Lab Chip* **2019,** *19* (4), 598-607.

23. Huang, S.; Abe, K.; Bennett, S.; Liang, T.; Ladd, P. D.; Yokobe, L.; Anderson, C. E.; Shah, K.; Bishop, J.; Purfield, M., Disposable autonomous device for swab-to-result diagnosis of influenza. *Analytical chemistry* **2017,** *89* (11), 5776-5783.

24. Apilux, A.; Ukita, Y.; Chikae, M.; Chailapakul, O.; Takamura, Y., Development of automated paper-based devices for sequential multistep sandwich enzyme-linked immunosorbent assays using inkjet printing. *Lab Chip* **2013,** *13* (1), 126-135.

25. Zhang, J.; Gui, X.; Zheng, Q.; Chen, Y.; Ge, S.; Zhang, J.; Xia, N., An HRP-labeled lateral flow immunoassay for rapid simultaneous detection and differentiation of influenza A and B viruses. *Journal of medical virology* **2019,** *91* (3), 503-507.

26. Ordutowski, H.; Dal Dosso, F.; De Wispelaere, W.; Van Tricht, C.; Vermeire, S.; Geukens, N.; Gils, A.; Spasic, D.; Lammertyn, J., Next generation point-of-care test for therapeutic drug monitoring of adalimumab in patients diagnosed with autoimmune diseases. *Biosensors and Bioelectronics* **2022,** *208*, 114189.

27. Yafia, M.; Ymbern, O.; Olanrewaju, A. O.; Parandakh, A.; Sohrabi Kashani, A.; Renault, J.; Jin, Z.; Kim, G.; Ng, A.; Juncker, D., Microfluidic chain reaction of structurally programmed capillary flow events. *Nature* **2022,** *605* (7910), 464-469.

28. Fu, E.; Liang, T.; Spicar-Mihalic, P.; Houghtaling, J.; Ramachandran, S.; Yager, P., Two-dimensional paper network format that enables simple multistep assays for use in low-resource settings in the context of malaria antigen detection. *Analytical chemistry* **2012,** *84* (10), 4574-4579.

29. Fridley, G. E.; Le, H.; Yager, P., Highly sensitive immunoassay based on controlled rehydration of patterned reagents in a 2-dimensional paper network. *Analytical chemistry* **2014,** *86* (13), 6447-6453.

30. Toley, B. J.; McKenzie, B.; Liang, T.; Buser, J. R.; Yager, P.; Fu, E., Tunable-delay shunts for paper microfluidic devices. *Analytical chemistry* **2013,** *85* (23), 11545-11552.

31. Shin, J. H.; Park, J.; Kim, S. H.; Park, J.-K., Programmed sample delivery on a pressurized paper. *Biomicrofluidics* **2014,** *8* (5), 054121.

32. Park, J.; Park, J.-K., Pressed region integrated 3D paper-based microfluidic device that enables vertical flow multistep assays for the detection of C-reactive protein based on programmed reagent loading. *Sensors and Actuators B: Chemical* **2017,** *246*, 1049-1055.

33. Channon, R. B.; Nguyen, M. P.; Scorzelli, A. G.; Henry, E. M.; Volckens, J.; Dandy, D. S.; Henry, C. S., Rapid flow in multilayer microfluidic paper-based analytical devices. *Lab on a Chip* **2018,** *18* (5), 793-802.

34. Ilhoon, J.; David S., D.; Brian J., G.; Charles, H.; Hyunwoong, K.; Simon, S., *Flow Control in a Laminate Capillary-Driven Microfluidic Device*. 2020.

35. Jang, I.; Carrão, D. B.; Menger, R. F.; Moraes de Oliveira, A. R.; Henry, C. S., Pump-Free Microfluidic Rapid Mixer Combined with a Paper-Based Channel. *ACS Sensors* **2020,** *5* (7), 2230-2238.

36. Call, Z. D.; Carrell, C. S.; Jang, I.; Geiss, B. J.; Dandy, D. S.; Henry, C. S., Paper-based pump-free magnetophoresis. *Analytical Methods* **2020,** *12* (43), 5177-5185.

37. Nguyen, M. P.; Meredith, N. A.; Kelly, S. P.; Henry, C. S., Design considerations for reducing sample loss in microfluidic paper-based analytical devices. *Analytica Chimica Acta* **2018,** *1017*, 20-25.

38. Ota, R.; Yamada, K.; Suzuki, K.; Citterio, D., Quantitative evaluation of analyte transport on microfluidic paper-based analytical devices (μPADs). *Analyst* **2018,** *143* (3), 643-653.

39. Carrell, C.; Jang, I.; Link, J.; Terry, J. S.; Michael S, S.; Call, Z.; Panraksa, Y.; Dandy, D. S.; Geiss, B. J.; Henry, C. S., Point-of-Need Disposable ELISA System for COVID-19 Serology Testing. *ChemRxiv* **2021**.

40. Panraksa, Y.; Jang, I.; Carrell, C. S.; Amin, A. G.; Chailapakul, O.; Chatterjee, D.; Henry, C. S., Simple manipulation of enzyme-linked immunosorbent assay (ELISA) using an automated microfluidic interface. *Analytical Methods* **2022**.

41. Ramachandran, S.; Fu, E.; Lutz, B.; Yager, P., Long-term dry storage of an enzyme-based reagent system for ELISA in point-of-care devices. *Analyst* **2014,** *139* (6), 1456-1462.

42. Terry, J. S.; Anderson, L. B. R.; Scherman, M. S.; McAlister, C. E.; Perera, R.; Schountz, T.; Geiss, B. J., Development of a SARS-CoV-2 nucleocapsid specific monoclonal antibody. *Virology* **2021,** *558*, 28-37.

43. Boehle, K. E.; Doan, E.; Henry, S.; Beveridge, J. R.; Pallickara, Sangmi L.; Henry, C. S., Single board computing system for automated colorimetric analysis on low-cost analytical devices. *Analytical Methods* **2018,** *10* (44), 5282-5290.

44. FDA In Vitro Diagnostics EUAs. https://www.fda.gov/medical-devices/coronavirus-disease-2019-covid-19-emergency-use-authorizations-medical-devices/vitro-diagnostics-euas (accessed 02/27/2021).

45. Koczula, K. M.; Gallotta, A., Lateral flow assays. *Essays Biochem* **2016,** *60* (1), 111-120.

46. Sapkal, G.; Shete-Aich, A.; Jain, R.; Yadav, P. D.; Sarkale, P.; Lakra, R.; Baradkar, S.; Deshpande, G. R.; Mali, D.; Tilekar, B. N.; Majumdar, T.; Kaushal, H.; Gurav, Y.; Gupta, N.; Mohandas, S.; Deshpande, K.; Kaduskar, O.; Salve, M.; Patil, S.; Gaikwad, S.; Sugunan, A. P.;

Ashok, M.; Giri, S.; Shastri, J.; Abraham, P.; Gangakhedkar, R. R.; Covid Support Team: Pawar S, P. S. S. V. N. V. M. V. M. B. J. A. S. P. M. R. K. R. S. D. K., Development of indigenous IgG ELISA for the detection of anti-SARS-CoV-2 IgG. *Indian J Med Res* **2020,** *151* (5), 444-449.

47. Roy, V.; Fischinger, S.; Atyeo, C.; Slein, M.; Loos, C.; Balazs, A.; Luedemann, C.; Astudillo, M. G.; Yang, D.; Wesemann, D. R.; Charles, R.; Lafrate, A. J.; Feldman, J.; Hauser, B.; Caradonna, T.; Miller, T. E.; Murali, M. R.; Baden, L.; Nilles, E.; Ryan, E.; Lauffenburger, D.; Beltran, W. G.; Alter, G., SARS-CoV-2-specific ELISA development. *Journal of Immunological Methods* **2020,** *484-485*, 112832.

48. Hamidon, N. N.; Salentijn, G. I.; Verpoorte, E., Enhanced passive mixing for paper microfluidics. *RSC advances* **2021,** *11* (41), 25677-25685.

49. Cate, D. M.; Bishop, J. D.; Hsieh, H. V.; Glukhova, V. A.; Alonzo, L. F.; Hermansky, H. G.; Barrios-Lopez, B.; Grant, B. D.; Anderson, C. E.; Spencer, E.; Kuhn, S.; Gallagher, R.; Rivera, R.; Bennett, C.; Byrnes, S. A.; Connelly, J. T.; Dewan, P. K.; Boyle, D. S.; Weigl, B. H.; Nichols, K. P., Antibody Screening Results for Anti-Nucleocapsid Antibodies Toward the Development of a Lateral Flow Assay to Detect SARS-CoV-2 Nucleocapsid Protein. *ACS Omega* **2021,** *6* (39), 25116-25123.

50. Schomburg, D. S., M.; Stephan, D., *Enzyme Handbook 7*. Springer Berlin, Heidelberg: 1994.

51. Huang, S.; Abe, K.; Bennett, S.; Liang, T.; Ladd, P. D.; Yokobe, L.; Anderson, C. E.; Shah, K.; Bishop, J.; Purfield, M.; Kauffman, P. C.; Paul, S.; Welch, A. E.; Strelitz, B.; Follmer, K.; Pullar, K.; Sanchez-Erebia, L.; Gerth-Guyette, E.; Domingo, G.; Klein, E.; Englund, J. A.; Fu, E.; Yager, P., Disposable Autonomous Device for Swab-to-Result Diagnosis of Influenza. *Analytical Chemistry* **2017,** *89* (11), 5776-5783.

# CHAPTER 3: DEVELOPMENT OF A CAPILLARY DRIVEN IMMUNOASSY FOR PROOF-OF-CONCEPT WITH CHEMILUMINESCENT DETECTION OF SARS-CoV-2 NUCLEOCAPSID PROTEIN

## 3.1 Chapter Overview:

In Chapter 2, I described a simple, affordable capillary driven immunoassays for rapid diagnostic devices. However, previous examples are limited to either visual or electrochemical readouts. One quantification method that has been unexplored to this point is the use of chemiluminescent substrates for detection. Chemiluminescence has been widely used in ELISAs, Western Blots, and other bioassays. These assays often boast more sensitive detection limits over their absorbance or visual counterparts but remain complicated and time consuming. Incorporating chemiluminescent readouts in the capillary-driven immunoassay (CaDI) devices previously described in Chapter 2 could pair higher sensitivity with the simplicity of the CaDI devices. In this Chapter, I describe the development of a chemiluminescent immunoassay for SARS-CoV-2 nucleocapsid protein (N-protein) in the CaDI device described in Chapter 2. Assay development and optimization tools are described. After initial optimization, a detection limit of 865 pg/mL was ascertained for recombinant N-protein from SARS-CoV-2 using a benchtop chemiluminescent imager. To our knowledge, this is the first example of an affordable, rapid, and near POC chemiluminescent assay for the detection of SARS-CoV-2 nucleocapsid protein. This work was primarily conducted as a collaboration of Burst Diagnostics, Inc as a part of a 6-month industry internship. The work will be submitted for publication after the appropriate intellectual property protections are in place. I will be an author on the paper and the patent application.

## 3.2 Introduction:

Immunoassays are a common tool for the detection of biological markers since their inception in the late 1950s. Although dangerous due to its radioactivity, the first reported radiation-based immunoassay was used to detect insulin in serum in 1959.[1] Since then, much safer labels have been used in diagnostic assays. The use of capture and signal antibodies, both of which are highly specific to the target of interest, make them a selective and sensitive method. In place of a radioactive label on the signal antibody, researchers began using safer alternatives following the invention of immunoassay, including fluorescent labels,[2-3] electrochemical labels,[4] and enzyme labels.[4-6] A substrate specific to an enzyme-labeled signal antibody can be added to react with the enzyme, enhancing signal that can be produced if target is present. This method, known as an enzyme-linked immunosorbent assay (ELISA) is especially popular to researchers since lower limits of detection can be obtained through this enzyme/substrate reaction. While electrochemical and absorbance methods are possible with ELISAs, luminescent products are another popular option for highly sensitive detection.

During luminescence, electrons return to ground state from an excited state, emitting radiation as light typically in the wavelength range of $\lambda$ = 300-800 nm.[7-8] Chemiluminescence (CL) occurs when electrons are moved to an excited state as a result of a chemical reaction, meaning an external source of excitation is unnecessary like in fluorescence (**Figure 3.1**). The lack of an external source means that common issues such as light scattering or error in the excitation source can be avoided.[8] CL assays also benefit from direct measurement of the photons emitted as opposed to indirect methods such as absorbance. Because of these advantages, chemiluminescent labels and assays have been investigated since the early 1970s.[9]

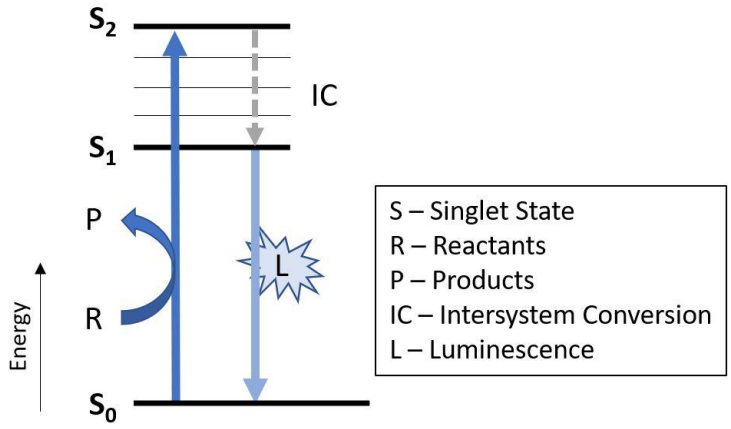


**Figure 3.1** A generic chemiluminescent Jablonski diagram is shown where the energy for electron citation is provided by a chemical reaction.

In recent years, CL assays seem to be primarily used for antibody detection and quantification for diagnostic purposes and medicine/vaccine development. These assays are highly specific and can be multiplexed, making them ideal for rapid screening of large panels of antibodies.[8, 10-11] In the previous decades, automated instrumentation has been created to capitalize on these advantages, making CL assays a powerful analytical tool.[12] While CL assays maintain the benefits of greater sensitivity, faster time-to-results than ELISAs, and automation, these benefits come with severe downsides. Large-scale instrumentation can cost >$100,000 for automated CL immunoassay systems.[13] Additionally, CL assays require trained technicians, multiple steps, and lab space, all of which increase cost further. These issues soften the appeal that comes from CL assay advantages. To maintain the advantages and mitigate the drawbacks, many attempts have been made to make the CL assay process more user-friendly.[14-17]

Lateral flow immunoassays are designed using a sequence of treated, fibrous membranes for sample and signal antibody delivery to a capture antibody.[18-20] Most lateral flow assays rely on gold nanoparticle labeled signal antibodies. An enzyme label would likely enhance signal produced, but washing steps would be required to reduce false positives from unbound signal

antibody. Devices that have been designed to make CL immunoassays more user-friendly still require multiple end-user steps after sample addition, and none have demonstrated effective on-device washing steps.[15-17]

Since CL assays have been heavily used in antibody detection and quantification for so long, it follows that many of the CL assays for SARS-CoV-2 antibodies and immune response was an appropriate application following the outbreak in late 2019.[21-23] By monitoring antibodies multiple antibodies for SARS-CoV-2 (IgG, IgM, and IgA), information can be gleaned about a patient's current state of infection and disease progression.[24] This information can assist in prognosis and treatment of patients, helping allocate hospital resources more effectively. Despite their power, antibody assays cannot diagnose active infection by themselves. The presence of antibodies against SARS-CoV-2 does indicate that a person has had the disease, but since it does not actively detect antigen or RNA form the virus, it can only indirectly indicate that an infection has occurred. Despite this, it seems as though very few CL assays for SARS-CoV-2 antigen have been developed, Therefore, PCR and ELISA remain the most popular methods for lab-based SARS-CoV-2 diagnostics.

For at-home diagnostics for SARS-CoV-2, the colloidal gold-nanoparticle lateral flow assay still dominates the field. These assays are much cheaper and are simple enough where the general public can operate and interpret results at home. In Chapter 2, I explain the advantages of the CaDI device over the traditional LFA. Briefly, the CaDI uses a simple microfluidic device to automate the steps of a well-plate ELISA from a single end-user step. This type of immunoassay, which typically takes dozens of pipetting steps and hours to complete, can be run in under 30 min on the CaDI system. Combining the benefits of the CaDI and a CL assay could potentially combine the advantages of both, namely, an even more sensitive assay on an affordable and rapid platform.

Despite the advantages of the CaDI device, assay development and proof of concept can still be time consuming and tedious. Reagent pad conditions, drying buffers, concentrations, and many other factors can influence the results on the NC membrane. Removing some of these variables would allow for a quicker screening of antibodies and assay feasibility. To this end, a single-channel device was developed in this work. Reagents for the sandwich immunoassay were pipetted individually to the reagent well, and the assay can be completed in 4 steps and 10 min.

Using the CaDI described in Chapter 2 of this thesis to provide sequential reagent delivery and washing steps, a fully automated CL immunoassay can be performed for SASRS-CoV-2 N-protein detection. Here, I present the use of a single-channel device used as an assay development tool. The single-channel device removes reagent pads, drying steps, and other variability that could influence the results on the NC. This device was used initially to show proof of concept for the CL assay on a NC membrane but could be used for rapid assay development for future targets. Once feasibility was shown on the single-channel device, the reagents used were dried on conjugate release pads and incorporated into the full CaDI device. The device can be operated in a single sample addition step, and images were capture with a benchtop CL imager. The CL CaDI assay conditions were optimized, and a quantitative limit of detection of 865 pg/mL N-protein was determined. This LOD is within the range found in the blood and saliva of clinically positive patients,[25-26] and we believe with further work and optimization, the LOD will continue to improve.

### 3.3 Materials and methods:

*Nitrocellulose preparation:*

Different 16x3 $mm^2$ nitrocellulose (NC) membranes (FF80HP Plus, FF120HP Plus, FF170HP Plus, Cytiva, Marlborough, MA, USA and Vivid90, Pall, NY, USA) were used for the assay. Capture antibody solution containing 0.88 mg/mL anti-SARS-CoV-2 nucleocapsid protein Ab (40143-MM08, Sino Biological, Beijing China), 0.44 M trehalose, and 4% glycerol was striped 5.5 mm from the top end of the strip using a BioSpot reagent printer (BioFluidix, Breisgau, Germany). A SARS-CoV-2 nucleocapsid protein solution containing 25 ng/mL NP (40143-V08B, Sino Biological), 50 mM NaCl, 1% glycerol, 0.8% trehalose, and 0.01% Tween80 was striped 5.5 mm from the bottom of the NC. The NC was then dried overnight in a desiccator at RT. The following day, the NC was blocked by allowing Stabilguard™ (SG01-1000, Surmodics Inc.) to wick through the NC from top to bottom in the direction that the device will flow once assembled. The NC was dried again at 37°C for 5 hrs, and yellow or red food dye diluted in DI water was striped 2 mm from the top and bottom of the NC respectively to ensure the NC is in the correct orientation when assembled in the device. The NC was lastly cut into 16x3 $mm^2$ strips.

*Single-channel immunoassay device assembly and operation:*

To quickly screen the intended antibody pair and CL reagent, a single-channel device was developed to simplify the reagent delivery process and remove any variability that may come from the full CaDI device. The single-channel device was assembled with 3 layers of transparency film (3M™ 9984, Saint Paul, MN, USA) and 2 layers of double-sided adhesive (3M™ 467MP). The layers were cut using a $CO_2$ laser (Epilog Zing, Golden, CO, USA) before assembling to create a 10.5x3 $mm^2$ channel and a reagent inlet of 5 mm Ø. A capture antibody solution of 0.88 mg/mL capture Ab (40143-MM08, Sino Biological) was made containing 4% glycerol and 44 mM trehalose. A 15x3 $mm^2$ nitrocellulose membrane (FF80HP Plus, Cytiva, Marlborough, MA, USA)

was spotted with 0.5 µL of capture antibody solution, pipetted by hand 0.25 µL at a time. The NC was dried at 37°C for 7 min between additions of capture antibody solution, and for an additional 30 min after the second addition. The membrane was blocked by allowing Stabilguard™ (SG01-1000, Surmodics Inc.) to wick through the membrane. The membrane was then dried again for 30 min at 37°C. The NC was then inserted into the single-channel device opposite from the reagent well. The NC was connected to a waste pad with an adhesive backing. A sample solution was made containing 0.5 µg/mL 2°Ab-HRP (40143-MM05-H, Sino Biological, Beijing, China), and 0, 1, 10, or 100 ng/mL of recombinant N-protein (40143-V08B, Sino Biological) in the "extraction buffer" descried in Chapter 1. To operate the device, 10 µL of sample solution was added to the reagent well. When the solution had completely drained through the NC membrane, 20 µL of blank extraction buffer was added to the well as a wash. After the wash buffer had drained, 10 µL of CL reagent (Pierce™ ECL Plus Western Blotting Substrate, ThermoFisher, Waltham, MA, USA) was added to the well. Within 30 s of adding the CL reagent, the device was placed into the CL imager, and an image was captured with a 5 s exposure. The device was removed, and an additional 20 µL of extraction buffer was added to wash. A second image was taken with 5 s exposure following the wash.

*Reagent pad preparation:*

Glass fiber (8980, Ahlstrom, Helsinki, Finland) was submerged in 1% PVP dissolved in 0.15 M PBS, pH 7.4, then dried overnight at 37°C. The blocked pads were then cut into 3x5 $mm^2$ rectangles. Varying volumes of different CL reagents (SuperSignal™ West Dura Extended Duration, 34075, ThermoFisher) were dried onto the CL reagent pad 7.5 µL at a time, drying for 8-10 min between each addition. After the final addition, the pads were dried for 2 hrs. The 2°Ab-

horseradish peroxidase (HRP) pads were blocked further with 15 µL of 0.5% aged casein[27] adding 7.5 µL at a time and allowing to dry for 30 min after the final addition. Once dry, 2°Ab-HRP (40143-MM05-H, Sino Biological) was diluted to 20 µg/mL in a drying buffer for long-term stability,[28] and 5 µL was added to each pad. The pads were then dried for 30 min at 37 °C before assembling in devices.

*CaDI Device assembly*:

The CaDI device assembly has been described in Chapter 2. Briefly, the patterns and dimensions are drawn in CorelDraw software (2017) and cut into alternating layers of polyester transparency film (3M™ 9984) and double-sided adhesive (3M™ 467MP) with a $CO_2$ laser cutter (Epilog Zing, Golden, CO, USA). The bottom four layers are then stacked and cold laminated to press the layers together. Before the top transparency film layer is added, the CL reagent pad and the 2°Ab-HRP pad are added to the device. The nitrocellulose test strip striped with capture antibody test line and NP control line are added to the outlet of the device. A waste pad (CFSP223000, MilliporeSigma Burlington, MA, USA) is pressed down on an adhesive backing to where it overlaps with the NC by 2 mm.

*Assay operation:*

Recombinant N-protein from SARS-CoV-2 (40143-V08B, Sino Biological) was diluted to varying concentrations in an extraction buffer made of 1.5x Pierce Stable Peroxide buffer (Thermo Fisher, 34062), 150 mM NaCl, 0.1% Tween-20, and 0.1% NP-40 at pH 6.5. After devices are assembled, 100 µL of sample is added to the sample inlet. The device is sealed within the CL camera assembly of the chemiluminescent imager (GE ImageQuant LAS 500). After waiting 15

min, images are captured every 30 s with 10 s exposures. The images are taken from that point until the signal begins to fade (typically around 30 min total).

*Image analysis:*

A series of images was captured every 30 s for each device from 15 min after sample addition until around 45 min. Each image in the series was uploaded to the free NIH software ImageJ and converted to 8-bit. A rectangular box was drawn around the test line (or where it would be in the case of a blank), and the integrated gray value of the surrounded pixels was gathered. For each device, the image with the highest mean gray value in the series was used in the analysis.

### 3.4 Results and Discussion:

Although the device function and operation is similar to that of the device in Chapter 2, the signal that is detected is light resulting of the chemical reaction of 5-amino-2,3-dihydro-1,4-phthalazinedione (luminol), $H_2O_2$, and HRP. Although the actual composition of the reagent used is proprietary, all of the CL reagents used are luminol based. The general luminol reaction is depicted in **Figure 3.2**. When in the presence of HRP and $H_2O_2$, luminol is oxidized, forming a peroxy intermediate, Double-bonded nitrogen makes an entropically favorable leaving group, so the electrons come back down to form carboxylate anions as $N_2$ gas is formed. This excited product is what emits energy as light as it relaxes to ground state.[29-31]

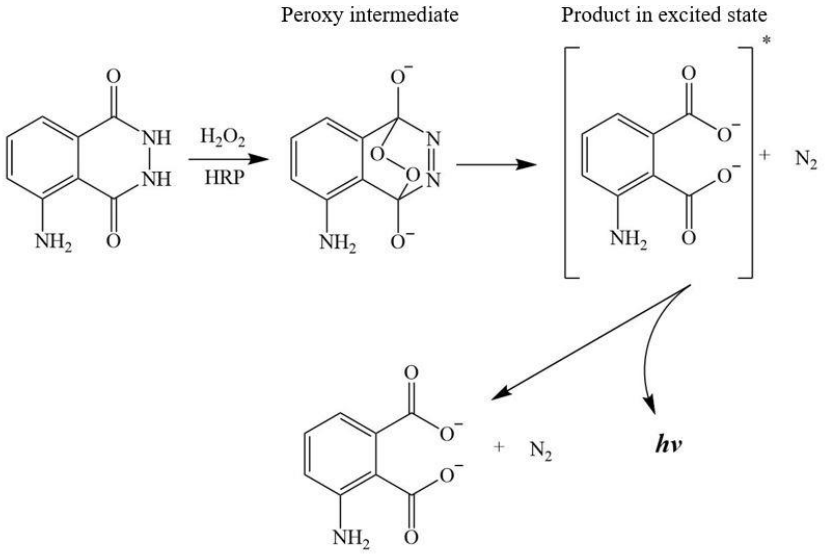


**Figure 3.2** The light producing reaction of HRP, $H_2O_2$, and luminol.

Since a CL sandwich immunoassay had not been performed in the CaDI before, we first wanted a way to ensure that the sandwich would form, and the CL reagent would react with HRP on the NC to generate signal. To test this, we developed a single-channel device that could be quickly assembled and tested to check the function of an assay. Because of its simplicity, this device (**Figure 3.3**) removes any variability or error that could be introduced by the full CaDI device, enabling faster screening of conditions. The device contains a single 10.5x3 $mm^2$ channel and a reagent well. Each step is added manually with a pipette, ensuring control over reagent delivery and timing. The channel and NC dimensions were selected to match the conditions in the full CaDI (**Figure 3.3A**).

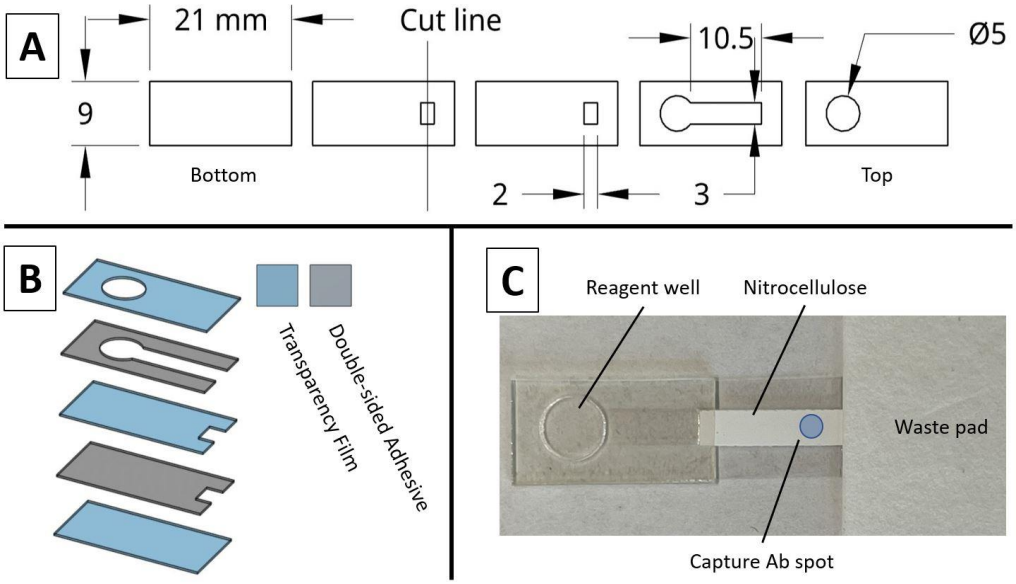


**Figure 3.3** (A) Dimensions for each layer of the single channel immunoassay device. (B) The cut layers of double-sided adhesive and transparency film are stacked to create a reagent addition well and a hollow channel. (C) Nitrocellulose with capture Ab connects the assembled device to a waste pad.

Recombinant N-protein and 2°Ab-HRP were mixed by pipetting before adding to the inlet on the device. By mixing before adding, the N-protein and 2°Ab-HRP can bind, and the sandwich immunoassay can be complete as the N-protein/2°Ab-HRP complex binds to the capture Ab on the NC. Excess target and 2°Ab-HRP are washed with extraction buffer before the CL reagent was added. An image was taken immediately after the CL reagent was added, and another was taken following the final wash step (**Figure 3.4**).

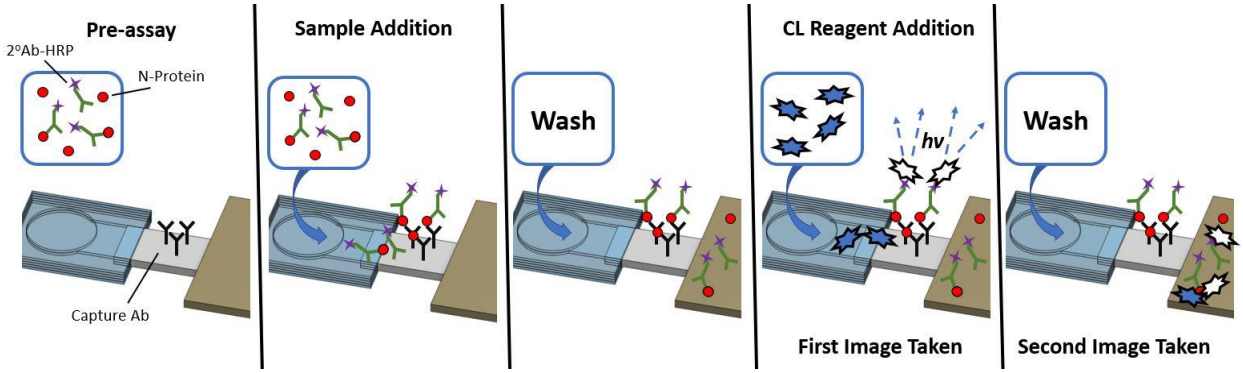


**Figure 3.4** The single-channel device is performed in 4 steps: sample addition, wash, CL reagent addition, and a second wash.

Using the single-channel device, a range of N-protein concentrations were test. With only a 5 s exposure time, signal was clearly visible for 100 ng/mL in the image immediately after the CL reagent was added. Each image was converted to 8-bit gray scale, contrast was adjusted (min 849, max 19000), a circular area around the test spot was selected in ImageJ. The average mean gray value for each test is plotted in **Figure 3.5.** Importantly, in contrast to the assay presented in Chapter 2, the product formed in this reaction is soluble, meaning it will be washed past the test spot after the final wash step. An example of this is shown for 100 ng/mL N-protein in **Figure 3.5B** where signal is no longer present at the test spot following a final wash step. Following the wash step, signal is no longer present at the test spot, and the signal coming from the waste pad is much higher (**Figure 3.5B**).

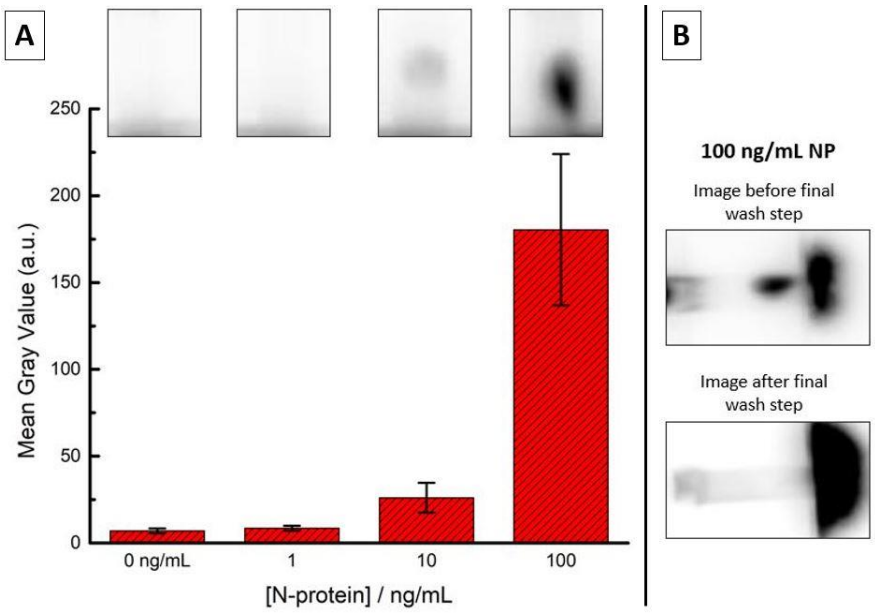


**Figure 3.5** (A) An initial test of the CL N-protein assay was performed on the single-channel devices. The images used in the plot were taken before the final wash step. (B) After the final wash step, a second image was taken. Following the wash, signal from the test spot is washed into the waste pad.

For this assay, the single-channel device was simply used to prove that the CL assay is possible with this antibody pair on NC membranes. However, the device present a powerful tool

for future assay development. Different antibody pairs, reagents, buffer conditions, and nitrocellulose types can rapidly screened using this device. This could help reduce time dedicated to troubleshooting in the full CaDI device and provide a helpful quaity assurance tool.

Following the initial studies in the single-channel device, we moved to the full CaDI device for the remaining experiments. The device operation and function are described in detail in Chapter 2 of this dissertation. Briefly, sample is added to the sample inlet of the device. The channels fill with sample passively via capillary action and rehydrate the 2°Ab-HRP and CL reagent dried on the conjugate release pads (**Figure 3.6**). Sample flows through the nitrocellulose, and target that may be present binds to the capture antibody. The reagents on the conjugate release pads are then sequentially delivered to the nitrocellulose via capillary action from the waste pad attached to the other end of the NC. The 2°Ab-HRP arrives first, binding to target that may be present at the test line, followed by a wash of buffer, and lastly the CL reagent. In the presence of HRP and $H_2O_2$ throughout the buffer, the luminol-based reagent produces detectable light.

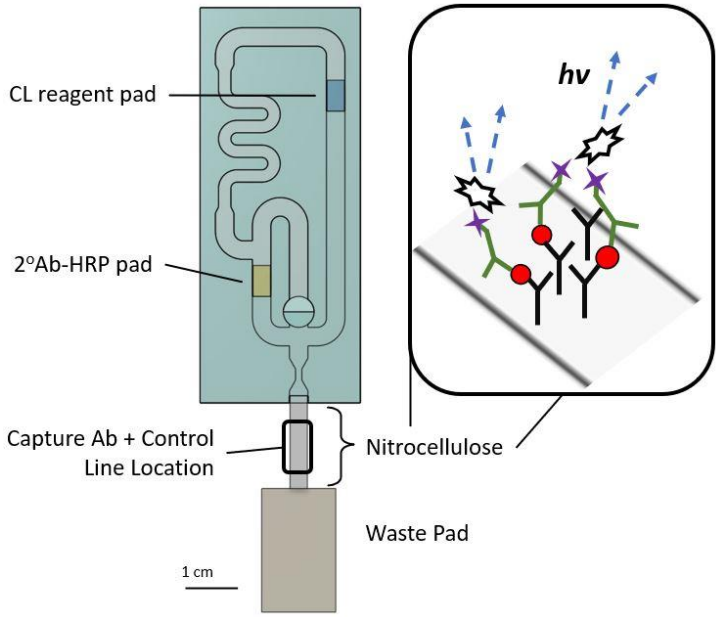

**Figure 3.6** The design and function of the CaDI device in this assay is similar to that of the device in Chapter 2. The main difference is the CL reagent pad, and the light emitted as a product of the assay.

To optimize the sensitivity of the assay in the full CaDI device, the flow rate of the device is crucial. Because the product of the luminol, $H_2O_2$, HRP reaction is soluble, consideration must be given to flow rate since solution is flowing through the NC for the entire assay. If the flow rate is too high, then the luminous product will travel past the test line in the time it takes the camera to capture an image. In that case, the test line will be smeared and not as densly concentrated. The simplest way to solve this problem would be to set a shorter exposure time; however, that would allow less light to enter the camera, lowering the sensitivity of the assay. Increasing the exposure time would allow more photons to enter the camera, but CL product would continue to run through the membrane while the shutter is open. Therefore, longer exposure times would lead to blury or smeared test lines. The flow rate through the NC membrane can affect how far the signal can diffuse/flow while the camera's shutter is open. Altering the flow rate in the device can be accomplished by simply changing the nitrocellulose material used. Four different NC types (FF80, FF120, FF170 and Viv90) with four different flow rate ranges from the manufacturers (40-67, 27-44, 20-29, and 36-57 mm/s respectively) were striped with capture antibody and wre run in device with 10 ng/mL N-protein. Since the devices were staggered to start, the image with the most intense signal as used for each test line was used process the data. An example of this image capture and data collection can be found in Figure A2.1. Despite having the slowest flow rate of the four, signal was weak in comparison to other NC types (**Figure 3.7A)**. Because flow is slowest through the NC, evaporation over the conjugate release pads can drive flow in their direction as well as through the NC. This causes the CL reagent to be pulled towards the 2$^o$Ab-HRP pad, preventing it from producing signal at the test line. This phenomenon was also seen in food dye flow experiments

done in the CaDI devices (Figure A2.2). The two fastest NC membranes (FF80 and Viv90) also perfomed poorly compared to FF120 (**Figure 3.7A**).

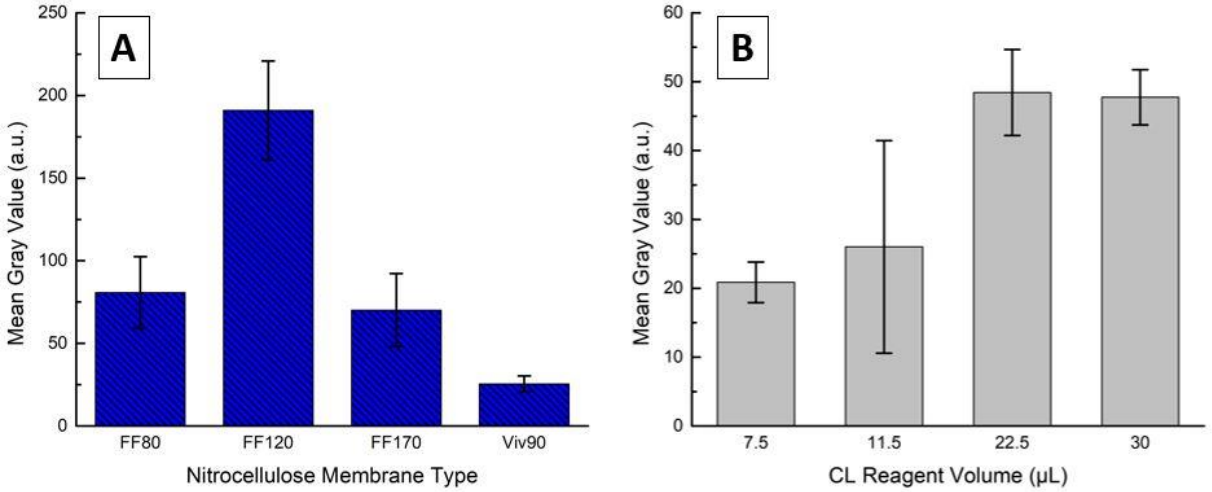


**Figure 3.7** (A) The type of NC membrane was varried and devices were run at 10 ng/mL NP. Devices were run in tripplicate, but 1 Viv90 device failed (did not flow, no control line), so the data for that NC type is n=2. (B) The CL reagent volume was varried and devices were run in tripplicate with 10 ng/mL N-protein.

The concentration of 2°Ab HRP had been optimized in Chapter 2, but the volume of CL reagent used still needed to be selected. Devices were run in triplicate with 10 ng/mL N-protein varying the CL reagent volume (**Figure 3.6B**). There was no statistical difference between the signal from 22.5 µL and 30 µL of CL reagent, so 22.5 µL was chosen to reduce the overall cost of the assay and to help prevent possible false positives from an excress of CL reagent.

With the optimzied conditions, a dose response cuve was gathered with recombinant N-protein spiked into extraction buffer at varying concentrations. The four points and a blank were fit to a four parameter logistic regression.[32] Although more points on the curve would be ideal, the fit of the curve is still acceptable with an $R^2$ value of 0.987 (**Figure 3.8**).

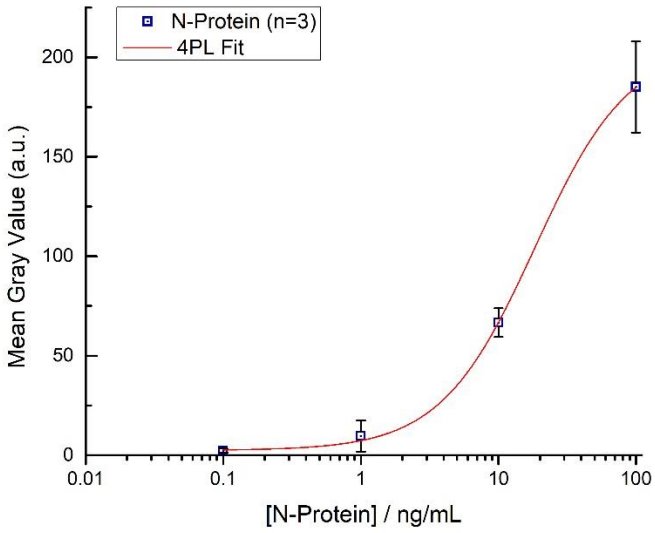


**Figure 3.8** A dose response curve for N-protein was gathered with 5 points, including a blank, n=3 for each point. The $R^2$ value is 0.987, and the LOD is 865 pg/mL.

The equation for a four parameter logistic regression is (eq. 3.1) was used to calculate the LOD, where *y* is the mean gray value, *x* is the concentration of N-protein, *a* is the thoretical limit for a blank sample, *d* is the theoretical limit with unlimited N-protein, *b* is a slope factor, and *c* is the inflection point.

$$y = d + \frac{a - d}{\left[1 + \left(\frac{x}{c}\right)^{b}\right]} \qquad (3.1)$$

$$y_{LOD} = y_B + (3 * \sigma_B) \qquad (3.2)$$

The LOD is the concentration (*x*) at $y_{LOD}$ found from eq. 3.2, where $y_{LOD}$ is the *y* value three standard deviation of the blank ($\sigma_B$) greater than the average blank signal ($y_B$). Rearranging eq. 3.1 to solve for *x*, yields eq. 3.3.

$$LOD = c\left[\left(\frac{a-d}{y_{LOD}-d}\right)-1\right]^{1/b} \quad (3.3)$$

Using eq. 3.1-3, we determined a LOD of 865 pg/mL for this assay. It is difficult to find a comparison for this LOD in the literature.

Many papers published on SARS-CoV-2 detection use the meadia tissue culture infectious dose ($TCID_{50}$) or plaque-forming uints (PFU) to quantify their results.[33-35] The use of these metrics for quantification is standard practice, but they are both indirect methods of quantification, not direct measurements of number of virus particles or protein. $TCID_{50}$ measures the median virus dilution required to infect 50% of a cell culture.[36] $TCID_{50}$ can predict a virus's infectivity, but a conversion to concentration of total viral particles or protein (like N-protein) would require many major assumptions. Similarly, PFU is the number of virus particles capable of forming plaques when plated.[37] This measurement helps determine the number of viable virus particles in a given sample but leaves out non-viable virus. A direct conversion from PFU/mL to concentration of a protein or total virus particles would skew the results. Some data has been collected that shows the concentration of N-protein can range from 3-4000 pg/mL in serum, and from 1-10,000 pg/mL in saliva for patients infected with SARS-CoV-2.[25-26] Although this CL detection study was performed in buffer, the limit of detection is well below some of the highest N-protein values detected in positive patients. With further optimization, we believe our limit of detection could significantly improve and continue to perform well when used in more complex samples.

### 3.5 Conclusion:

This chapter describes the assay development and proof of concept for a CL assay for the detection of SARS-CoV-2 N-protein. The single-channel device was used to assess assay

feasability, and can be used in the future to decrease assay development time and effort. The single-channel device has been used in other assays to screen antibody pairs, reagent conditions, and troubleshoot nitrocellulose conditions (data not shown). Once the CL assay was shown to work in the single-channel device, the reagents used in that assay were dried on conjugte release pads and incorportaed into the full CaDI device. The device operates from a single sample addition step, and fully automates the steps required for a sandwich CL immunoassay. With this assay, a LOD of 865 pg/mL was found for N-protein diluted in buffer. This detection limit is within the range of N-protein found in the blood and saliva of SARS-CoV-2 infected patients, but with further optimization, longer exposure times for imaging, and better instrumentation, we believe the LOD will continue to improve. Future work will focus on adjusting the deivce to handle more complex, clinical samples. For example, on device filtering may be necessary for saliva or nasopharyngeal swab samples. Multiplexed analysis may also be explored to improve the value of this diagnostic tool.

## CHAPTER 3 CITATIONS


1. Yalow, R. S.; Berson, S. A., Immunoassay of endogenous plasma insulin in man. *J Clin Invest* **1960,** *39* (7), 1157-75.

2. Hemmilä, I., Fluoroimmunoassays and immunofluorometric assays. *Clinical Chemistry* **1985,** *31* (3), 359-370.

3. Rizzo, F., Optical Immunoassays Methods in Protein Analysis: An Overview. *Chemosensors* **2022,** *10* (8), 326.

4. Darwish, I. A., Immunoassay Methods and their Applications in Pharmaceutical Analysis: Basic Methodology and Recent Advances. *International journal of biomedical science : IJBS* **2006,** *2* (3), 217-35.

5. Davies, C., Chapter 2.1 - Principles of Competitive and Immunometric Assays (Including ELISA)1. In *The Immunoassay Handbook (Fourth Edition)*, Wild, D., Ed. Elsevier: Oxford, 2013; pp 29-59.

6. Aydin, S., A short history, principles, and types of ELISA, and our laboratory experience with peptide/protein analyses using ELISA. *Peptides* **2015,** *72*, 4-15.

7. Cinquanta, L.; Fontana, D. E.; Bizzaro, N., Chemiluminescent immunoassay technology: what does it change in autoantibody detection? *Auto- immunity highlights* **2017,** *8* (1), 9.

8. Dodeigne, C.; Thunus, L.; Lejeune, R., Chemiluminescence as diagnostic tool. A review. *Talanta* **2000,** *51* (3), 415-439.

9. Kricka, L. J., 15 - CHEMILUMINESCENCE IMMUNOASSAY. In *Immunoassay*, Diamandis, E. P.; Christopoulos, T. K., Eds. Academic Press: San Diego, 1996; pp 337-353.

10. Mahler, M.; Bentow, C.; Serra, J.; Fritzler, M. J., Detection of autoantibodies using chemiluminescence technologies. *Immunopharmacology and Immunotoxicology* **2016,** *38* (1), 14-20.

11. Espejo, A. P.; Akgun, Y.; Al Mana, A. F.; Tjendra, Y.; Millan, N. C.; Gomez-Fernandez, C.; Cray, C., Review of Current Advances in Serologic Testing for COVID-19. *American Journal of Clinical Pathology* **2020,** *154* (3), 293-304.

12. Zhao, L.; Sun, L.; Chu, X., Chemiluminescence immunoassay. *TrAC Trends in Analytical Chemistry* **2009,** *28* (4), 404-415.

13. Beckman Coulter UniCel DxI 600 Access Immunoassay System. https://www.allstatesmed.com/products/beckman-coulter-unicel-dxi-600-access-immunoassay-system?variant=31917317128269&currency=USD&utm_medium=product_sync&utm_source=google&utm_content=sag_organic&utm_campaign=sag_organic&_vsrefdom=googleads&gclid=CjwKCAiAjPyfBhBMEiwAB2CCImR_15nJzvmDbOlIHjC0E3u8ZyZqO1EKNdazqwuVUn_exvCJJPe4mBoCod8QAvD_BwE.

14. Zangheri, M.; Di Nardo, F.; Mirasoli, M.; Anfossi, L.; Nascetti, A.; Caputo, D.; De Cesare, G.; Guardigli, M.; Baggiani, C.; Roda, A., Chemiluminescence lateral flow immunoassay cartridge with integrated amorphous silicon photosensors array for human serum albumin detection in urine samples. *Analytical and Bioanalytical Chemistry* **2016,** *408* (30), 8869-8879.

15. Park, J.-M.; Jung, H.-W.; Chang, Y. W.; Kim, H.-S.; Kang, M.-J.; Pyun, J.-C., Chemiluminescence lateral flow immunoassay based on Pt nanoparticle with peroxidase activity. *Analytica Chimica Acta* **2015,** *853*, 360-367.

16. Zangheri, M.; Cevenini, L.; Anfossi, L.; Baggiani, C.; Simoni, P.; Di Nardo, F.; Roda, A., A simple and compact smartphone accessory for quantitative chemiluminescence-based lateral flow immunoassay for salivary cortisol detection. *Biosensors and Bioelectronics* **2015,** *64*, 63-68.

17. Deng, J.; Yang, M.; Wu, J.; Zhang, W.; Jiang, X., A Self-Contained Chemiluminescent Lateral Flow Assay for Point-of-Care Testing. *Analytical Chemistry* **2018,** *90* (15), 9132-9137.

18. Parolo, C.; Sena-Torralba, A.; Bergua, J. F.; Calucho, E.; Fuentes-Chust, C.; Hu, L.; Rivas, L.; Álvarez-Diduk, R.; Nguyen, E. P.; Cinti, S.; Quesada-González, D.; Merkoçi, A., Tutorial: design and fabrication of nanoparticle-based lateral-flow immunoassays. *Nature Protocols* **2020,** *15* (12), 3788-3816.

19. Sena-Torralba, A.; Álvarez-Diduk, R.; Parolo, C.; Piper, A.; Merkoçi, A., Toward Next Generation Lateral Flow Assays: Integration of Nanomaterials. *Chemical Reviews* **2022,** *122* (18), 14881-14910.

20. Carrell, C.; Kava, A.; Nguyen, M.; Menger, R.; Munshi, Z.; Call, Z.; Nussbaum, M.; Henry, C., Beyond the lateral flow assay: A review of paper-based microfluidics. *Microelectronic Engineering* **2019,** *206*, 45-54.

21. Liu, B.; Su, X.; Yu, G.; Yang, S.; Wang, F.; Huang, T.; Zhou, L.; Hui, Z.; Liao, Y.; Qiu, Y.; Huang, J.; Gao, H.; Liu, J.; Zhong, Y., An automated chemiluminescent immunoassay (CLIA) detects SARS-CoV-2 neutralizing antibody levels in COVID-19 patients and vaccinees. *International Journal of Infectious Diseases* **2022,** *115*, 116-125.

22. Horn, M. P.; Jonsdottir, H. R.; Brigger, D.; Damonti, L.; Suter-Riniker, F.; Endrich, O.; Froehlich, T. K.; Fiedler, M.; Largiadèr, C. R.; Marschall, J.; Weber, B.; Eggel, A.; Nagler, M.,

Serological testing for SARS-CoV-2 antibodies in clinical practice: A comparative diagnostic accuracy study. *Allergy* **2022,** *77* (7), 2090-2103.

23. Weber, M. C.; Risch, M.; Thiel, S. L.; Grossmann, K.; Nigg, S.; Wohlwend, N.; Lung, T.; Hillmann, D.; Ritzler, M.; Ferrara, F.; Bigler, S.; Egli, K.; Bodmer, T.; Imperiali, M.; Salimi, Y.; Fleisch, F.; Cusini, A.; Heer, S.; Renz, H.; Paprotny, M.; Kohler, P.; Vernazza, P.; Risch, L.; Kahlert, C. R., Characteristics of Three Different Chemiluminescence Assays for Testing for SARS-CoV-2 Antibodies. *Disease Markers* **2021,** *2021*, 8810196.

24. Grossberg, A. N.; Koza, L. A.; Ledreux, A.; Prusmack, C.; Krishnamurthy, H. K.; Jayaraman, V.; Granholm, A.-C.; Linseman, D. A., A multiplex chemiluminescent immunoassay for serological profiling of COVID-19-positive symptomatic and asymptomatic patients. *Nature Communications* **2021,** *12* (1), 740.

25. Zhang, Y.; Ong, C. M.; Yun, C.; Mo, W.; Whitman, J. D.; Lynch, K. L.; Wu, A. H. B., Diagnostic Value of Nucleocapsid Protein in Blood for SARS-CoV-2 Infection. *Clin Chem* **2021,** *68* (1), 240-248.

26. Shan, D.; Johnson, J. M.; Fernandes, S. C.; Suib, H.; Hwang, S.; Wuelfing, D.; Mendes, M.; Holdridge, M.; Burke, E. M.; Beauregard, K.; Zhang, Y.; Cleary, M.; Xu, S.; Yao, X.; Patel, P. P.; Plavina, T.; Wilson, D. H.; Chang, L.; Kaiser, K. M.; Nattermann, J.; Schmidt, S. V.; Latz, E.; Hrusovsky, K.; Mattoon, D.; Ball, A. J., N-protein presents early in blood, dried blood and saliva during asymptomatic and symptomatic SARS-CoV-2 infection. *Nature Communications* **2021,** *12* (1), 1931.

27. Grant, B. D.; Anderson, C. E.; Williford, J. R.; Alonzo, L. F.; Glukhova, V. A.; Boyle, D. S.; Weigl, B. H.; Nichols, K. P., SARS-CoV-2 Coronavirus Nucleocapsid Antigen-Detecting

Half-Strip Lateral Flow Assay Toward the Development of Point of Care Tests Using Commercially Available Reagents. *Analytical chemistry* **2020,** *92* (16), 11305-11309.

28. Ramachandran, S.; Fu, E.; Lutz, B.; Yager, P., Long-term dry storage of an enzyme-based reagent system for ELISA in point-of-care devices. *Analyst* **2014,** *139* (6), 1456-1462.

29. Kim, H.-S.; Pyun, J.-C., Hyper Sensitive Strip Test with Chemi-luminescence Signal Band. *Procedia Chemistry* **2009,** *1* (1), 1043-1046.

30. Villaverde, A.; Netherton, J.; Baker, M. A., From Past to Present: The Link Between Reactive Oxygen Species in Sperm and Male Infertility. *Antioxidants (Basel, Switzerland)* **2019,** *8* (12).

31. Kazemi, S. Y.; Abedirad, S. M., Effect of human and bovine serum albumin on kinetic chemiluminescence of Mn (III)-Tetrakis (4-sulfonatophenyl) porphyrin-luminol-hydrogen peroxide system. *TheScientificWorldJournal* **2012,** *2012*, 913412.

32. Dunn, J.; Wild, D., Chapter 3.6 - Calibration Curve Fitting. In *The Immunoassay Handbook (Fourth Edition)*, Wild, D., Ed. Elsevier: Oxford, 2013; pp 323-336.

33. Bullen, C. K.; Davis, S. L.; Looney, M. M., Quantification of Infectious SARS-CoV-2 by the 50% Tissue Culture Infectious Dose Endpoint Dilution Assay. *Methods Mol Biol* **2022,** *2452*, 131-146.

34. Uhteg, K.; Jarrett, J.; Richards, M.; Howard, C.; Morehead, E.; Geahr, M.; Gluck, L.; Hanlon, A.; Ellis, B.; Kaur, H.; Simner, P.; Carroll, K. C.; Mostafa, H. H., Comparing the analytical performance of three SARS-CoV-2 molecular diagnostic assays. *Journal of clinical virology : the official publication of the Pan American Society for Clinical Virology* **2020,** *127*, 104384.

35. Fukuta, M.; Mao, Z. Q.; Morita, K.; Moi, M. L., Stability and Infectivity of SARS-CoV-2 and Viral RNA in Water, Commercial Beverages, and Bodily Fluids. *Front Microbiol* **2021,** *12*.

36. Lei, C.; Yang, J.; Hu, J.; Sun, X., On the Calculation of TCID(50) for Quantitation of Virus Infectivity. *Virologica Sinica* **2021,** *36* (1), 141-144.

37. Lin, Y.-C.; Malott, R. J.; Ward, L.; Kiplagat, L.; Pabbaraju, K.; Gill, K.; Berenger, B. M.; Hu, J.; Fonseca, K.; Noyce, R. S.; Louie, T.; Evans, D. H.; Conly, J. M., Detection and quantification of infectious severe acute respiratory coronavirus-2 in diverse clinical and environmental samples. *Scientific Reports* **2022,** *12* (1), 5418.

# CHAPTER 4: MULTIPLEXED CAPILLARY-FLOW IMMUNOASSAY

## 4.1 Chapter Overview:

Multiplexed analysis in medical diagnostics is widely accepted as a more thorough and complete method compared to single analyte detection. While analytical methods like PCR and ELISA exist for multiplexed detection of biomarkers, they remain time consuming and expensive. Lateral flow assays (LFAs) are an attractive option for point-of-care testing, and examples of multiplexed LFAs exist. However, these devices are limited by spatial resolution of test lines, large sample volumes, cross-reactivity, and poor sensitivity. Recent work by the Henry lab has developed capillary-flow microfluidic ELISA platforms as a more sensitive alternative to LFAs, however, multiplexed detection on these types of devices has yet to be demonstrated. In the aftermath of the initial SARS-CoV-2 pandemic, the need for rapid, sensitive point of care devices has become apparent. Moving forward, devices that can distinguish between diseases with similar presenting symptoms would be the ideal home diagnostic. In this chapter, I present the first example of a multiplexed capillary-flow immunoassay device for the simultaneous detection of multiple biomarkers. From a single sample addition step, the reagents and washing steps required for two simultaneous ELISAs are delivered to spatially separated test strips. Visual results can be obtained in <15 min, and images captured with a smartphone can be captured for quantitative data. This device was used to distinguish between and quantify H1N1 hemagglutinin (HA) and SARS-CoV-2 nucleocapsid protein (N-protein). Using this device, analytical detection limits of 840 pg/mL was gathered for hemagglutinin, and 133 pg/mL for nucleocapsid protein. The presence of one target in the device did not increase the signal on the other test line, indicating no cross reactivity between the assays. Additionally, simultaneous detection of both N-protein and HA was

performed as well as simultaneous detection of N-protein and human C-reactive protein (CRP). While simultaneous detection of SARS-CoV-2 and H1N1 might rarely be necessary, simultaneous detection of two biomarkers in an automated ELISA device has never been shown in the literature. Elevated levels of C-reactive protein in a patient infected with SARS-CoV-2 has been shown to correlate with more severe patient outcomes. To further expand on simultaneous detection of two biomarkers, CRP and N-protein were also detected simultaneously. This work was conducted by myself with lab assistance by two undergraduate research assistants. The data in this chapter will be submitted to the journal, Analytical Chemistry, in the near-term future.

## 4.2 Introduction:

The results of medical testing influences accurate diagnosis, prognosis, treatment, and timely discharge of patients from a medical facility. It follows that early and affordable diagnosis is a crucial part of the treatment process. The sooner a patient with chronic illnesses like cancer or Alzheimer's can be diagnosed, the more effectively the diseases can be slowed, halted, or prevented.[1-3] Rapid testing for communicable diseases is also crucial for patient outcome. The need for reliable testing has been a theme for decades, and the world seems to get a grim reminder of this need every few decades with new or reemerging infectious diseases. In recent history, HIV/AIDS in the 1980's to present,[4-5] SARS-CoV in the early 2000s,[6] H1N1 in the 2009,[7] and SARS-CoV-2 in early 2019 have posed great stress to diagnostic infrastructure in place. In both cases, communicable or non-communicable, diagnostics that can detect multiple targets are preferred to systems that can only detect one.

One of the most common ways to detect biological targets is enzyme-linked immunosorbent assays (ELISAs). Laboratory-based ELISAs are performed in 96-well microtiter

plates. In this format, wells can be coated with a variety of capture proteins or antibodies. This spatial separation makes them ideal tools for multiplexing biological assays.[8] Unfortunately, ELISAs are time consuming, requiring multiple pipetting steps and trained personnel to perform. These drawbacks hinder the ability for regular testing to occur, making it difficult to diagnose and treat patients. Rapid, onsite or point of care (POC) testing is especially important in rural and resource limited setting where a patient may have difficulty traveling to and from medical facilities.[9-10]

Point of care (POC) testing is an attractive alternative to traditional medical diagnostics in many ways. Reliable POC tests allow for faster time-to-results, more affordable and regular testing, and the opportunity for home testing and personalized medicine. In recent years, lateral flow assays (LFAs) have been a popular solution to POC diagnostics. LFAs consist of a series of membranes containing different reagents required for a sandwich immunoassay to occur from a single sample addition with a gold nanoparticle-based readout.[11] LFAs can be used to assess environmental contaminants,[12] food safety,[13-15] and disease biomarkers.[14, 16-17] There has also been considerable effort in developing multiplexed LFA devices. The simplest approach to multiplex LFAs (xLFAs) is adding multiple test lines to a single test strip.[13, 18-20] This allows for multiple targets to be captured and screened in a single strip, but spatial constraints limit the number of analytes that can be targeted. Mathematical modeling has shown that test lines should be at least 2 mm apart for good detection.[21] Extending the length of the test strip membrane could increase room for additional test lines, but assay time would increase exponentially according to the Lucas-Washburn equation.[22-23] Microarrays of test spots offer another alternative for increasing the number of detection zones, but spatial resolution and cross-reactivity between signal and capture antibodies may still pose issues.[24-26] Spatially separating multiple test strip membranes reduces the

number of test line/targets per membrane. Successful devices have been designed where 10 individual LFA test strips radiate around a single sample inlet.[15, 27] This removes the possibility of cross-reactivity between antibody pairs and spatially separates test lines, but increases the total sample volume required to operate. Another example of multiple test strips on a single device comes from *Han et. al.* In their work, stacked paper channels controls sample and enhancer delivery to two separate test strips with three total test lines. This device sequentially delivers gold nanoparticle conjugated signal antibodies followed by an enhancer solution.[28] While this delivery method is impressive, it does not allow for washing between steps, a highly desirable step for other applications like paper-based ELISAs.

Paper-based ELISA has been used for more than a decade in various ways.[29-30] The simplest version of a paper-based ELISA replaces a 96 well plate with wax patterned paper microwells.[29] While using paper may cut costs and improve portability, the manual pipetting steps required for this type of paper-based ELISA are still tedious. Several attempts have been made to simplify or automate the sample addition, washing, and regent delivery steps associated with an ELISA with the goal of making them more user friendly.[31-33] While these examples are simpler than traditional ELISAs, they still require multiple steps after sample addition, disqualifying them as an ideal POC device. The Henry group has developed multiple automated, capillary driven immunoassay devices that fully automate sample delivery, washing, and reagent delivery steps to test strips, but multiplexing on these devices has yet to be shown, remaining an elusive future goal.[34-36]

In this work, I describe a capillary-driven device that passively delivers the reagent and washing steps associated with an ELISA to two, spatially separated test strips in under 15 min

from a single sample addition step. The device uses horseradish peroxidase (HRP) as a signal enzyme, and 3,3',5,5'-tetramethylbenzydine (TMB) as the amplification substrate. The device is assembled from inexpensive double-sided adhesive and transparency film to create the microfluidic front end that leads to two nitrocellulose test strips. The channels of the device are oriented in such a way that, after sample addition, sample, signal antibody, wash steps, and substrate are delivered to two separate test strips simultaneously. The device is also designed so that reagents for one target will never interact with reagents from on the other side of the device. This separation prevents cross reactivity that may occur between capture and signal antibodies from the other assay.

Multiplexed detection was shown in two motifs. The first demonstrates the device's ability to distinguish between two conditions. For this example of multiplexed detection, the device was used to distinguish between H1N1 and SARS-CoV-2 infections from a single sample. These two are of special interest because many of their symptoms (fever, muscle soreness, cough, headaches, etc.) mimic one another, making it difficult to distinguish between the two solely on the symptoms a patient presents.[37] The device was optimized to detect hemagglutinin from H1N1 on one test strip, and nucleocapsid protein (N-protein) from SARS-CoV-2 on the other. Initial optimization for the H1N1 assay was performed on a single-channel device that was developed in Chapter 2 of this dissertation. Once conditions were chosen, dose response curves were generated for H1N1 hemagglutinin and SARS-CoV-2 nucleocapsid protein (N-protein) were performed on the multiplex device with detection limits of 840 pg/mL and 133 pg/mL respectively. The amount of SARS-CoV-2 N-protein found in blood and saliva from positive patients ranges from 1 - $1x10^5$ pg/mL during the first two weeks after infection; our device is well within that range.[38] Although it is difficult to determine hemagglutinin concentration in positive patients (most studies use

PFU/mL or $TCID_{50}$), other similar POC devices claim LODs of 0.23-29 ng/mL[39-41] To show the devices function in complex sample matrix, devices were run in nasal swabs spiked with varying concentrations of N-protein or HA. Results for our device can be read visually in under 15 min and can be quantified with a smartphone.

The second motif of multiplexed detection is simultaneous detection of two targets. To demonstrate this type of multiplexed detection, two examples are shown. Although the likelihood of a patient being infected with both H1N1 and SARS-CoV-2 are small, devices were run with 5 and 100 ng/mL of both N-protein and HA simultaneously to show proof of concept for simultaneous detection of two target analytes. To further demonstrate this concept, N-protein from inactivated SARS-CoV-2 virus and C-reactive protein (CRP) were also detected simultaneously. Elevated levels of CRP have been found in patients infected with SARS-CoV-2.[42-43] Subsequently, it has been suggested that elevated levels of CRP could be used as a predictor for the severity of a patient's condition.[44] Therefore, simultaneously detecting a SARS-CoV-2 infection and quantifying the amount of CRP in the same sample may be useful to the decision making of healthcare providers. The multiplexed device in this work was run with 1100 PFU/mL of inactivated SARS-CoV-2 and 100 ng/mL of CRP simultaneously, and signal on both test strips was visible in under 15 min.

### 4.3 Materials and Methods:

*Nitrocellulose test strip preparation:*

Nitrocellulose (NC) membranes (Vivid 90 LFNC, Pall, NY, USA) were striped with capture and control antibodies for each assay. For the N-protein test strips, 0.88 mg/mL capture antibody (40143-MM08, Sino Biological, Beijing China) and goat anti-mouse control line

antibody (AB6708, Abcam, Cambridge UK) were striped using a BioSpot reagent printer (BioFluidix, Breisgau, Germany). For the HA test strips, 0.88 mg/mL capture antibody (11055-RM10, Sino Biological) and goat anti-rabbit control line antibody (R1131, Millipore Sigma, Burlington MA, USA) were striped. For the CRP test strips, 0.88 mg/mL capture antibody (PAB7943, Abnova, Taipei, Taiwan) and a CRP (30-AC05S, Fitzgerald, Acton MA, USA) control line was striped. All test line and control line solutions also contained 4% glycerol and 4 mM trehalose for improved drying and longevity. All NC membranes were dried overnight in a desiccator before blocking with Stabilguard™ (SG01-1000, Surmodics Inc.) to prevent non-specific adsorption to the membrane during the assay. The NC membranes were then cut into 15x3 $mm^2$ individual test strips using a $CO_2$ laser cutter (Epilog Zing, Golden, CO, USA). NC membranes then was stored at 4 ºC before until used.

*Reagent pad preparation:*

Glass fiber pads (GFDX203000, MilliporeSigma Burlington, MA, USA) were used for both TMB and secondary antibody-HRP (2ºAb-HRP) pads, but the pretreatment/blocking conditions for each were slightly different. For TMB pad, glass fiber sheets were completely submerged in a blocking solution containing 10 mM PBS (Thermo Scientific, Rockford, IL, USA), 3% sucrose, 0.5% Tween-20, and 0.1% thimerosal (MilliporeSigma) for 15 min. The sheets were removed from the solution and dried overnight at 37 ºC before use. The dried, blocked membranes were then cut into 3 x 5 $mm^2$ reagent pads with a razor blade. TMB (TMBM-0100-01, Surmodics Inc., Eden Prairie, MN, USA) was pipetted onto the pads in 7.5 µL aliquots, drying for 7-8 min between additions. After the final TMB addition, the pads were dried for 2 hr before assembling in the microfluidic device. For 2ºAb-HRP pads, blank glass fiber membranes were cut into 3 x 5

$mm^2$ reagent pads before any pretreatment. "Aged casein" was prepared following the procedures outlined in work from *Grant et. al.*[45] The aged casein was diluted to 0.5% in 10 mM PBS, and 15 µL was added to each 2°Ab-HRP pad, 7.5 µL at a time. The pads were dried for 7-8 minutes at 37°C between additions, and for an additional 30 minutes after the second. 2°Ab-HRP for the N-protein assay (40143-MM05-H, Sino Biological) and the HA assay (11055-RP07, Sino Biological) were diluted in a drying buffer designed for long-term stability.[46] 5 µL of each diluted 2°Ab-HRP was added to separate treated pads and dried for 30 minutes at 37°C before adding to the device. For the CRP assay, 200 µg/mL of 2°Ab conjugated to biotin (MAB5101, Abnova) was mixed 1:1 with 200 µg/mL streptavidin conjugated HRP (21123, Thermo Fisher Scientific). The resulting solution was then diluted in a ratio of 1:5 in drying buffer, and 5 µL was added to treated glass fiber pads and dried for 30 min.

*Device assembly*:

Patterns for the device channels were designed in the CAD program, OnShape, and cut into alternating layers of transparency film (3M™ 9984, Saint Paul, MN, USA) and double-sided adhesive (3M™ 467MP, Saint Paul, MN, USA) with a $CO_2$ laser cutter (**Figure 4.1A and 4.1B**). The first four layers of the device were assembled before the conjugate release pads were added. The final layer of transparency film was added last, completing the hollow channels and securing the conjugate release pads in place. The devices were cut at the bottom to open the channels for the insertion of the NC test strips. Conjugate release pads and NC test strip for the HA assay were assembled into the left half of the device, and N-protein pads and test strip were assembled into the right side (**Figure 4.1C**). The entire device was adhered to an adhesive backing, and a waste

pad (CFSP223000, Millipore Sigma, Burlington MA, USA) was pressed down, overlapping with the end of the NC membrane.

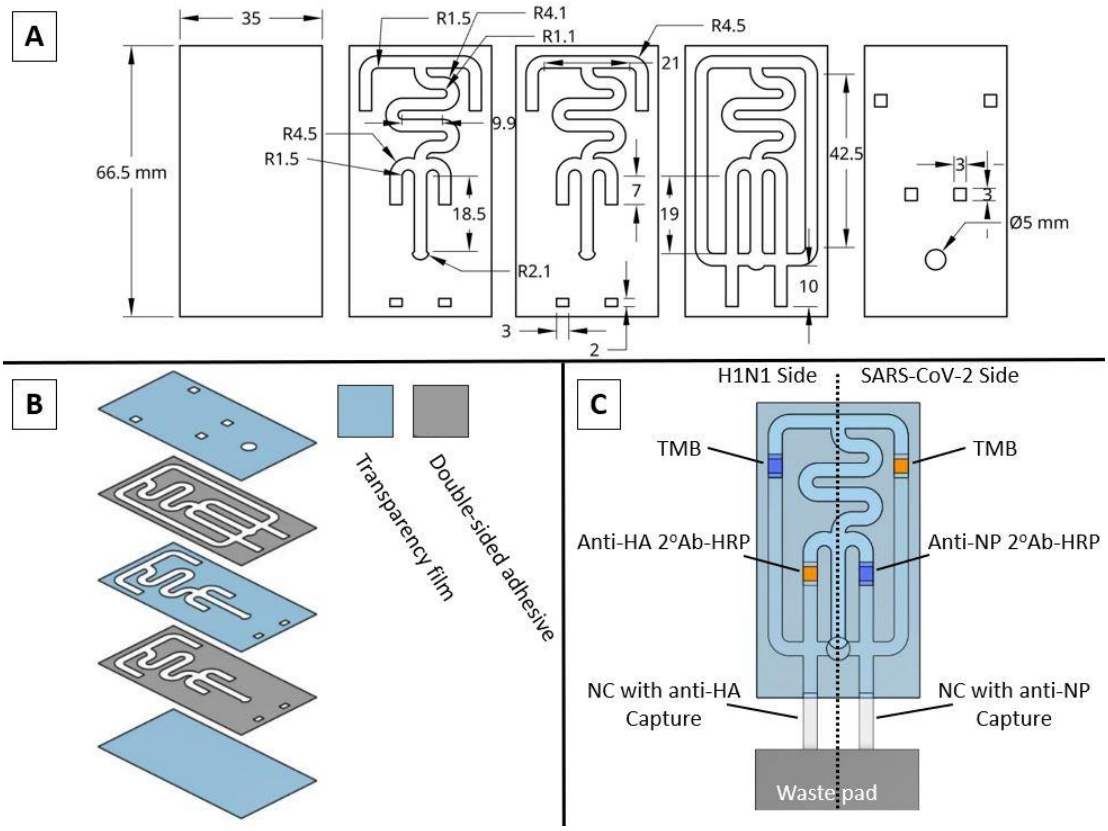


**Figure 4.1** (A) Schematic with dimensions for each layer of the multiplexed CaDI. (B) Order in which the 5 layers are assembled. (C) Location of reagent pads and NC membranes containing TMB, 2°Ab-HRP for each assay, and NC with capture and control antibodies for each assay.

*Assay optimization:*

The N-protein assay has been previously studied extensively. Therefore, the concentrations of 2°Ab-HRP and volume of TMB substrate used in the N-protein assay were pulled from chapter 2 of this dissertation. The buffer is made using 1.5X stable peroxide buffer (Thermo Fisher, 34062) at pH 6.5 with 150 mM NaCl, 0.1% Igepal CA630, and 0.1% Tween-20. The influenza A H1N1 assay has never been performed on this type of capillary driven immunoassay device (CaDI). To

optimize the conditions for the HA side of the multiplex device, the HA assay was performed on the single channel CaDI device outlined in chapter 2. First, TMB volume was held constant at 30 µL while the 2°Ab-HRP concentration was adjusted between 5 and 60 µg/mL. Devices were run in triplicate with running buffer containing either 0 or 50 ng/mL HA. 100 µL of sample was added to the sample inlet, and when the devices had completed, the NC was removed and imaged with a smartphone (Motorola 1) under a lightbox containing 16 LEDs. Based on the analyzed results, the 2°Ab-HRP concentration was held at 40 µg/mL while the TMB volume was varied from 7.5-37.5 µL. Devices were run again in triplicate with 0 or 50 ng/mL HA, and 22.5 µL of TMB was chosen moving forward.

*Multiplex assay operation:*

After HA assay conditions were optimized in the single-channel CaDI, dose response curves for both assays were collected in the multiplex device. First, a range of HA concentrations were diluted in running buffer, and 160 µL of each concentration was added to the sample inlet of the multiplex device. Sample completely fills the channels and delivers target to both NC test strips. Afterwards, reagents for each side of the device are delivered passively to the NC membrane from the device. The device is complete when the buffer above the TMB pads is drained from the channels through the NC membrane, to the waste pad. After the assay was complete (<15 min), NC membranes were removed, allowed to dry for 5 min at RT before imaging with a Motorola 1 smartphone under the light box. The same procedures were performed with varying concentrations of N-protein spiked into running buffer. Devices were also run with 5 and 100 ng/mL of both targets simultaneously spiked into running buffer. For simultaneous SARS-CoV-2 and CRP detection, one side of the device was prepared with the N-protein conjugate release pads and test

strip while the other contained reagents for the CRP assay described above. These devices were run at 1100 PFU/mL inactivated SARS-CoV-2 (USA-WA1/2020)[47] and 100 ng/mL CRP.

*Spiked Nasal Swab Samples:*

Anterior nares swab was performed under IRB approved conditions. A foam swab (FoamTec Medical, MP1301AST) was swirled in each nostril 3-5x. To each swab, 50 µL of extraction buffer spiked with N-protein, HA, or both was added to the swab. The swabs were submerged in 300 µL of running buffer for 15 s and then pressed through a 0.2 µm syringe filter (Fisher, 13-1001-14). 160 µL of the filtered sample was then added to the multiplexed device. When devices had finished, the NC membranes were removed and allowed to dry at RT for 5 min. NC membranes were imaged under an LED lightbox with a smartphone (Motorola 1).

*Image/Data Analysis:*

NC membranes were allowed to dry for 5 min at RT before being imaged under a light box. Images were uploaded to the free NIH software, ImageJ. Images were converted to 8-bit gray scale and inverted to provide a positive correlation with increasing target concentration. A rectangular area of interest was drawn around the area of the test line (or the blank area where the test line would be in the case of blank samples). A mean gray value measurement was taken of the test line area, and another measurement was taken in the area between the test line and control line. The ratio of these values is called the “mean gray ratio” and was used for quantification purposes.

## 4.4 Results and Discussion:

*Flu assay optimization:*

The multiplex device used in this work consists of two, separate immunoassays. Conditions for the N-protein assay had been optimized previously in chapter 2 of this dissertation. To optimize the HA assay, the single channel CaDI device described in that previous work was used, and the location of conjugate release pads and NC membrane are chosen in **Figure 4.2A**. Manufacturing the single channel devices in bulk is slightly easier, giving us a quick way to determine the optimal 2°Ab-HRP concentrations and TMB volumes to use. First, the volume of TMB dried on the TMB pad was held constant at 30 µL while the concentration of 2°Ab-HRP dried was varied. The optimal concentration of 2°Ab-HRP was based on the results that gave the greatest signal for 50 ng/mL HA in running buffer and no signal with 0 ng/mL HA. The lowest concentration of 2°Ab-HRP where those criteria were met was 40 µg/mL. Despite having excess 2°Ab-HRP, more than 40 µg/mL did not improve signal and had a slightly higher signal for the blank samples (**Figure 4.2B**). Next, 2°Ab-HRP was held constant at 40 µg/mL while the volume of TMB substrate dried was varied. Devices were again run at 0 and 50 ng/mL HA. Although all TMB volumes above 15 µL performed similarly for signal intensity, 22.5 µL was chosen to ensure an excess of TMB is present in the device (**Figure 4.2B**). Along with benefiting the multiplex device, this HA assay development is the first example in the literature of an automated, capillary-driven immunoassay for HA.

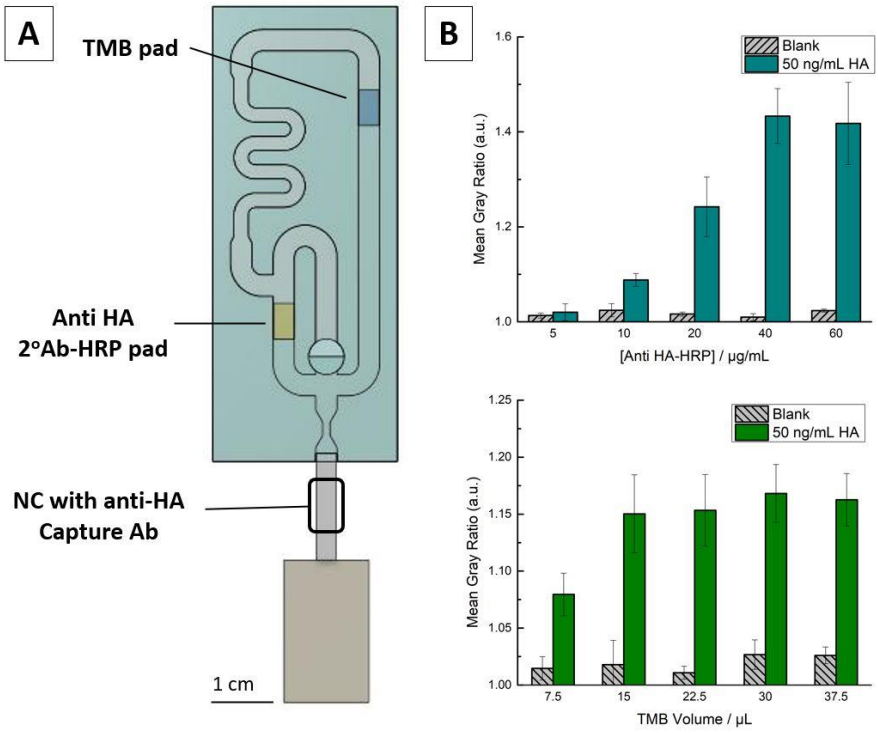


**Figure 4.1** (A) The single NC CaDI device was used to optimize conditions for the H1N1 assay. (B) TMB volume was held at 30 µL while the anti-HA 2°Ab-HRP concentration was varied. Following that, the anti-HA 2°Ab-HRP was held at 40 µg/mL while the TMB volume dried on the TMB pad was varied.

*Multiplex device function and theory:*

The optimized reagent pad conditions for the N-protein assay from chapter 2 and for the HA assay described above were incorporated into the multiplexed microfluidic device. A NC test strip for each assay was inserted on its corresponding side, and the device was pressed down on an adhesive backing with a waste pad connected to the membrane. To operate the device, 160 µL of sample is added to the sample inlet. No other end user steps are required after sample addition. Whaen sample is added, the solution fills the hollow channels in the device. Sample rehydrates 2°Ab-HRP and TMB from the conjugate release pads and flows through each NC membrane. If either target is present, it will bind to the capture antibody striped on its NC membrane. After this initial filling step, the buffer in the channels begins to drain into the waste pad through capillary

forces of the waste pad and the NC membranes. As the channels drain, an air bubble forms in the center channel above the sample inlet. Because of this air gap, 2°Ab-HRP from one side of the device cannot cross over to the other. 2°Ab-HRP is the next reagent delivered to the NC, followed by a gap of sample buffer that washes any excess from the test lines. Lastly, TMB is delivered to each test line. The assay operation is shown in **Figure 4.2A and B** with blue and yellow food dye dried on the conjugate release pads to help visualize flow. Mismatched colors were chosen to show that there was no cross over from one side of the device to the other when reagents are delivered to the test strips. If target is present at one or both test lines, 2°Ab-HRP will also be present. TMB can with HRP and $H_2O_2$ in the running buffer to form a solid blue test line. Control lines consisting of anti-mouse and anti-rabbit antibodies for NP and HA assay respectively should always be present.

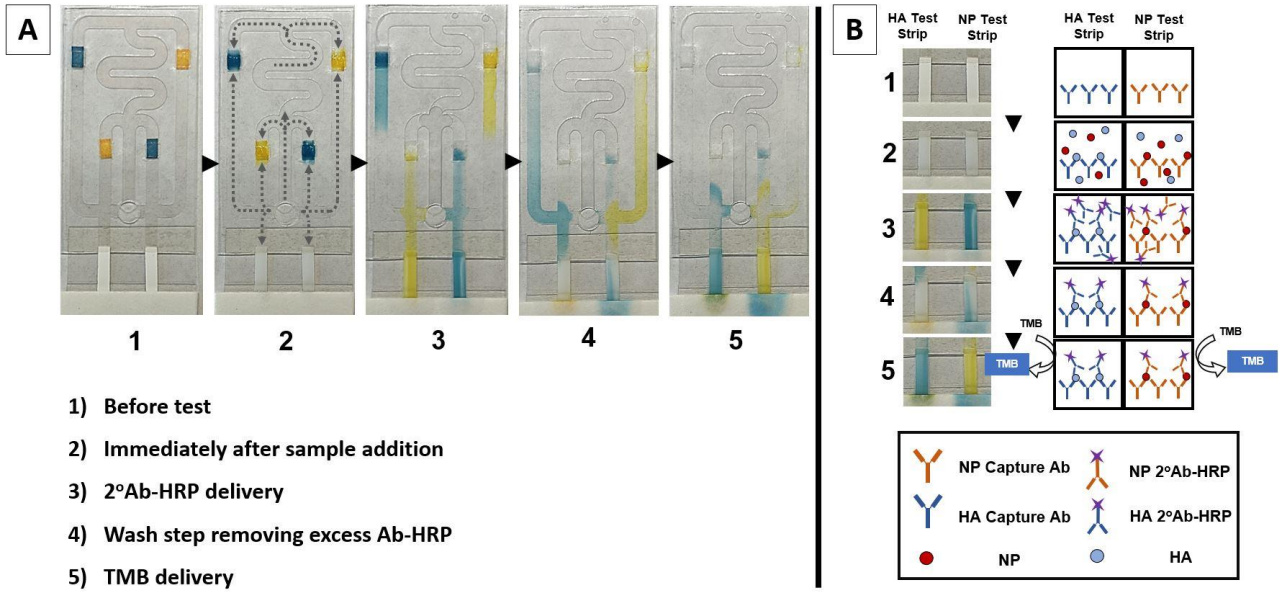


**Figure 4.2** (A) The device function is broken down into 5 distinct key points. Image 1 depicts the device before sample is added. Image 2 is immediately after sample is added. Sample and buffer fill the channels (direction of flow is depicted with gray arrows), and dried reagents are rehydrated. Target present flows through NC membranes and binds to the corresponding capture antibodies. In image 3, 2°Ab-HRP for each side of the device is delivered to its respective test strip. In image

4, excess 2°Ab-HRP is washed from each test strip. Lastly, in image 5, TMB is delivered to each test/control line, reacting with $H_2O_2$ in the buffer and HRP on the NC if it's present. (B) Images focused on the NC are accompanied by a molecular level schematic for each crucial step outlined in A.

*Dose response curves and simultaneously detection:*

Separate dose response curves were gathered for both sides of the device. One target was diluted in a running buffer containing hydrogen peroxide for the HRP reaction. The running buffer also contains NaCl for protein stability, and surfactants to encourage release of reagents from the conjugate release padas and prevent non-specific binding on the test lines. Varying concentrations of N-protein were run in triplicate with no HA present, and the resulting signal was fit to 4 parameter logistic regression (4PL). The LOD for N-protein was determined to be three standard deviations above the signal of the blank sample, meaning the LOD was 133 pg/mL. Ideally, regardless of the increase in concentration of N-protein, the signal in the HA assay NC membrane should never be present. If that's the case, a linear fit to the HA data should have a slope of 0. In this case, the slope of a linear fit to the HA signal was 0.00823 (**Figure 4.3A**). The same procedures were done holding the N-protein concentration at 0 and varying the concentration of HA. For that data, the LOD of HA is 840 pg/mL, and the slope of a linear fit for the N-protein side of the device is 0.00118 (**Figure 4.3B**).

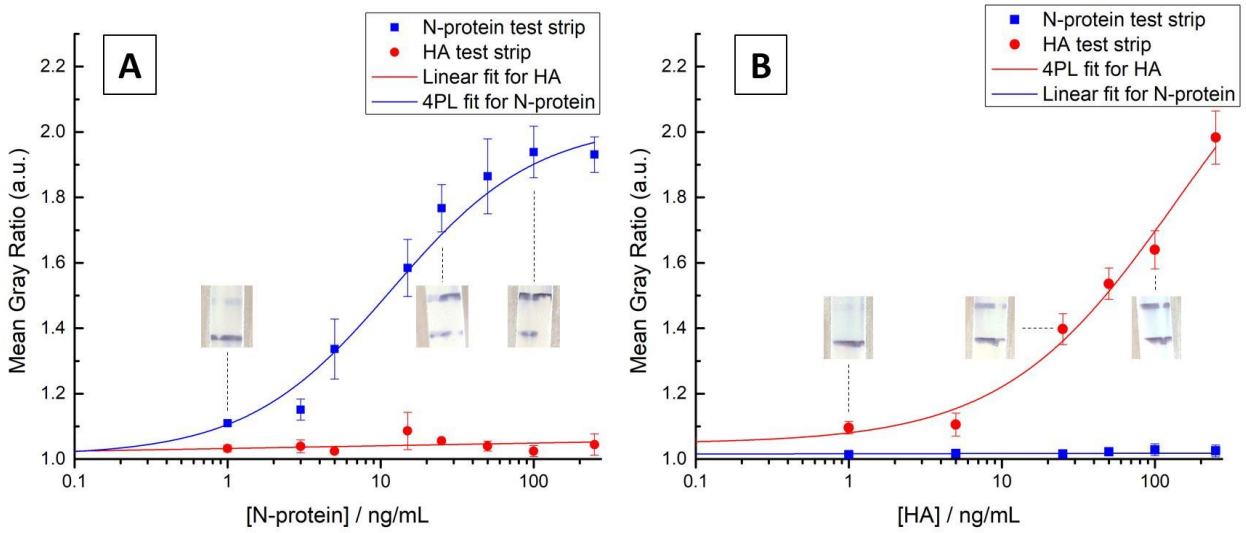


**Figure 4.3** Dose response curves were run for both targets separately, and representative images are shown for selected points. (A) SARS-CoV-2 N-protein dose response curve was run while holding HA concentration at 0. The N-protein signal was fitted to a 4PL ($R^2$ = 0.98) and the HA side is fitted to a linear fit with a slope of 0.00823. (B) H1N1 HA dose response was run holding the N-protein concentration at 0. The signal for HA was fit to a 4PL fit ($R^2$ = 0.97), and the linear fit for the N-protein signal had a slope of 0.00118.

A patient presenting with a fever and cough would not likely be infected with both SARS-CoV-2 and H1N1. However, to show the effectiveness of this multiplex device to detect two analytes at the same time, one relatively low and one relatively high concentration of both HA and N-protein was spiked into running buffer. These samples containing both targets were run in triplicate, and the images for both sides of the devices were processed as described above (**Figure 4.4**).

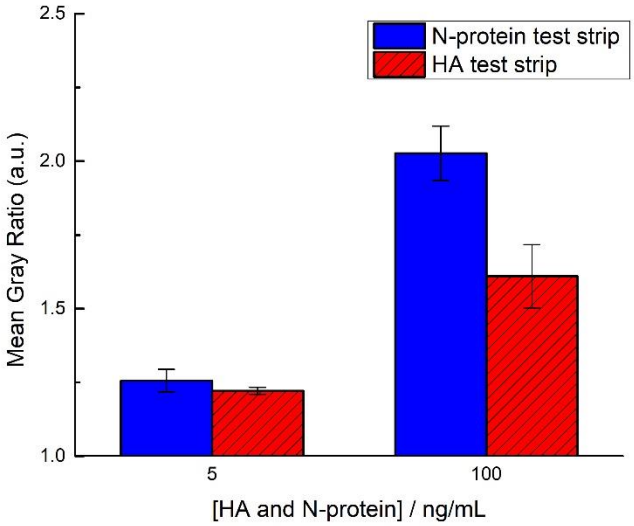


**Figure 4.4** Devices were run with 5 ng/mL and 100 ng/mL of both HA and N-protein in running buffer simultaneously.

At both concentrations, signal was present on both test strips after the devices had run. It did not appear that the presence of one target hindered the other side's ability to detect its intended target. Continuing the expand on multiplex applications, simultaneous detection of SARS-CoV-2 and CRP was investigated. Elevated levels of CRP in patients infected with SARS-CoV-2 has been correlated with worse patient outcomes.[44] Therefore, simultaneous diagnosis of a SARS-CoV-2 infection and quantification of CRP would greatly help in prognosis and treatment. Devices were assembled with SARS-CoV-2 reagents and test strip on one side, and with CRP reagents and test strip on the other. Extraction buffer was spiked with 1100 PFU/mL of inactivated SARS-CoV-2 and 100 ng/mL CRP before running in the multiplex device. As a control, one device was run with no sample present.

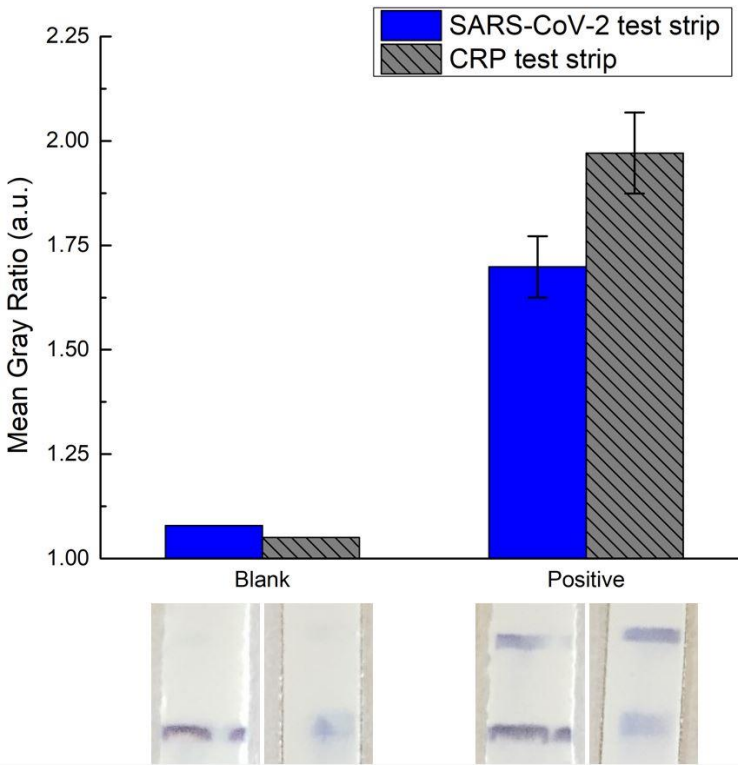


**Figure 4.5** Devices were run with one side containing reagents and test strip for the N-protein immunoassay, and the other side with reagents for the CRP assay. Blank devices were run with neither target present as a control, and positive devices were run in triplicate with running buffer containing both 1100 PFU/mL SARS-CoV-2 virus and 100 ng/mL CRP. Representative images for each assay are shown.

Lastly, to show that both the N-protein and HA immunoassays would work in more complex samples, spiked nasal swabs were run for both targets separately and together. Anterior nares swabs were collected from two participants, and varying amounts of N-protein, HA, or both simultaneously was spiked onto the swab. The swabs were submerged in running buffer, filtered with a syringe filter, and sample was added to the devices. The results showed varying success. Signal was very low for swabs spiked with 10 ng/mL of either target. This is understandable, however, since the 50 µL spiked onto the swab is then diluted when submerged in 300 µL of running buffer. Some target may be lost to the swab, the filter, or both, resulting in lower signal than expected. For swabs spiked with only N-protein, signal was detectable at 100 ng/mL, although

the signal varied greatly between the three replicates (Figure 4.6A). For swabs spiked only with HA, signal was again detectable at 100 ng/mL, but signal was low, likely due to the reasons described above (Figure 4.6B). Encouragingly, when swabs were spiked with both 100 ng/mL N-protein *and* HA, signal for both aligned well with the signal of when each target was spiked individually (Figure 4.6C).

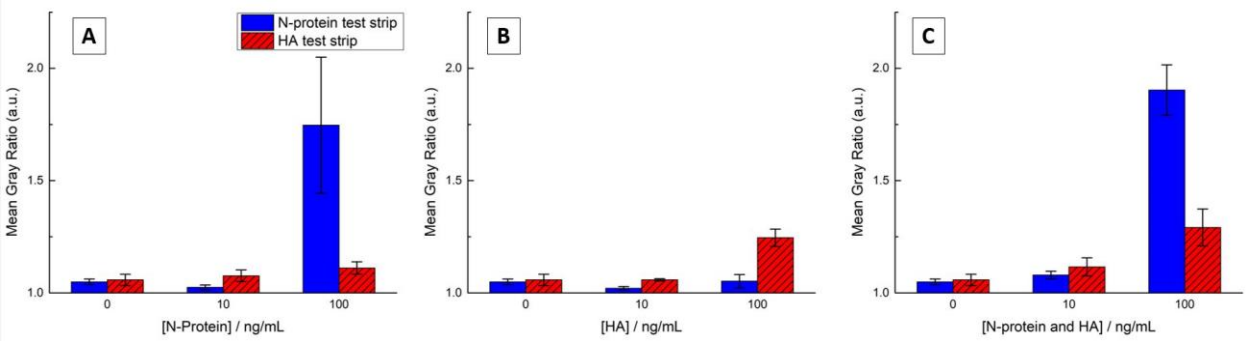


**Figure 4.6** (A) 50 µL of 10 and 100 ng/mL N-protein, (B) 50 µL of 10 and 100 ng/mL HA, and (C) 50 µL of 10 and 100 ng/mL of *both* N-protein and HA was spiked onto nasal swabs. Swabs were submerged in running buffer, filtered, and sample was added to the device sample inlet.

Although not the case for 10 ng/mL of either target, for 100 ng/mL, every scenario had a significantly higher signal than the blank. This shows that the assay still operates as intended in complex sample; however more data points should be collected in the future to complete a full dose response curve in contrived nasal swab samples.

## 4.5 Conclusion:

In this work, we show the first example of an automated, multiplexed ELISA on a POC-style device. Using hollow microfluidic channels, spatially separated NC test strips, and conjugate release pads device operates in a single sample addition step and outputs visually detectable signal in under 15 min. The device can detect HA from H1N1 in with an LOD of 840 pg/mL and N-

protein from SARS-CoV-2 with an LOD of 133 pg/mL when spiked in running buffer, and preliminary data for nasal swab samples is also shown. While this device was designed to determine between a SARS-CoV-2 or H1N1 infection, the device can also be used for simultaneous detection of two targets. To demonstrate this concept, N-protein and HA were detected simultaneously, and inactivated SARS-CoV-2 and CRP were detected simultaneously. The effectiveness of simultaneous detection on this device, and the spatial separation of the test strips points towards numerous future applications. In addition, future work will aim to further multiplex the device, adding additional test lines to each test strip, increasing the number of targets that can be detected.

# CHAPTER 4 CITATIONS


1. Rasmussen, J.; Langerman, H., Alzheimer's Disease - Why We Need Early Diagnosis. *Degenerative neurological and neuromuscular disease* **2019,** *9*, 123-130.

2. Kashyap, D.; Kaur, H., Cell-free miRNAs as non-invasive biomarkers in breast cancer: Significance in early diagnosis and metastasis prediction. *Life Sciences* **2020,** *246*, 117417.

3. Bohunicky, B.; Mousa, S. A., Biosensors: the new wave in cancer diagnosis. *Nanotechnology, Science and Applications* **2011,** *4*, 1-10.

4. Clinton, W. J., Turning the Tide on the AIDS Pandemic. *New England Journal of Medicine* **2003,** *348* (18), 1800-1802.

5. Gayle, H. D., Curbing the Global AIDS Epidemic. *New England Journal of Medicine* **2003,** *348* (18), 1802-1805.

6. Nitsche, A.; Schweiger, B.; Ellerbrok, H.; Niedrig, M.; Pauli, G., SARS coronavirus detection. *Emerg Infect Dis* **2004,** *10* (7), 1300-3.

7. Al Hajjar, S.; McIntosh, K., The first influenza pandemic of the 21st century. *Annals of Saudi medicine* **2010,** *30* (1), 1-10.

8. Otoo, J. A.; Schlappi, T. S., REASSURED Multiplex Diagnostics: A Critical Review and Forecast. *Biosensors (Basel)* **2022,** *12* (2).

9. Petti, C. A.; Polage, C. R.; Quinn, T. C.; Ronald, A. R.; Sande, M. A., Laboratory Medicine in Africa: A Barrier to Effective Health Care. *Clinical Infectious Diseases* **2006,** *42* (3), 377-382.

10. Herd, G. C. E.; Musaad, S. M. A., Point-of-Care Testing in Rural and Remote Settings to Improve Access and Improve Outcomes: A Snapshot of the New Zealand Experience. *Archives of Pathology & Laboratory Medicine* **2020,** *145* (3), 327-335.

11. Noviana, E.; Ozer, T.; Carrell, C. S.; Link, J. S.; McMahon, C.; Jang, I.; Henry, C. S., Microfluidic Paper-Based Analytical Devices: From Design to Applications. *Chemical Reviews* **2021,** *121* (19), 11835-11885.

12. Jara, M. D. L.; Alvarez, L. A. C.; Guimarães, M. C. C.; Antunes, P. W. P.; de Oliveira, J. P., Lateral flow assay applied to pesticides detection: recent trends and progress. *Environmental science and pollution research international* **2022,** *29* (31), 46487-46508.

13. Chen, Y.; Chen, Q.; Han, M.; Zhou, J.; Gong, L.; Niu, Y.; Zhang, Y.; He, L.; Zhang, L., Development and optimization of a multiplex lateral flow immunoassay for the simultaneous determination of three mycotoxins in corn, rice and peanut. *Food Chemistry* **2016,** *213*, 478-484.

14. Tominaga, T., Rapid detection of coliform bacteria using a lateral flow test strip assay. *Journal of Microbiological Methods* **2019,** *160*, 29-35.

15. Zhao, Y.; Wang, H.; Zhang, P.; Sun, C.; Wang, X.; Wang, X.; Yang, R.; Wang, C.; Zhou, L., Rapid multiplex detection of 10 foodborne pathogens with an up-converting phosphor technology-based 10-channel lateral flow assay. *Scientific Reports* **2016,** *6* (1), 21342.

16. Yin, M.; Nie, Y.; Liu, H.; Liu, L.; Tang, L.; Dong, Y.; Hu, C.; Wang, H., Development of a europium nanoparticles lateral flow immunoassay for NGAL detection in urine and diagnosis of acute kidney injury. *BMC Nephrology* **2022,** *23* (1), 30.

17. Koczula, K. M.; Gallotta, A., Lateral flow assays. *Essays Biochem* **2016,** *60* (1), 111-120.

18. Peng, J.; Wang, Y.; Liu, L.; Kuang, H.; Li, A.; Xu, C., Multiplex lateral flow immunoassay for five antibiotics detection based on gold nanoparticle aggregations. *RSC Advances* **2016,** *6* (10), 7798-7805.

19. Wang, Q.; Liu, Y.; Wang, M.; Chen, Y.; Jiang, W., A multiplex immunochromatographic test using gold nanoparticles for the rapid and simultaneous detection of four nitrofuran metabolites in fish samples. *Analytical and Bioanalytical Chemistry* **2018,** *410* (1), 223-233.

20. Parolo, C.; Sena-Torralba, A.; Bergua, J. F.; Calucho, E.; Fuentes-Chust, C.; Hu, L.; Rivas, L.; Álvarez-Diduk, R.; Nguyen, E. P.; Cinti, S.; Quesada-González, D.; Merkoçi, A., Tutorial: design and fabrication of nanoparticle-based lateral-flow immunoassays. *Nature Protocols* **2020,** *15* (12), 3788-3816.

21. Ragavendar, M. S.; Anmol, C. M. In *A mathematical model to predict the optimal test line location and sample volume for lateral flow immunoassays*, 2012 Annual International Conference of the IEEE Engineering in Medicine and Biology Society, 28 Aug.-1 Sept. 2012; 2012; pp 2408-2411.

22. Sena-Torralba, A.; Álvarez-Diduk, R.; Parolo, C.; Piper, A.; Merkoçi, A., Toward Next Generation Lateral Flow Assays: Integration of Nanomaterials. *Chemical Reviews* **2022,** *122* (18), 14881-14910.

23. Washburn, E. W., The Dynamics of Capillary Flow. *Physical Review* **1921,** *17* (3), 273-283.

24. Gomez-Martinez, J.; Silvy, M.; Chiaroni, J.; Fournier-Wirth, C.; Roubinet, F.; Bailly, P.; Brès, J.-C., Multiplex Lateral Flow Assay for Rapid Visual Blood Group Genotyping. *Analytical Chemistry* **2018,** *90* (12), 7502-7509.

25. Taranova, N. A.; Byzova, N. A.; Zaiko, V. V.; Starovoitova, T. A.; Vengerov, Y. Y.; Zherdev, A. V.; Dzantiev, B. B., Integration of lateral flow and microarray technologies for multiplex immunoassay: application to the determination of drugs of abuse. *Microchimica Acta* **2013,** *180* (11), 1165-1172.

26. Dincer, C.; Bruch, R.; Kling, A.; Dittrich, P. S.; Urban, G. A., Multiplexed Point-of-Care Testing - xPOCT. *Trends Biotechnol* **2017,** *35* (8), 728-742.

27. Hong, W.; Huang, L.; Wang, H.; Qu, J.; Guo, Z.; Xie, C.; Zhu, Z.; Zhang, Y.; Du, Z.; Yan, Y.; Zheng, Y.; Huang, H.; Yang, R.; Zhou, L., Development of an up-converting phosphor technology-based 10-channel lateral flow assay for profiling antibodies against Yersinia pestis. *Journal of Microbiological Methods* **2010,** *83* (2), 133-140.

28. Han, D. K.; Oh, J.; Lee, J.; Cho, Y. G.; Park, J. S.; Choi, J. S.; Kim, D. S.; Kwon, J., Paper-based multiplex analytical device for simultaneous detection of Clostridioides difficile toxins and glutamate dehydrogenase. *Biosensors and Bioelectronics* **2021,** *176*, 112894.

29. Cheng, C.-M.; Martinez, A. W.; Gong, J.; Mace, C. R.; Phillips, S. T.; Carrilho, E.; Mirica, K. A.; Whitesides, G. M., Paper-Based ELISA. *Angewandte Chemie International Edition* **2010,** *49* (28), 4771-4774.

30. Fabiani, L.; Mazzaracchio, V.; Moscone, D.; Fillo, S.; De Santis, R.; Monte, A.; Amatore, D.; Lista, F.; Arduini, F., Paper-based immunoassay based on 96-well wax-printed paper plate combined with magnetic beads and colorimetric smartphone-assisted measure for reliable detection of SARS-CoV-2 in saliva. *Biosensors and Bioelectronics* **2022,** *200*, 113909.

31. Verma, M. S.; Tsaloglou, M.-N.; Sisley, T.; Christodouleas, D.; Chen, A.; Milette, J.; Whitesides, G. M., Sliding-strip microfluidic device enables ELISA on paper. *Biosensors and Bioelectronics* **2018,** *99*, 77-84.

32. Carrell, C. S.; Wydallis, R. M.; Bontha, M.; Boehle, K. E.; Beveridge, J. R.; Geiss, B. J.; Henry, C. S., Rotary manifold for automating a paper-based Salmonella immunoassay. *RSC Advances* **2019,** *9* (50), 29078-29086.

33. Mu, X.; Zhang, L.; Chang, S.; Cui, W.; Zheng, Z., Multiplex Microfluidic Paper-based Immunoassay for the Diagnosis of Hepatitis C Virus Infection. *Analytical Chemistry* **2014,** *86* (11), 5338-5344.

34. Samper, I. C.; Sánchez-Cano, A.; Khamcharoen, W.; Jang, I.; Siangproh, W.; Baldrich, E.; Geiss, B. J.; Dandy, D. S.; Henry, C. S., Electrochemical Capillary-Flow Immunoassay for Detecting Anti-SARS-CoV-2 Nucleocapsid Protein Antibodies at the Point of Care. *ACS Sensors* **2021,** *6* (11), 4067-4075.

35. Clark, K. M.; Schenkel, M. S.; Pittman, T. W.; Samper, I. C.; Anderson, L. B. R.; Khamcharoen, W.; Elmegerhi, S.; Perera, R.; Siangproh, W.; Kennan, A. J.; Geiss, B. J.; Dandy, D. S.; Henry, C. S., Electrochemical Capillary Driven Immunoassay for Detection of SARS-CoV-2. *ACS Measurement Science Au* **2022**.

36. Panraksa, Y.; Jang, I.; Carrell, C. S.; Amin, A. G.; Chailapakul, O.; Chatterjee, D.; Henry, C. S., Simple manipulation of enzyme-linked immunosorbent assay (ELISA) using an automated microfluidic interface. *Analytical Methods* **2022**.

37. Similarities and Differences between Flu and COVID-19. https://www.cdc.gov/flu/symptoms/flu-vs-covid19.htm (accessed 1/27/2023).

38. Shan, D.; Johnson, J. M.; Fernandes, S. C.; Suib, H.; Hwang, S.; Wuelfing, D.; Mendes, M.; Holdridge, M.; Burke, E. M.; Beauregard, K.; Zhang, Y.; Cleary, M.; Xu, S.; Yao, X.; Patel, P. P.; Plavina, T.; Wilson, D. H.; Chang, L.; Kaiser, K. M.; Nattermann, J.; Schmidt, S. V.; Latz, E.; Hrusovsky, K.; Mattoon, D.; Ball, A. J., N-protein presents early in blood, dried blood and saliva during asymptomatic and symptomatic SARS-CoV-2 infection. *Nature Communications* **2021,** *12* (1), 1931.

39. Anderson, C. E.; Holstein, C. A.; Strauch, E.-M.; Bennett, S.; Chevalier, A.; Nelson, J.; Fu, E.; Baker, D.; Yager, P., Rapid Diagnostic Assay for Intact Influenza Virus Using a High Affinity Hemagglutinin Binding Protein. *Analytical Chemistry* **2017,** *89* (12), 6608-6615.

40. Chávez Ramos, K.; Nishiyama, K.; Maeki, M.; Ishida, A.; Tani, H.; Kasama, T.; Baba, Y.; Tokeshi, M., Rapid, Sensitive, and Selective Detection of H5 Hemagglutinin from Avian Influenza Virus Using an Immunowall Device. *ACS Omega* **2019,** *4* (15), 16683-16688.

41. Wang, Z.; Zhao, Q.; Huang, M.; Duan, Y.; Li, F.; Wang, T., Dual Detection of Hemagglutinin Proteins of H5N1 and H1N1 Influenza Viruses Based on FRET Combined With DNase I. *Front Microbiol* **2022,** *13*.

42. Chen, N.; Zhou, M.; Dong, X.; Qu, J.; Gong, F.; Han, Y.; Qiu, Y.; Wang, J.; Liu, Y.; Wei, Y.; Xia, J. a.; Yu, T.; Zhang, X.; Zhang, L., Epidemiological and clinical characteristics of 99 cases of 2019 novel coronavirus pneumonia in Wuhan, China: a descriptive study. *The Lancet* **2020,** *395* (10223), 507-513.

43. Gao, Y.; Li, T.; Han, M.; Li, X.; Wu, D.; Xu, Y.; Zhu, Y.; Liu, Y.; Wang, X.; Wang, L., Diagnostic utility of clinical laboratory data determinations for patients with the severe COVID-19. *Journal of Medical Virology* **2020,** *92* (7), 791-796.

44. Ali, N., Elevated level of C-reactive protein may be an early marker to predict risk for severity of COVID-19. *J Med Virol* **2020,** *92* (11), 2409-2411.

45. Grant, B. D.; Anderson, C. E.; Williford, J. R.; Alonzo, L. F.; Glukhova, V. A.; Boyle, D. S.; Weigl, B. H.; Nichols, K. P., SARS-CoV-2 Coronavirus Nucleocapsid Antigen-Detecting Half-Strip Lateral Flow Assay Toward the Development of Point of Care Tests Using Commercially Available Reagents. *Analytical chemistry* **2020,** *92* (16), 11305-11309.

46. Ramachandran, S.; Fu, E.; Lutz, B.; Yager, P., Long-term dry storage of an enzyme-based reagent system for ELISA in point-of-care devices. *Analyst* **2014,** *139* (6), 1456-1462.

47. Terry, J. S.; Anderson, L. B. R.; Scherman, M. S.; McAlister, C. E.; Perera, R.; Schountz, T.; Geiss, B. J., Development of a SARS-CoV-2 nucleocapsid specific monoclonal antibody. *Virology* **2021,** *558*, 28-37.

# CHAPTER 5: CONCLUSION AND FUTURE DIRECTIONS

Reliable medical diagnostics are a crucial part of patient treatment, preventing transmission of communicable diseases, and community health.[1-3] Despite the importance, there is still significant need for improvement in affordable, regular diagnostic devices. Laboratory methods for medical diagnostics, such as bacterial culturing, PCR, and immunoassays, are well understood and reliable; however, they also require trained personnel to perform, are time consuming, and are expensive.[4-5] The combination of these limitations can hinder the access a patient might have to regular testing. In the case of communicable diseases, a lack in regular testing can be especially detrimental. Early in the COVID-19 pandemic, many researchers argued that robust contact tracing, social distancing, and access to regular, dependable diagnostics were the most crucial aspects to preventing or slowing the spread of the virus.[6-8] Unfortunately, the infrastructure in place in response to the COVID-19 pandemic was overwhelmed, and faults in health-care systems were noticed.[9-10] Rapid antigen tests for SARS-CoV-2 proteins emerged as a response to fill this gap in diagnostic tools. Most of these rapid tests rely on a lateral flow assay (LFA) design. Although dozens of these tests have been granted emergency use authorization by the FDA,[11] when tested independently, many fail to meet the manufacturer's claims with nasal swab samples.[12] LFAs are simple to perform, but this failure in analytical sensitivity makes them less reliable than laboratory based tests like ELISA and PCR. The capillary-driven immunoassay devices in this dissertation merge the gap between the simplicity of an LFA and the signal enhancement gained from an enzyme-based detection method like ELISA.

In this dissertation, I presented multiple examples of capillary-driven immunoassay devices that automate the steps of a traditional well-plate ELISA from a single sample addition

step. These devices are constructed using patterned and laser cut transparency film and double-sided adhesive layers to create hollow channels for fluid transport. Reagents required for an ELISA are dried in conjugate release pads that are incorporated into the channels of the device. Upon sample addition, the microfluidic channels fill, dried reagents are rehydrated, and target present in the sample is delivered to a capture antibody on a nitrocellulose test strip. Passively via capillary action, the remaining reagent delivery and wash steps required for an ELISA are delivered to the nitrocellulose membrane.

In Chapter 2 of this dissertation, I describe the first colorimetric application of a capillary driven immunoassay for rapid detection of SARS-CoV-2 antigen. Lateral flow assays for SARS-CoV-2 nucleocapsid protein exist as lateral flow assays, but when independently evaluated, many of them fail to meet the manufacturers claimed detection limits in nasal swab samples.[12] The device in Chapter 2 was first compared to a traditional well-plate ELISA with inactivated SARS-CoV-2 virus. Detection limits of 86 and 8 PFU/mL were determined for the capillary-driven immunoassay device and the well-plate ELISA respectively. Although these detection limits varied by an order of magnitude, the ELISA required 17 separate pipetting steps, >5 hours to perform, and a plate reader for quantification. The capillary-driven immunoassay required only a single sample addition step, and the signal is visibly present in under 20 min. SARS-CoV-2 spiked nasal swab samples were also tested, yielding a detection limit of 222 PFU/mL form quantifying signal intensity of smartphone images. Although this detection limit is higher than when the assay was performed in buffer, the nasal swab samples are a more complex sample matrix, and the swabs were diluted in additional extraction buffer before running. Even with these drawbacks, this detection limit is below the FDAs recommended 500 PFU/mL for these types of diagnostic

devices.[12] Lastly, a visual detection limit of 100 PFU/mL was determined by polling 20 untrained end users, asking them to correctly identify positive and negative results.

Visual detection of SARS-CoV-2 antigen is the simplest form of signal detection for point-of-care settings. However, chemiluminescent immunoassays offer a more sensitive alternative when paired with an imager. Chemiluminescent (CL) immunoassays rely on light produced as the result of a chemical reaction.[13-14] CL immunoassays have been performed for decades, but they maintain the limitations described previously: time consuming, expensive, and tedious to perform.[15-16] Some CL immunoassays attempt to ease these limitations through the use of lateral flow assays, but none have been able to incorporate the washing and reagent delivery steps required to prevent non-specific binding into the design.[17-18] In Chapter 3, I describe the use chemiluminescent substrate can be used in a capillary-driven immunoassay for the detection of SARS-CoV-2 nucleocapsid protein. The assay/device is the first automated CL immunoassay to be performed from a single end-user step. It is also the first CL immunoassay of its kind for the detection of SARS-CoV-2. A detection limit of 864 pg/mL for SARS-CoV-2 nucleocapsid protein was obtained using this device and a benchtop CL imager. This limit of detection is well within the range of nucleocapsid protein found in the blood and saliva of patients positive for COVID-19.[19-20]

Single analyte detection is suitable for many applications in medical diagnostics. In the example of SARS-CoV-2 detection, a device designed for a single biomarker from the virus can give a yes/no results to whether or not someone has the disease. However, for more complex analysis, multiplexed detection of biomarkers is of increasing interest.[21] In Chapter 4, I describe a multiplex capillary-driven device with two spatially separated test strips that can be used in two different types of assays. In the first example, the device is used to distinguish between H1N1

and SARS-CoV-2. Since H1N1 and SARS-CoV-2 infections normally present with similar symptoms,[22] the multiplex device in Chapter 4 would tell a patient which infection they have. Dose response curves were generated for both sides of the device with detection limits of 840 pg/mL H1N1 hemagglutinin and 133 pg/mL SARS-CoV-2 nucleocapsid protein. In both cases, the presence of one target did not result in signal on the other test strip, allowing the user to distinguish between the two diseases. Distinguishing between illnesses is important, but simultaneous detection is also useful for a number of applications. For example, elevated levels of C-reactive protein (CRP) in patients with COVID-19 can be indicative of more severe outcomes.[23-24] Therefore, the multiplexed device was also used to simultaneous detect nucleocapsid protein from SARS-CoV-2 and CRP to demonstrate another form of multiplexed detection.

The devices described in this dissertation are some of the first examples of this class of affordable capillary driven immunoassay. Future work will expand upon the types of biomarkers and analytes detected with these types of devices. For example, chronic illnesses like cardiovascular diseases can be monitored more effectively if a patient has access to regular and reliable testing. Being able to self-administer tests and communicate the results to a health-care professional would prevent regular trips to a clinic or could help monitor a patient's response to treatment. Additionally, very few biomarkers in human serum are specifically related to cardiovascular disease, so a multiplexed assay for these complicated illnesses would be more ideal. C-reactive protein is commonly used as a biomarker for overall heart health, but elevated levels of CRP can be indicative of several diseases like Crohn's disease, cancer, or tissue damage.[25-27] Therefore, using the multiplexed device to monitor a panel of biomarkers associated

with heart health would give patients and practitioners more wholistic information from the results.

Detecting other biomarkers would inherently mean testing in different sample types. In this dissertation, samples were primarily run in buffer or spiked nasal swab samples. In the future, whole blood or plasma, urine, saliva, or unfiltered swab samples may need to be performed. Previous examples of on device plasma separation have been published in capillary driven immunoassays to detect SARS-CoV-2 IgG antibodies from whole blood.[28-29] These devices had a two step process for the end user; through dilution of the sample or further on device filtering, ideally this could be reduced to one step. Urine samples would be ideal for testing urinary tract infections, but the salinity pH, and concentration of urine can change dramatically from person to person or even in the same person throughout the day.[30-31] Buffer components would have to be considered that could adjust the pH of urine samples, and antibodies that can specifically handle high salt concentrations would need to be selected. Saliva and nasal swab samples are also too complex to be added to the device without some sort of pretreatment. In this dissertation, a filtering step was necessary whenever nasal swab samples were used. In the future, on device filtering will need to be explored to remove that step and simplify the process. I have done some initial work to incorporate a cellulose filter membrane over the sample inlet of a capillary driven device. With a filter over the sample inlet, air that normally enters the device through the sample inlet as buffer begins to flow through the nitrocellulose membrane cannot pass through the filter as easily. Therefore, an air inlet was cut into the design of the device immediately above the sample inlet/filter (Figure 5.1).

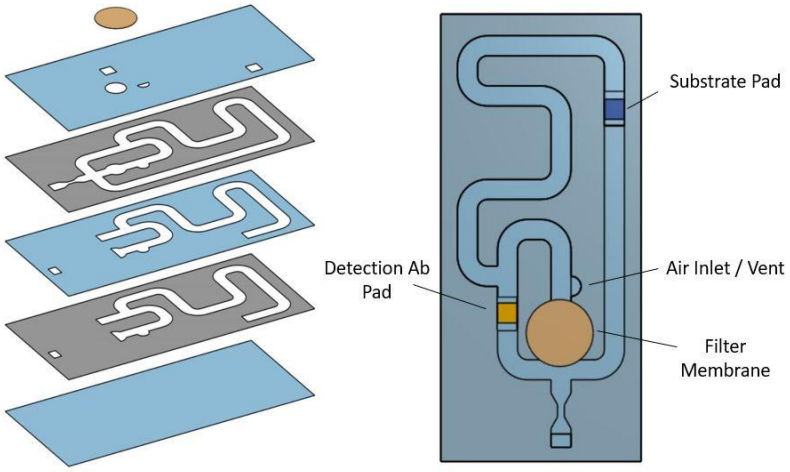


**Figure 5.1** The layers of transparency film (blue) and double-sided adhesive (gray) for a device that incorporates a filter membrane are shown on the left. A top-down view shows the locations of the reagent pads, filter, and air inlet/vent.

Initial tests using this device with nasal swab samples and food dye in place of reagents showed that devices finished in under 25 min on average (n = 3). While this is slightly slower than when running devices with buffer or filtered nasal swab samples, it would still give users results in under 30 min without additional pretreatment steps off device.

The work in this dissertation has shown advancements in rapid, affordable diagnostic devices in three different ways. The devices described are made of inexpensive materials, simple to manufacture, and reduce the complexity of laboratory-based ELISAs without sacrificing sensitivity. The assays have been performed in biological samples, and the robustness of the assays have been shown. With the single device or the multiplex device, the detection motifs and future clinical application are innumerable.

## CHAPTER 5 CITATIONS


1. Saber Tehrani, A. S.; Lee, H.; Mathews, S. C.; Shore, A.; Makary, M. A.; Pronovost, P. J.; Newman-Toker, D. E., 25-Year summary of US malpractice claims for diagnostic errors 1986–2010: an analysis from the National Practitioner Data Bank. *BMJ Quality & Safety* **2013,** *22* (8), 672-680.

2. Herd, G. C. E.; Musaad, S. M. A., Point-of-Care Testing in Rural and Remote Settings to Improve Access and Improve Outcomes: A Snapshot of the New Zealand Experience. *Archives of Pathology & Laboratory Medicine* **2020,** *145* (3), 327-335.

3. Yager, P.; Edwards, T.; Fu, E.; Helton, K.; Nelson, K.; Tam, M. R.; Weigl, B. H., Microfluidic diagnostic technologies for global public health. *Nature* **2006,** *442* (7101), 412-418.

4. Darwish, I. A., Immunoassay Methods and their Applications in Pharmaceutical Analysis: Basic Methodology and Recent Advances. *International journal of biomedical science : IJBS* **2006,** *2* (3), 217-35.

5. Noviana, E.; Ozer, T.; Carrell, C. S.; Link, J. S.; McMahon, C.; Jang, I.; Henry, C. S., Microfluidic Paper-Based Analytical Devices: From Design to Applications. *Chemical Reviews* **2021,** *121* (19), 11835-11885.

6. Kelly-Cirino, C. D.; Nkengasong, J.; Kettler, H.; Tongio, I.; Gay-Andrieu, F.; Escadafal, C.; Piot, P.; Peeling, R. W.; Gadde, R.; Boehme, C., Importance of diagnostics in epidemic and pandemic preparedness. *BMJ Global Health* **2019,** *4* (Suppl 2), e001179.

7. Kretzschmar, M. E.; Rozhnova, G.; Bootsma, M. C. J.; van Boven, M.; van de Wijgert, J. H. H. M.; Bonten, M. J. M., Impact of delays on effectiveness of contact tracing strategies for COVID-19: a modelling study. *The Lancet Public Health* **2020,** *5* (8), e452-e459.

8. Cevik, M.; Kuppalli, K.; Kindrachuk, J.; Peiris, M., Virology, transmission, and pathogenesis of SARS-CoV-2. *BMJ* **2020,** *371*, m3862.

9. Peeling, R. W.; Heymann, D. L.; Teo, Y. Y.; Garcia, P. J., Diagnostics for COVID-19: moving from pandemic response to control. *Lancet* **2022,** *399* (10326), 757-768.

10. Rethinking diagnostics for pandemic readiness. *Nature Biomedical Engineering* **2022,** *6* (3), 221-222.

11. In Vitro Diagnostics EUAs - Antigen Diagnostic Tests for SARS-CoV-2. https://www.fda.gov/medical-devices/coronavirus-disease-2019-covid-19-emergency-use-authorizations-medical-devices/in-vitro-diagnostics-euas-antigen-diagnostic-tests-sars-cov-2 (accessed 2/22/23).

12. Cubas-Atienzar, A. I.; Kontogianni, K.; Edwards, T.; Wooding, D.; Buist, K.; Thompson, C. R.; Williams, C. T.; Patterson, E. I.; Hughes, G. L.; Baldwin, L.; Escadafal, C.; Sacks, J. A.; Adams, E. R., Limit of detection in different matrices of 19 commercially available rapid antigen tests for the detection of SARS-CoV-2. *Scientific Reports* **2021,** *11* (1), 18313.

13. Dodeigne, C.; Thunus, L.; Lejeune, R., Chemiluminescence as diagnostic tool. A review. *Talanta* **2000,** *51* (3), 415-439.

14. Cinquanta, L.; Fontana, D. E.; Bizzaro, N., Chemiluminescent immunoassay technology: what does it change in autoantibody detection? *Auto- immunity highlights* **2017,** *8* (1), 9.

15. Kricka, L. J., 15 - CHEMILUMINESCENCE IMMUNOASSAY. In *Immunoassay*, Diamandis, E. P.; Christopoulos, T. K., Eds. Academic Press: San Diego, 1996; pp 337-353.

16. Zhao, L.; Sun, L.; Chu, X., Chemiluminescence immunoassay. *TrAC Trends in Analytical Chemistry* **2009,** *28* (4), 404-415.

17. Park, J.-M.; Jung, H.-W.; Chang, Y. W.; Kim, H.-S.; Kang, M.-J.; Pyun, J.-C., Chemiluminescence lateral flow immunoassay based on Pt nanoparticle with peroxidase activity. *Analytica Chimica Acta* **2015,** *853*, 360-367.

18. Zangheri, M.; Cevenini, L.; Anfossi, L.; Baggiani, C.; Simoni, P.; Di Nardo, F.; Roda, A., A simple and compact smartphone accessory for quantitative chemiluminescence-based lateral flow immunoassay for salivary cortisol detection. *Biosensors and Bioelectronics* **2015,** *64*, 63-68.

19. Zhang, Y.; Ong, C. M.; Yun, C.; Mo, W.; Whitman, J. D.; Lynch, K. L.; Wu, A. H. B., Diagnostic Value of Nucleocapsid Protein in Blood for SARS-CoV-2 Infection. *Clin Chem* **2021,** *68* (1), 240-248.

20. Shan, D.; Johnson, J. M.; Fernandes, S. C.; Suib, H.; Hwang, S.; Wuelfing, D.; Mendes, M.; Holdridge, M.; Burke, E. M.; Beauregard, K.; Zhang, Y.; Cleary, M.; Xu, S.; Yao, X.; Patel, P. P.; Plavina, T.; Wilson, D. H.; Chang, L.; Kaiser, K. M.; Nattermann, J.; Schmidt, S. V.; Latz, E.; Hrusovsky, K.; Mattoon, D.; Ball, A. J., N-protein presents early in blood, dried blood and saliva during asymptomatic and symptomatic SARS-CoV-2 infection. *Nature Communications* **2021,** *12* (1), 1931.

21. Dincer, C.; Bruch, R.; Kling, A.; Dittrich, P. S.; Urban, G. A., Multiplexed Point-of-Care Testing - xPOCT. *Trends Biotechnol* **2017,** *35* (8), 728-742.

22. Similarities and Differences between Flu and COVID-19. https://www.cdc.gov/flu/symptoms/flu-vs-covid19.htm (accessed 1/27/2023).

23. Chen, N.; Zhou, M.; Dong, X.; Qu, J.; Gong, F.; Han, Y.; Qiu, Y.; Wang, J.; Liu, Y.; Wei, Y.; Xia, J. a.; Yu, T.; Zhang, X.; Zhang, L., Epidemiological and clinical characteristics of

99 cases of 2019 novel coronavirus pneumonia in Wuhan, China: a descriptive study. *The Lancet* **2020,** *395* (10223), 507-513.

24. Gao, Y.; Li, T.; Han, M.; Li, X.; Wu, D.; Xu, Y.; Zhu, Y.; Liu, Y.; Wang, X.; Wang, L., Diagnostic utility of clinical laboratory data determinations for patients with the severe COVID-19. *Journal of Medical Virology* **2020,** *92* (7), 791-796.

25. Pepys, M. B.; Hirschfield, G. M., C-reactive protein: a critical update. *J Clin Invest* **2003,** *111* (12), 1805-1812.

26. Nadar, S. K.; Shaikh, M. M., Biomarkers in Routine Heart Failure Clinical Care. *Cardiac failure review* **2019,** *5* (1), 50-56.

27. Sanders-van Wijk, S.; van Empel, V.; Davarzani, N.; Maeder, M. T.; Handschin, R.; Pfisterer, M. E.; Brunner-La Rocca, H. P.; investigators, f. t. T.-C., Circulating biomarkers of distinct pathophysiological pathways in heart failure with preserved vs. reduced left ventricular ejection fraction. *European Journal of Heart Failure* **2015,** *17* (10), 1006-1014.

28. Samper, I. C.; Sánchez-Cano, A.; Khamcharoen, W.; Jang, I.; Siangproh, W.; Baldrich, E.; Geiss, B. J.; Dandy, D. S.; Henry, C. S., Electrochemical Capillary-Flow Immunoassay for Detecting Anti-SARS-CoV-2 Nucleocapsid Protein Antibodies at the Point of Care. *ACS Sensors* **2021,** *6* (11), 4067-4075.

29. Carrell, C.; Jang, I.; Link, J.; Terry, J. S.; Michael S, S.; Call, Z.; Panraksa, Y.; Dandy, D. S.; Geiss, B. J.; Henry, C. S., Point-of-Need Disposable ELISA System for COVID-19 Serology Testing. *ChemRxiv* **2021**.

30. Sarigul, N.; Korkmaz, F.; Kurultak, İ., A New Artificial Urine Protocol to Better Imitate Human Urine. *Sci Rep* **2019,** *9* (1), 20159.

31. Yaroshenko, I.; Kirsanov, D.; Kartsova, L.; Sidorova, A.; Borisova, I.; Legin, A., Determination of urine ionic composition with potentiometric multisensor system. *Talanta* **2015,** *131*, 556-561.

## APPENDIX 1

This appendix corresponds to Chapter 2 of this dissertation. Table A1 compares other pseudo automated ELISA devices to the CaDI device described in Chapter 2. The number of end-user steps, the assay time, and the enzyme/substrate pair are all considered.

**Table A1.** Other automated ELISA based systems, the number of user steps required, the time to results, and the enzyme/substrate pair used.

| Manual steps after sample addition | Time to Results (min) | Enzyme/substrate | Reference |
|---|---|---|---|
| 4 | 65 | β-galactosidase/CPRG | [1] |
| 5 | 60 | ALP/BCIP | [2] |
| 4 | 7 | HRP/TMB | [3] |
| 1 | 35 | HRP/DAB | [4] |
| 1 | 20 | HRP/TMB | [5] |
| 0 | 15 | ALP/BCIP | [6] |
| 0 | 15-20 | HRP/TMB | This work |
| 6+ | >60 | ----- | ELISA |
| 0 | <15 | Au Nanoparticles | LFA |

### A1.1 Device Design and Assembly:

The device channels were designed using the CAD program, Onshape, and CorelDraw. Figure A1.1 shows the dimensions of the features in the device that were cut with a laser cutter.

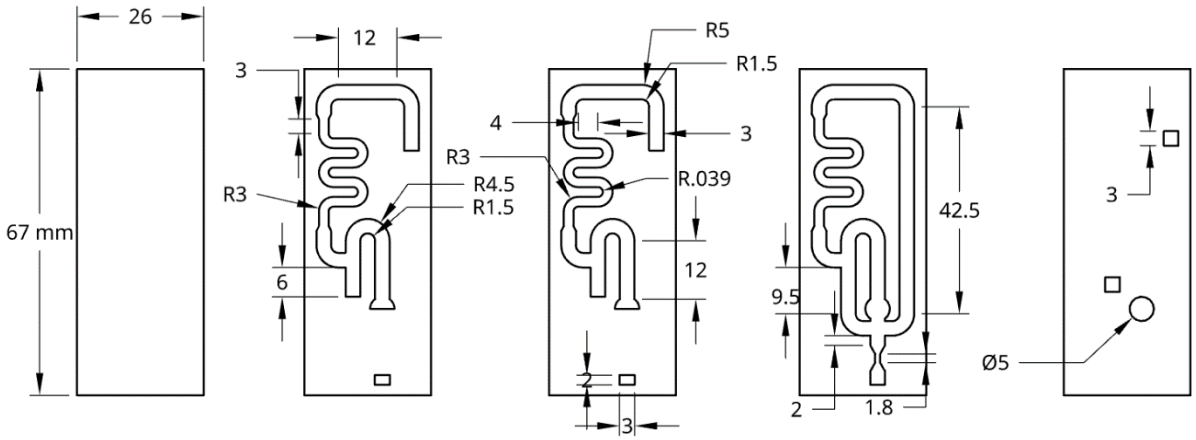


**Figure A1.1** Shown above are feature dimensions of the device layers.

The layers are cut into either transparency film (3M 9984) or double-sided adhesive (3M 467MP). The layers are then stacked in the order shown in Figure A1.2. The conjugate release pads described in the chapter 2 of this dissertation are added to the channels before the top layer of transparency film is added, and the device is pressed together with a laminator (TruLam).

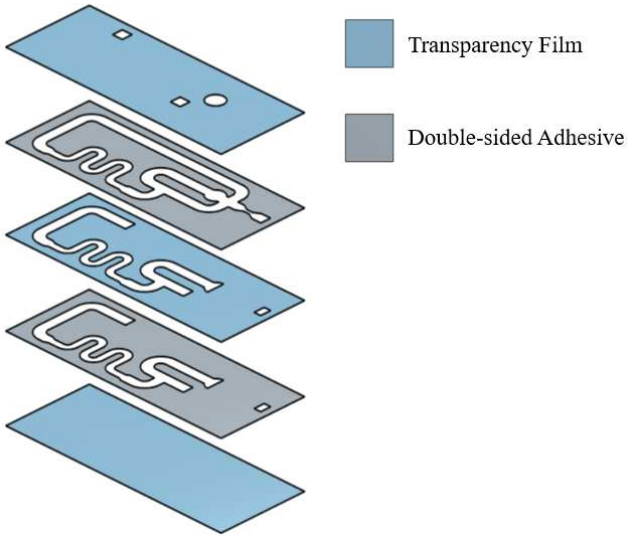


**Figure A1.2** After laser cutting the channel patterns into either double-sided adhesive or transparency film, the layers are assembled in the order shown above.

### A1.2 Antibody Selection

Five anti-SARS-CoV-2 nucleocapsid antibodies from Sino Biological (40143-MM05, 40143-MM08, 40143-R001, 40143-R004, and 40143-R040) were ordered at 1 mg/mL both unconjugated and conjugated to HRP. To simplify the selection process and select the best capture/secondary Ab pair, a 1:1:1:1:1 mixture of all HRP conjugated antibodies and a 1:1:1:1:1 mixture of unconjugated antibodies was made.

To determine the ideal capture antibody, 1 mL of each unconjugated antibody and the unconjugated mixture was spotted with a micropipette onto nitrocellulose test strips, 0.25 mL at a time, drying for 5-7 min at 37 $^{o}$C between each addition. The nitrocellulose was dried for 1 hour at 37 $^{o}$C after the final addition. The membranes were blocked by allowing Stabilguard$^{TM}$ (Surmodics Inc.) to wick through and fully saturate the membrane. The strips then dried for an additional 45 min at 37 $^{o}$C before use. The mixture of HRP-conjugated antibodies was diluted to a total antibody concentration of 20 mg/mL in drying buffer (described in the main work), and 5 mL was added to the conjugate release pad in the device. Each spotted capture antibody (including the mixture) was run in triplicate with devices containing the mixture of HRP-conjugated secondary antibody.

The same process was used to determine the best HRP-conjugated secondary antibody. The mixture of unconjugated antibody was spotted on nitrocellulose as described above, and each individual HRP-conjugated antibody (and the mixture) was diluted to 20 ug/mL before adding to the conjugate release pad. Each HRP-conjugated antibody (including the mixture) was run with a mixture of capture antibody on the test spot. Images of the results were captured with a smartphone and were processed using the method described in the main work (Figure A1.3).

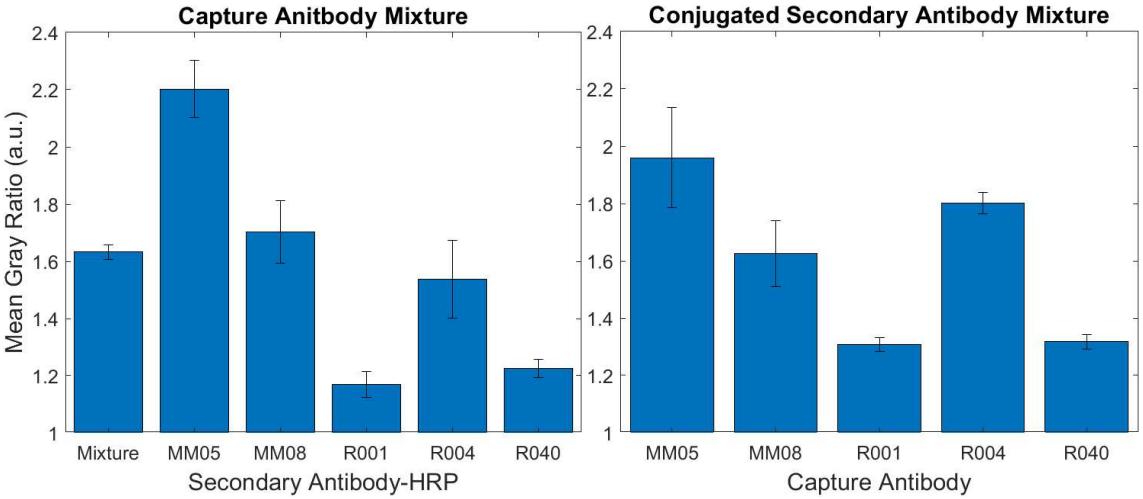


**Figure A1.3** (A) The mixture of unconjugated antibodies was spotted on nitrocellulose, and each HRP conjugated secondary antibody was used in the device with 5500 PFU/mL inactivated virus. (B) Each unconjugated antibody was spotted as on the nitrocellulose, and the mixture of HRP-conjugated antibodies was used in the device with 5500 PFU/mL inactivated virus.

From this initial study (Figure A1.3) we determined that MM05, MM08, and R004 worked well as both a capture and/or a detection antibody. We decided to use HRP conjugated MM05 as the secondary antibody. Conjugated MM05 was then tested against MM08, R004, and a 1:1 mixture of the two as the capture antibody. Of those combinations, MM08 by itself performed best as the capture antibody with MM05-HRP as the secondary (Figure A1.4).

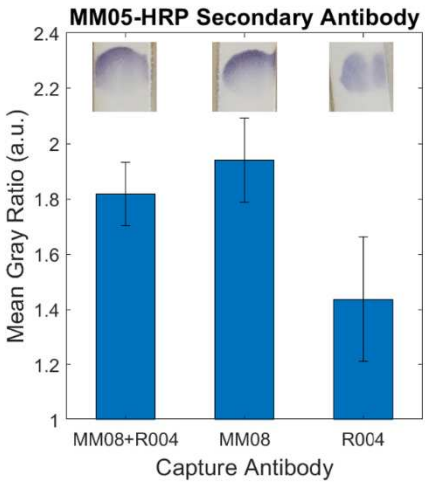


**Figure A1.4** Using MM05-HRP as the secondary antibody, MM08 outperformed R004 or a combination of both as the capture.

### A1.3 Extraction Buffer Optimization

NaCl concentration and pH of the extraction buffer were optimized using a well-plate ELISA as described in the main text. Virus was diluted in extraction buffer containing varying concentrations of NaCl and with varied pH, but each condition also contained 0.1% Tween-20 and 0.1% Igepal CA630. The results of that study are shown in Figure A1.5. The buffer conditions in Figure A1.5 were only used when making dilutions of the inactivated virus, meaning they only influence the antibody/antigen binding step. It makes sense that antibodies have a greater binding affinity at a pH close to physiological (7.4), but HRP functions best at a lower pH (6-6.5). For this reason, 150 mM NaCl and pH 6.5 was chosen for the extraction buffer.

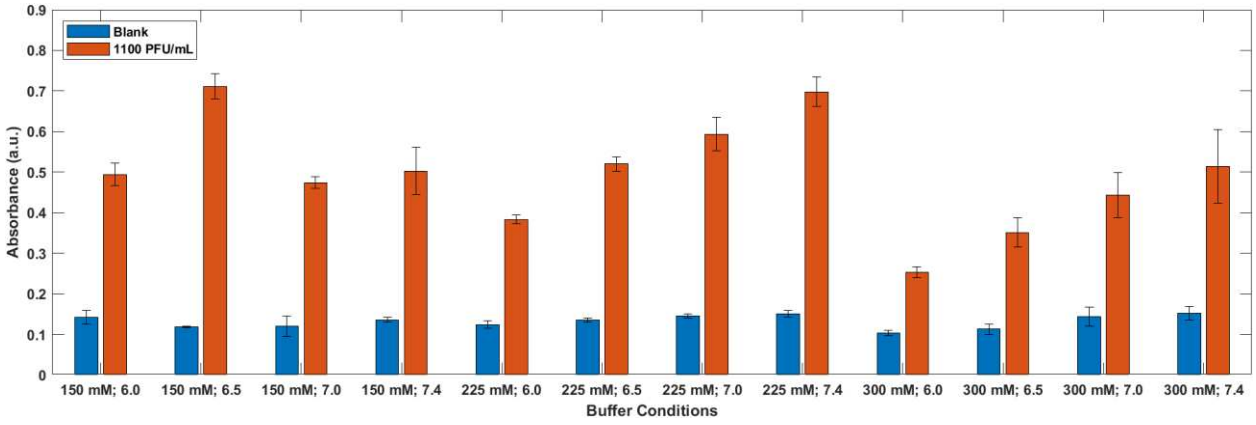


**Figure A1.5.** A well plate ELISA was performed at varying NaCl concentrations and pH.

### A1.4 Images from Dose Response Curve in Buffer

After varying concentrations of virus were diluted in extraction buffer and run in the device, images were captured with a Motorola One smartphone, and the mean gray ratio was generated using ImageJ. The images for the curve generated in Figure 2.4 are shown in Figure A1.6.

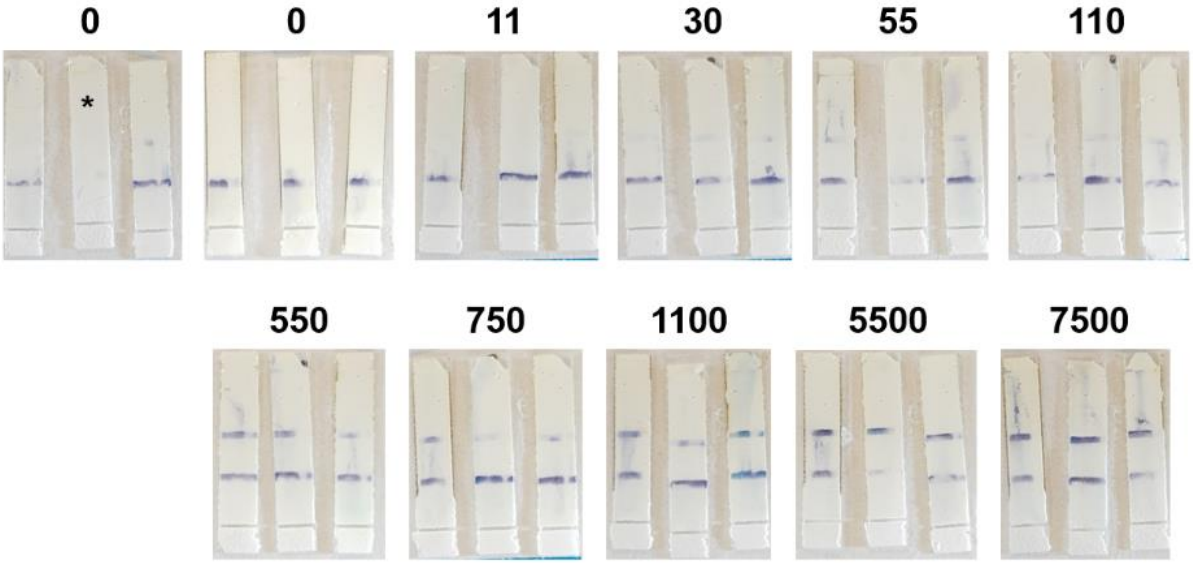


**Figure A1.6.** Images of the points for the dose response curve in Figure 2.4. The numbers indicate the concentration of virus in PFU/mL. The asterisk (*) on 0 indicates a failed test because no control line appeared. Because of this, three more blanks were run, giving an n=5 for 0 PFU/mL.

# APPENDIX 1 CITATIONS


1. Carrell, C. S.; Wydallis, R. M.; Bontha, M.; Boehle, K. E.; Beveridge, J. R.; Geiss, B. J.; Henry, C. S., Rotary manifold for automating a paper-based Salmonella immunoassay. *RSC Advances* **2019,** *9* (50), 29078-29086.

2. Verma, M. S.; Tsaloglou, M.-N.; Sisley, T.; Christodouleas, D.; Chen, A.; Milette, J.; Whitesides, G. M., Sliding-strip microfluidic device enables ELISA on paper. *Biosensors and Bioelectronics* **2018,** *99*, 77-84.

3. Chen, C.-A.; Yeh, W.-S.; Tsai, T.-T.; Li, Y.-D.; Chen, C.-F., Three-dimensional origami paper-based device for portable immunoassay applications. *Lab on a Chip* **2019,** *19* (4), 598-607.

4. Huang, S.; Abe, K.; Bennett, S.; Liang, T.; Ladd, P. D.; Yokobe, L.; Anderson, C. E.; Shah, K.; Bishop, J.; Purfield, M.; Kauffman, P. C.; Paul, S.; Welch, A. E.; Strelitz, B.; Follmer, K.; Pullar, K.; Sanchez-Erebia, L.; Gerth-Guyette, E.; Domingo, G.; Klein, E.; Englund, J. A.; Fu, E.; Yager, P., Disposable Autonomous Device for Swab-to-Result Diagnosis of Influenza. *Analytical Chemistry* **2017,** *89* (11), 5776-5783.

5. Zhang, J.; Gui, X.; Zheng, Q.; Chen, Y.; Ge, S.; Zhang, J.; Xia, N., An HRP-labeled lateral flow immunoassay for rapid simultaneous detection and differentiation of influenza A and B viruses. *Journal of Medical Virology* **2019,** *91* (3), 503-507.

6. Apilux, A.; Ukita, Y.; Chikae, M.; Chailapakul, O.; Takamura, Y., Development of automated paper-based devices for sequential multistep sandwich enzyme-linked immunosorbent assays using inkjet printing. *Lab on a Chip* **2013,** *13* (1), 126-135.

## APPENDIX 2

This appendix corresponds to Chapter 3 of this dissertation, and discusses image/data processing as well as nitrocellulose flow issues.

### A2.1 Image Capture and Selection:

Chemiluminescent (CL) images in Chapter 3 were captured 1 per minute while the devices were running. Those images were processed with the NIH software, ImageJ, as described in Chapter 3. Because three devices were run simultaneously under the imager, there are delays between sample additions for each. These delays in addition to slight differences in the devices and lead to differences in when signal appears and when it is strongest. Therefore, the greatest signal value for each device in the image set was chosen for data work up rather than an image form a set time point. An example of this type of image process can be found in **figure A2.1.** A sharp increase in signal is apparent as images progress, and plateaus as the CL reagent flows over the enzyme present at the test line. Then, as the CL reagent is washed past the test line and no more remains, signal sharply drops.

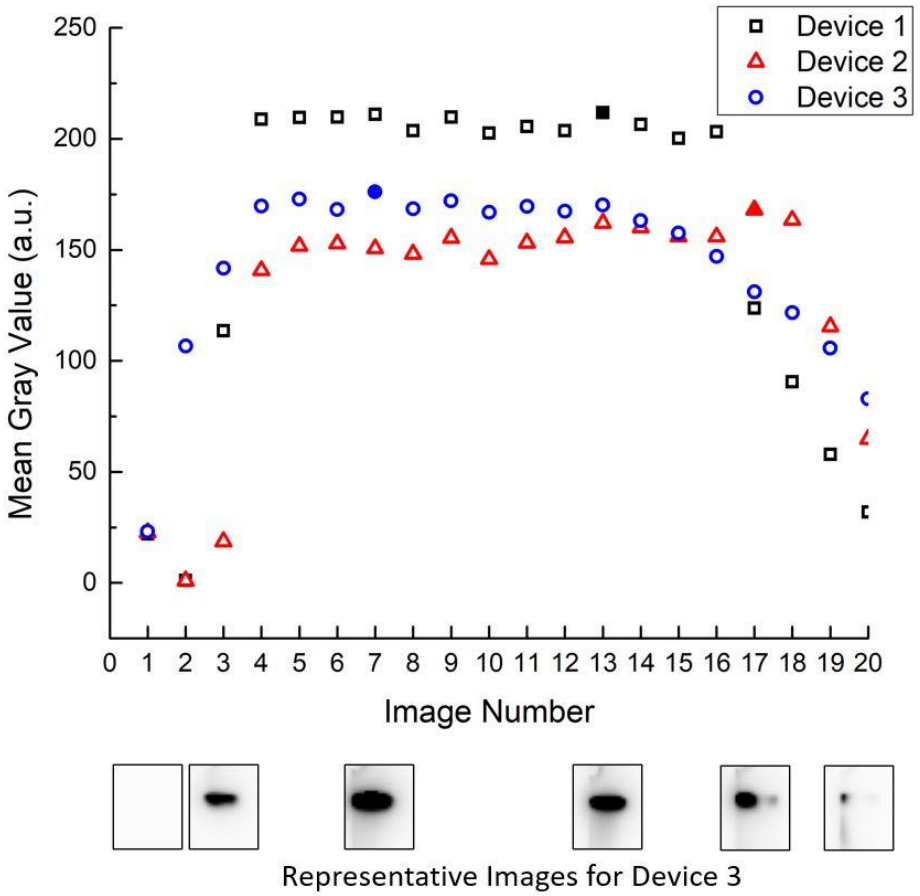


**Figure A2.1** Devices were run in triplicate under the CL imager at 100 ng/mL N-protein. The signal for each device was monitored over time. The maximum signal for each individual device (filled markers) was used for data work up. Representative images at different timepoint along the signal development are shown under the plot for device #3.

### A2.2 Nitrocellulose Considerations:

As discussed in the main body of Chapter 3, various types of nitrocellulose were used in the CL assay in an attempt to control flow rate. With a longer exposure time from the CL imager (20-30s), a high flow rate would cause the CL reagent to flow past the test line and appear blurred or smeared in the final image. However, a slow rate that is too slow causes issues in the device. If the flow rate is too slow, evaporation over the vents of the reagent pads can occur, driving flow in their direction rather than through the nitrocellulose (NC) membrane. Evaporation over the NC itself can also prevent fluid from entering the waste pad, leading to

poor washing. These phenomena were initially posited after running the CL devices on the NC with the slowest flow rate, FF170. These theories were then tested with food dye in place of CL reagents to better visualize where reagents are flowing and when. These results and key issues are highlighted in **Figure A2.2.**

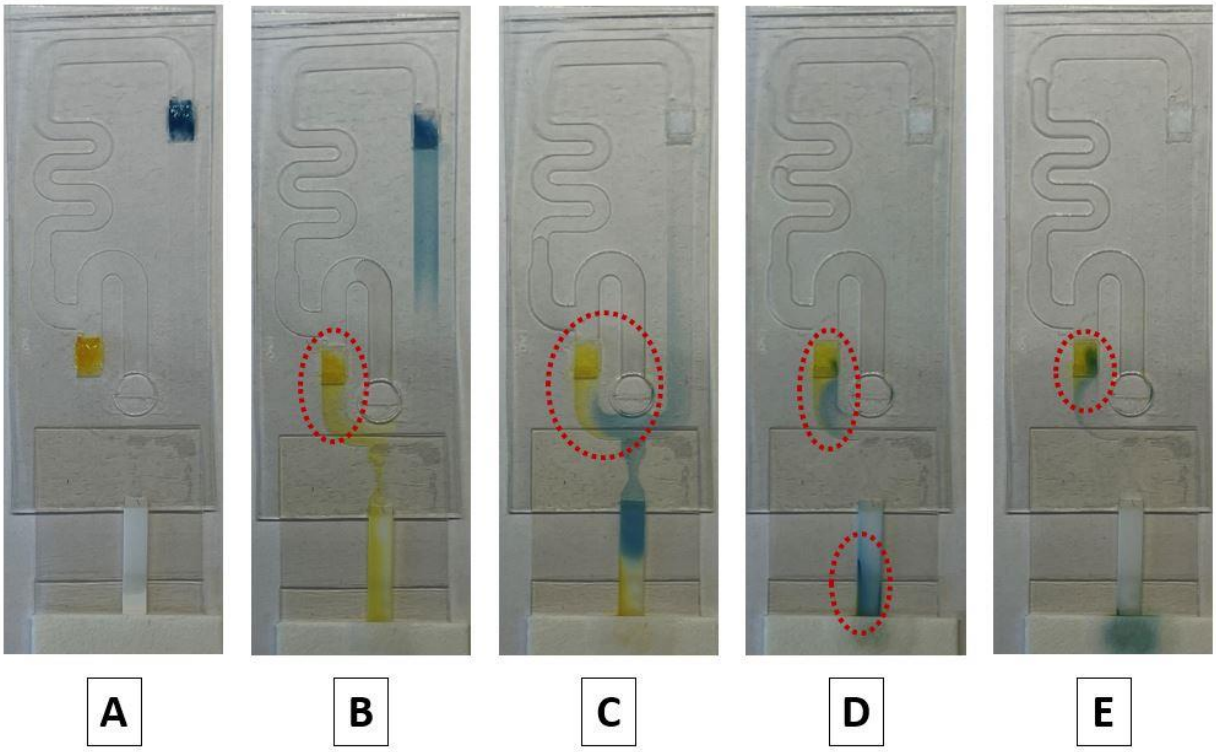


**Figure A2.2** FF170 NC was cut into a 3x16 $mm^2$ test strip and inserted into a device with blue food dye representing the 2°Ab-HRP and yellow dye representing the CL reagent. Images were captured as the device flowed, and relevant aspects are highlighted with red circles. (A) Initially following sample addition (100 µL of extraction buffer). (B) Slow/poor release from 2°Ab-HRP pad. (C) 2°Ab-HRP still present in pad while CL reagent reaches NC. (D) Evaporation over the 2°Ab-HRP drives CL reagent in that direction as well as through the NC. Poor washing in NC caused by evaporation over NC. (E) Near device completion, much of the CL reagent and 2°Ab-HRP are still present in 2°Ab-HRP pad.

Most importantly, it was noted that the 2°Ab-HRP pad released very slowly when the NC flow rate was too low. Additionally, evaporation over the 2°Ab-HRP pad caused CL reagent to flow in that direction instead of to the NC. Using FF170 prevented a significant amount of 2°Ab-

HRP and CL reagent to reach the test strip, inevitably lowering the signal that would be present, as seen in Figure 3.6A in Chapter 3 of this dissertation.

## APPENDIX 3

This appendix is work that was conducted before the laboratory was closed due to the COVID-19 pandemic. The work in this appendix was progressing towards publication, but time did not allow me to revisit it.

### A3.1 Appendix Introduction:

In the main body of this dissertation, I discussed the development and operation of three different automated immunoassays. While varying in other ways, one similarity between the three assays is the use of nitrocellulose as a membrane for the test and control lines. Nitrocellulose is a common material for lateral flow and western blotting assays because of its ability to bind proteins to its surface. Nitrate groups extending from the 2, 3, and 6 carbons of a cellulose backbone typically occupied by hydroxyl groups each glucose unit.[1] Under physiological conditions, these zwitterionic groups are able to interact with the polar surface of proteins and bind them to the surface.[2] Because the interaction is non-covalent, factors like pH, ionic strength, and sample composition can greatly influence the interaction between protein and nitrocellulose. Because of these variables, the interaction between protein and nitrocellulose is poorly understood. Some research has suggested that even under optimal conditions, only 21% of the original protein remains bound to the surface of nitrocellulose after depositing.[3] In order to avoid the variability that comes with nitrocellulose, I developed a method to covalently attach protein to the surface of glass fiber membranes.

The use of (3-aminopropyl)triethoxysilane (APTES) to bind to glass surfaces has been widely explored.[4-7] APTES undergoes hydrolysis and can bind to hydroxyl groups on a surface via

condensation, leaving siloxane bonds at the surface interface and exposed amine groups in the solution.[8-10] Next, a cross-linker like glutaraldehyde can be used to react with amines on the surface and amines present in amino acids of a protein.[4, 11-13] Researcher have used this reaction before on the surface of glass slides and silicon wafers;[4] however, to my knowledge, it has never been performed on glass fiber. Glass fiber is an attractive surface for immunoassays. It is a porous membrane with greater surface area than a glass slide or silicon wafer. This should allow for more protein to bind to a surface treated with APTES-glutaraldehyde. In this appendix, I demonstrate an immunoassay with capture antibodies covalently bound to the surface of glass fiber using APTES-glutaraldehyde. This immunoassay was developed for C-reactive protein (CRP) as a model. CRP is a biomarker for inflammation commonly used to help diagnose the risk of heart failure with a dynamic range from 1-50 µg/ml circulating in blood.[14-16]

## A3.2 Materials and Methods:

*Optimizing silanizing and crosslinking conditions:*

The optimal APTES solvent, the APTES concentration, glutaraldehyde concentration, and wash buffer volume were determined. Glass fiber membranes (Cytiva, Fisher Scientific) were cut into 8 mm diameter discs with a laser cutter (Zing 10000, Epilog Laser). The discs were then plasma treated (Harrick PDC-32G) for 30 seconds to thoroughly clean the surface and expose hydroxyl groups. Immediately following, the discs were immersed in a solution of APTES (Milipore-Sigma) of various concentrations diluted in either deionized water or toluene for 30 minutes while shaking. They were then removed, washed thoroughly to a waste pad placed under the discs, and dried at 100 $^{o}$C for an hour. The discs were then immersed in a solution with varying

concentrations of glutaraldehyde diluted in DI water for 30 minutes while shaking. They were removed, washed again, and 10 µL of 5 ng/mL horseradish peroxidase (HRP) was added and left to incubate at room temperature (RT) for 15 minutes. The discs were washed again with wash buffer (0.01 M PBS with 0.05% Tween-20) to remove unbound HRP. Lastly, 5 µL of a solution containing 3,3',5,5'-tetramethylbenzidine (TMB) and $H_2O_2$ (1-Step™ Ultra TMB-ELISA Substrate Solution, Thermo Fisher) was added and left to develop at RT for 15 minutes. Images were captured using a smartphone under a 12 LED light box.

*CRP assay:*

An ELISA to detect CRP was performed using the optimized protein binding conditions. 8 mm diameter glass fiber discs were immersed in 0.5% APTES in toluene for 30 minutes while shaking. They were then removed and washed twice with 20 µL of toluene, twice with 20 µL of EtOH, and twice with 20 µL of DI water over a waste pad. The discs were then dried at 100ºC for an hour, then immersed in 0.5% glutaraldehyde in water for 30 minutes while shaking. They were removed and washed twice with 20 µL of wash buffer. 10 µL of 30 µg/mL polyclonal anti-CRP was added to the discs and incubated at RT for 10 minutes, then washed again with wash buffer. The discs were then blocked by adding 20 µL of SuperBlock™ (Thermo Fisher Scientific, Waltham, MA) and incubating for 30 minutes.

To perform the assay, PBS was spiked with CRP (Fitzgerald Industries, Acton MA). 20 µL of spiked PBS was added to each disc and incubated at RT for 10 minutes. Each disc was then washed twice with 20 µL of wash buffer. Monoclonal, biotinylated anti-CRP (25 µg/mL) was added and incubated at RT for 10 min and washed out as described before. Streptavidin-labeled HRP (5 ng/mL) was added to each disc, incubated at RT for 10 minutes, and washed. Lastly, 10

μL of TMB solution was added and color was left to develop for 15 minutes. Images were captured under a light box with a smart phone.

*Data analysis:*

Inverted gray scale values were obtained for each disc using the ImageJ (NIH). When the images were taken, an additional glass fiber disc was included in the picture to serve as a reference. The gray values of the discs from the assay were divided by the reference to account for any differences in lighting that could have occurred.

**A3.3 Results and Discussion:**

For detecting human-CRP, glass fiber membranes were chosen over cellulose membranes for several reasons. Glass fiber empirically appears lighter in color compared to cellulose, making the contrast of a colorimetric reaction against it appear more intense. The membrane selected also has a larger pore size, leading to lower capillary pressure and a faster and more uniform flow.[17] Glass fiber is commonly used as a conjugate release pad in lateral flow assays due to its chemically inert nature, making non-specific adsorption of proteins less likely.[18-19] To emphasize these benefits and optimize washing procedures, HRP was added to both cellulose (Whatman 1, GE) and glass fiber discs. Both membranes were allowed to incubate for 5 minutes at room temperature before washing using varying volumes of wash buffer. The gray scale values of the discs that contained HRP were divided by the value of a blank membrane to ensure that the intensity is representative of the TMB color change and not a result of the color of the membrane or lighting differences. Statistically, there were no differences in signal ratio between cellulose and glass fiber after any wash volume was added. However, without washing, the mean gray ratio is greater for

glass fiber, meaning the signal appears stronger in contrast with blank glass fiber (**Figure A1**). From this, glass fiber was chosen as the membrane for the assay, and a minimum wash volume of 40 µL was chosen.

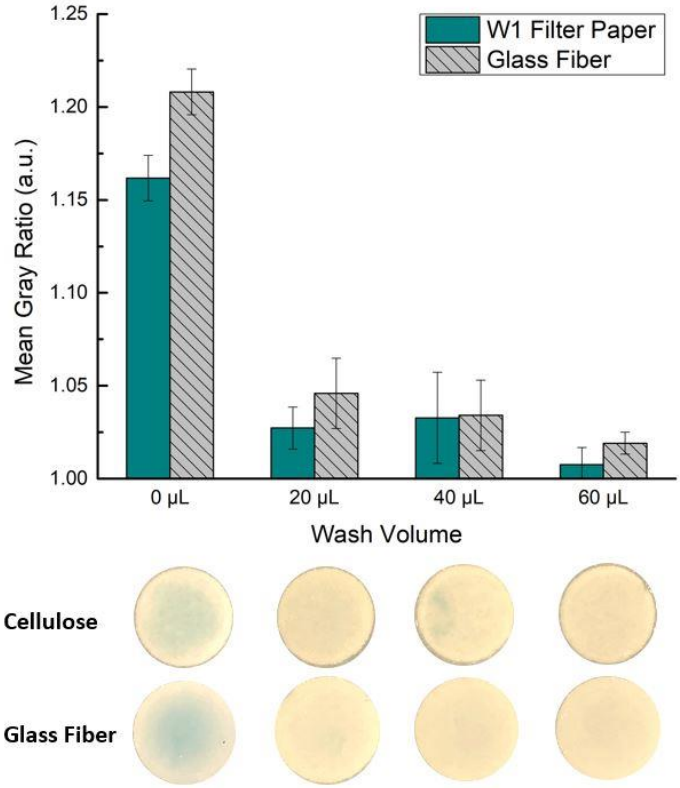


**Figure A3.1** HRP was added and washed out of 8 mm diameter punches with varying volumes of wash buffer (n=3).

A variety of procedures exist to covalently bind proteins to $SiO_x$ surfaces such as glass. One of the most common is the use of a silanizing agent and a cross linker. In this study, (3-aminopropyl)triethoxysilane (APTES) was chosen for its terminal amine, and glutaraldehyde was chosen to crosslink that amine group with one on the surface of HRP or an antibody (**Figure A3.2**).

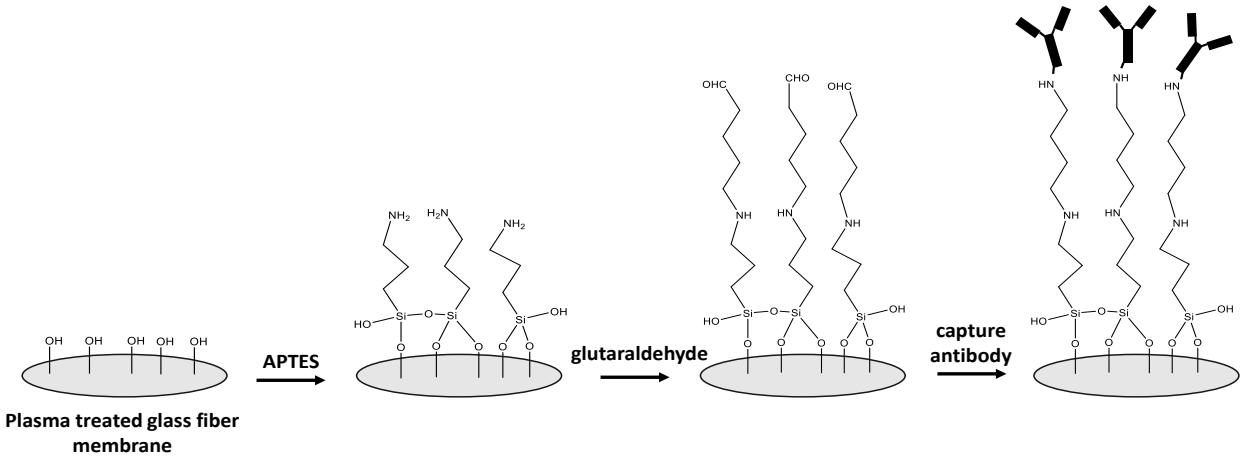


**Figure A3.2** The schematic for covalently binding proteins to the surface of glass fiber membranes using APTES as a silanizing agent and glutaraldehyde as a crosslinker.

The solvent in which APTES is dissolved in is an important factor in the orientation and thickness of the APTES layer.[8, 20] A number of solvents have been reported for silanization, but water or toluene are common.[21-23] Because of water's role in the hydrolysis reaction that occurs with APTES, using aqueous solvents can cause polymerization of APTES in solution or at the surface of the glass fiber. The result of this would be an uneven, thicker layer of APTES bound to the surface of glass fiber. It is generally understood that, under ambient conditions, a thin layer of water molecules can adsorb to the surface of glass from the atmosphere. Therefore, in organic solvents, the only water available for the reaction to take place between APTES and the glass membrane is at the surface of the glass fiber. Studies have reported that using anhydrous toluene as a solvent produces even, self-assembling monolayers.[24-25] In order to confirm this method on glass fiber membranes, 1% APTES was dissolved in both DI water and anhydrous toluene and the procedures outlined in **Figure A3.2** were carried out. Glass fiber discs were immersed in these solutions, washed, and dried at 100 $^{o}$C for 30 min to evaporate any excess solvent. The treated discs were then placed into a 1% glutaraldehyde solution. One end of glutaraldehyde reacts via a Mannich reaction with the primary amine from APTES present at the surface of the membrane.[26] The membranes were washed again, and HRP was incubated on the discs, where the other aldehyde

now present on the surface can react with a basic amino acid residue at the protein's surface. A TMB solution containing $H_2O_2$ was added, and the blue color that developed was quantified in gray scale values (**Figure A3.3**). The two solvents were also compared to discs where no APTES treatment took place as controls. The data shows an increase in signal when APTES is dissolved in toluene, and toluene was further used in this project based on these results.

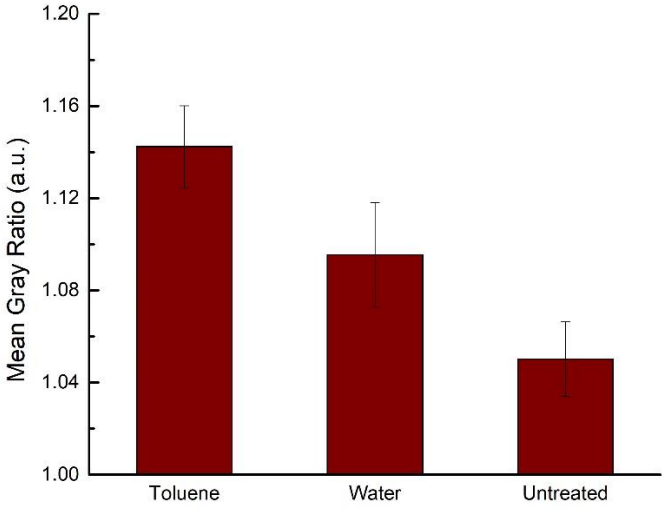


**Figure A3.3** APTES was diluted in both toluene and water. The signal of the reaction between bound HRP and TMB was compared to non-specifically adsorbed HRP on untreated glass fiber.

The optimal concentrations of APTES and glutaraldehyde were then investigated. The same approach was taken as described in the previous paragraph. For the optimization of each condition, the concentration of the other was held constant at 1% for the process. It was determined that 0.5% APTES and 0.5% glutaraldehyde were best for both (**figure A3.4**). However, if no HRP is bound, the expected value for the mean gray ratio should be 1. Notably in both cases, when the concentration of APEST or glutaraldehyde is 0%, there is still signal present well above 1. In the absence of glutaraldehyde, this could be due to the addition of amine groups from the APTES. In

a study the water contact angle was measured following APTES treatment, the contact angle was smaller flowing treatment, indicating that the hydrophilic amine groups were successfully added to the surface.[27] Due to the polar nature of a protein's exterior, HRP could still be non-covalently adsorbed to these amine groups at the glass fiber even after washing thoroughly. This could explain why signal was still present in the absence of glutaraldehyde. In the absence of APTES, aldehyde groups can still react with hydroxyl groups present on the glass fiber surface to create a hemiacetal group. Because this reaction is reversable, it could explain why signal is weakly present in the absence of APTES.[28]

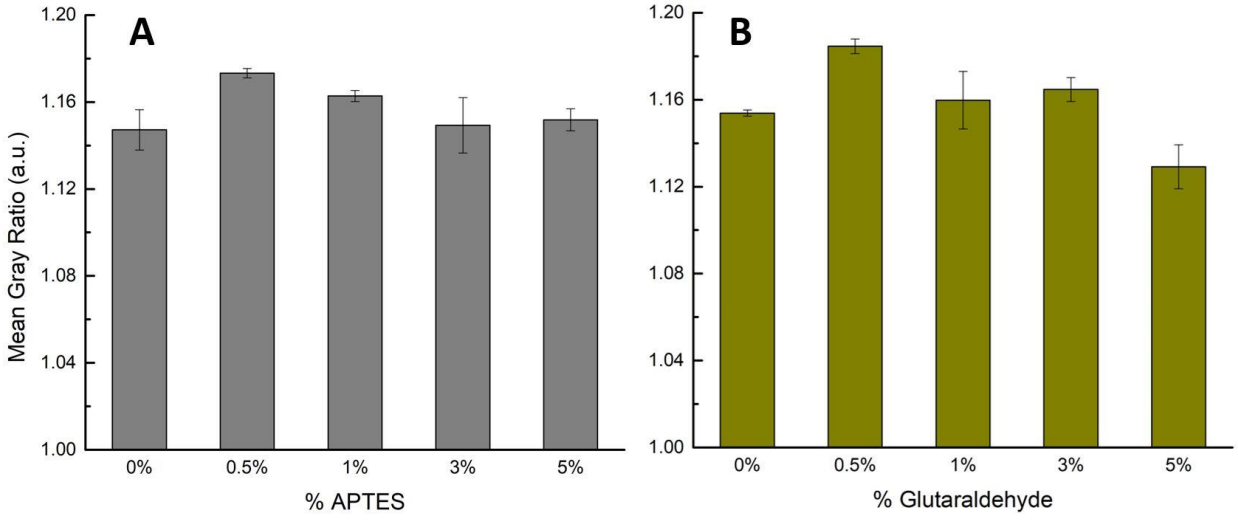


**Figure A3.4** The concentration of A) APTES and B) Glutaraldehyde were determined by binding HRP to APTES treated glass fiber membranes. For each condition tested, the other was held constant at 1%.

Glass fiber membranes were treated with the optimized conditions, and anti-CRP antibodies were bound to the membranes for the assay to be carried out as depicted in **Figure A3.5**. CRP spiked into PBS was added at varying concentrations to the treated membranes, and a sandwich antibody labeled with biotin was added after washing. The interaction between biotin

and streptavidin is one of the strongest natural non-covalent interactions between a protein and a ligand having a $K_d$ on the order of $10^{-14}$.[29] Because of this strong interaction, any signal present at the surface after washing is likely the result of the sandwich assay being successful.

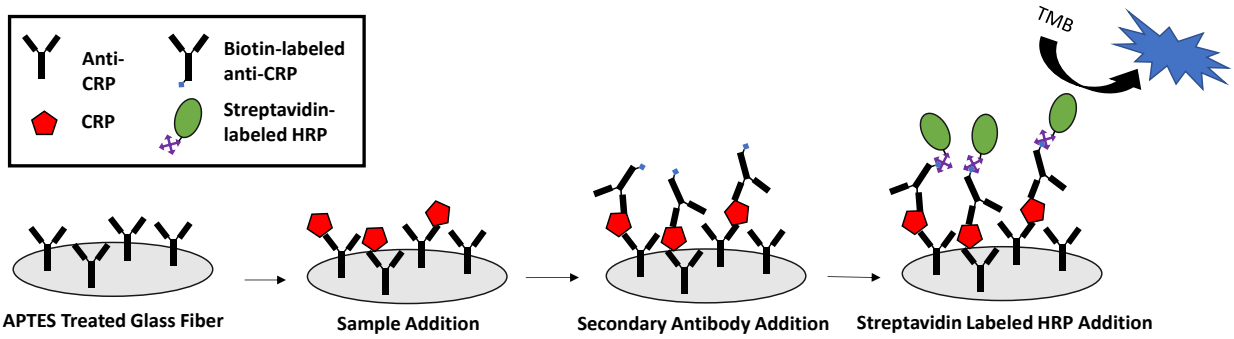


**Figure A3.5** The assay for the detection of human-CRP is depicted above. The assay was performed using polyclonal anti-CRP antibodies covalently bound to glass fiber via APTES and glutaraldehyde.

After the addition of TMB, a dose response curve was gathered (**Figure A6**). A limit of detection at 40 ng/ml was gathered using this data. These results show the efficacy of using glass fiber, APTES, and glutaraldehyde as a method by which to covalently bind capture antibodies on a glass fiber surface where a simple ELISA can be subsequently performed.

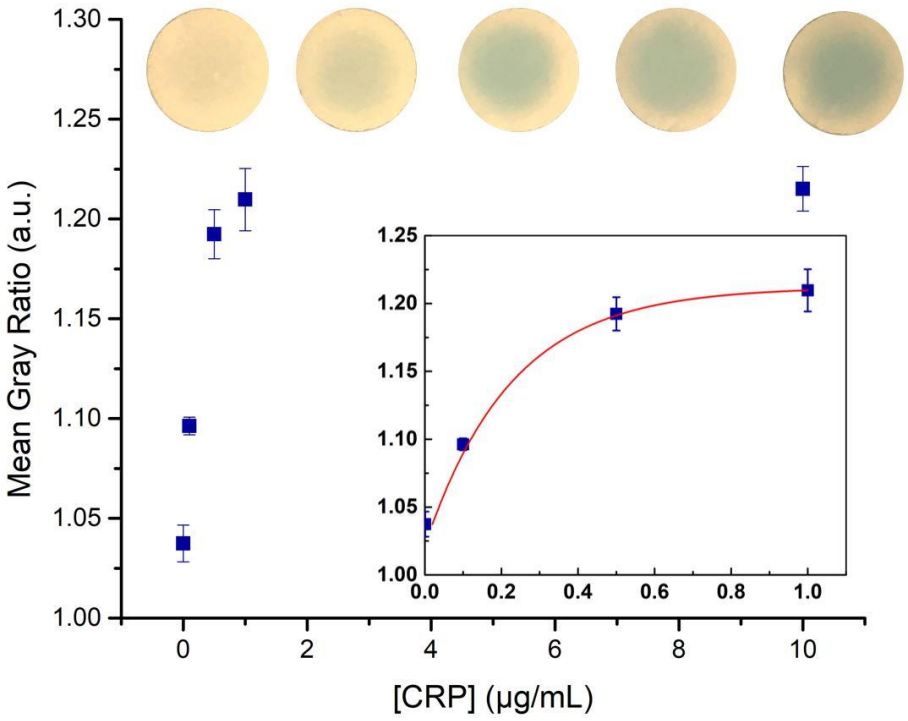


**Figure A3.6** Performing the glass-fiber based immunoassay with spiked buffer and covalently bound antibodies resulted in the data above. Representative images are shown above the plot, and the data was fit to a logarithmic fit ($y = 0.463\ln(x) + 1.2139$) with an $R^2 = 0.986$. Using the fit and the standard deviation of the blank, the LOD for this assay is 40 ng/ml CRP.

## A3.4 Conclusion:

This appendix demonstrates the proof of concept and optimization for a novel method of covalently binding protein to the surface of glass fiber using APTES and glutaraldehyde. The application of this was shown using CRP detection as a model with a limit of detection of 40 ng/mL. While this limit of detection is near that of comparable paper-based assays,[18, 30-31] further optimization of reagent volumes, timing steps, and washing steps can be investigated to lower this LOD further. This work also presents an alternative to nitrocellulose as a surface for point of care style devices. Using APTES-glutaraldehyde pretreatment, researchers may have greater control of the surface conditions they are using in their devices.

## APPENDIX 3 CITATIONS


1. Ashter, S. A., 5 - Types of Biodegradable Polymers. In *Introduction to Bioplastics Engineering*, Ashter, S. A., Ed. William Andrew Publishing: Oxford, 2016; pp 81-151.

2. Lu, Y.; Shi, W.; Qin, J.; Lin, B., Fabrication and Characterization of Paper-Based Microfluidics Prepared in Nitrocellulose Membrane By Wax Printing. *Analytical Chemistry* **2010,** *82* (1), 329-335.

3. Tanyolaç, D.; Işık Yürüksoy, B.; Özdural, A. R., Immobilization of a thermostable α-amylase, Termamyl®, onto nitrocellulose membrane by Cibacron Blue F3GA dye binding. *Biochemical Engineering Journal* **1998,** *2* (3), 179-186.

4. Gunda, N. S. K.; Singh, M.; Norman, L.; Kaur, K.; Mitra, S. K., Optimization and characterization of biomolecule immobilization on silicon substrates using (3-aminopropyl)triethoxysilane (APTES) and glutaraldehyde linker. *Applied Surface Science* **2014,** *305*, 522-530.

5. Awsiuk, K.; Psarouli, A.; Petrou, P.; Budkowski, A.; Kakabakos, S.; Bernasik, A.; Rysz, J.; Raptis, I., Spectroscopic and microscopic examination of protein adsorption and blocking of non-specific binding to silicon surfaces modified with APTES and GOPS. *Procedia Engineering* **2011,** *25*, 334-337.

6. Nicholas, M. P.; Rao, L.; Gennerich, A., Covalent immobilization of microtubules on glass surfaces for molecular motor force measurements and other single-molecule assays. *Methods Mol Biol* **2014,** *1136*, 137-169.

7. Wang, Z.-H.; Jin, G., Covalent immobilization of proteins for the biosensor based on imaging ellipsometry. *Journal of Immunological Methods* **2004,** *285* (2), 237-243.

8. Acres, R. G.; Ellis, A. V.; Alvino, J.; Lenahan, C. E.; Khodakov, D. A.; Metha, G. F.; Andersson, G. G., Molecular Structure of 3-Aminopropyltriethoxysilane Layers Formed on Silanol-Terminated Silicon Surfaces. *The Journal of Physical Chemistry C* **2012,** *116* (10), 6289-6297.

9. Shlyakhtenko, L. S.; Gall, A. A.; Lyubchenko, Y. L., Mica functionalization for imaging of DNA and protein-DNA complexes with atomic force microscopy. *Methods Mol Biol* **2013,** *931*, 295-312.

10. Sypabekova, M.; Hagemann, A.; Rho, D.; Kim, S., Review: 3-Aminopropyltriethoxysilane (APTES) Deposition Methods on Oxide Surfaces in Solution and Vapor Phases for Biosensing Applications. *Biosensors (Basel)* **2023,** *13* (1), 36.

11. Syga, Ł.; Spakman, D.; Punter, C. M.; Poolman, B., Method for immobilization of living and synthetic cells for high-resolution imaging and single-particle tracking. *Scientific Reports* **2018,** *8* (1), 13789.

12. Chen, Y.; Yu, F.; Yang, C.; Song, J.; Tang, L.; Li, M.; He, J.-J., Label-free biosensing using cascaded double-microring resonators integrated with microfluidic channels. *Optics Communications* **2015,** *344*, 129-133.

13. Saengdee, P.; Chaisriratanakul, W.; Bunjongpru, W.; Sripumkhai, W.; Srisuwan, A.; Hruanun, C.; Poyai, A.; Phunpae, P.; Pata, S.; Jeamsaksiri, W.; Kasinreak, W.; Promptmas, C., A silicon nitride ISFET based immunosensor for Ag85B detection of tuberculosis. *Analyst* **2016,** *141* (20), 5767-5775.

14. Anand, I. S.; Latini, R.; Florea, V. G.; Kuskowski, M. A.; Rector, T.; Masson, S.; Signorini, S.; Mocarelli, P.; Hester, A.; Glazer, R.; Cohn, J. N., C-Reactive Protein in Heart Failure. *Circulation* **2005,** *112* (10), 1428-1434.

15. Shrivastava, A. K.; Singh, H. V.; Raizada, A.; Singh, S. K., C-reactive protein, inflammation and coronary heart disease. *The Egyptian Heart Journal* **2015,** *67* (2), 89-97.

16. Ouyang, P. Assessing Cardiovascular Risk with C-Reactive Protein. https://www.hopkinsmedicine.org/heart_vascular_institute/centers_excellence/women_cardiovascular_health_center/patient_information/health_topics/c_reactive_protein.html (accessed Sept. 7).

17. Das, D.; Dsouza, A.; Kaur, N.; Soni, S.; Toley, B. J., Paper Stacks for Uniform Rehydration of Dried Reagents in Paper Microfluidic Devices. *Scientific Reports* **2019,** *9* (1), 15755.

18. Dong, M.; Wu, J.; Ma, Z.; Peretz-Soroka, H.; Zhang, M.; Komenda, P.; Tangri, N.; Liu, Y.; Rigatto, C.; Lin, F., Rapid and Low-Cost CRP Measurement by Integrating a Paper-Based Microfluidic Immunoassay with Smartphone (CRP-Chip). *Sensors (Basel)* **2017,** *17* (4), 684.

19. Delmulle, B. S.; De Saeger, S. M. D. G.; Sibanda, L.; Barna-Vetro, I.; Van Peteghem, C. H., Development of an Immunoassay-Based Lateral Flow Dipstick for the Rapid Detection of Aflatoxin B1 in Pig Feed. *Journal of Agricultural and Food Chemistry* **2005,** *53* (9), 3364-3368.

20. Vandenberg, E. T.; Bertilsson, L.; Liedberg, B.; Uvdal, K.; Erlandsson, R.; Elwing, H.; Lundström, I., Structure of 3-aminopropyl triethoxy silane on silicon oxide. *Journal of Colloid and Interface Science* **1991,** *147* (1), 103-118.

21. Sabek, J.; Torrijos-Morán, L.; Griol, A.; Díaz Betancor, Z.; Bañuls Polo, M.-J.; Maquieira, Á.; García-Rupérez, J., Real Time Monitoring of a UV Light-Assisted Biofunctionalization Protocol Using a Nanophotonic Biosensor. *Biosensors (Basel)* **2018,** *9* (1), 6.

22. Smith, E. A.; Chen, W., How to prevent the loss of surface functionality derived from aminosilanes. *Langmuir : the ACS journal of surfaces and colloids* **2008,** *24* (21), 12405-12409.

23. Howarter, J. A.; Youngblood, J. P., Optimization of Silica Silanization by 3-Aminopropyltriethoxysilane. *Langmuir* **2006,** *22* (26), 11142-11147.

24. Zhu, M.; Lerum, M. Z.; Chen, W., How to prepare reproducible, homogeneous, and hydrolytically stable aminosilane-derived layers on silica. *Langmuir : the ACS journal of surfaces and colloids* **2012,** *28* (1), 416-423.

25. Zhang, F.; Srinivasan, M. P., Self-Assembled Molecular Films of Aminosilanes and Their Immobilization Capacities. *Langmuir* **2004,** *20* (6), 2309-2314.

26. List, B., The Direct Catalytic Asymmetric Three-Component Mannich Reaction. *Journal of the American Chemical Society* **2000,** *122* (38), 9336-9337.

27. Liu, J.; Xi, T., Enhanced Anti-corrosion Ability and Biocompatibility of PLGA Coatings on MgZnYNd Alloy by BTSE-APTES Pre-treatment for Cardiovascular Stent. *Journal of Materials Science & Technology* **2016,** *32* (9), 845-857.

28. Vollhardt, P. S., N., *Organic Chemistry: Structure and Function*. 6th ed.; W.H. Freeman and Company: New York, NY, 2009.

29. Michael Green, N., [5] Avidin and streptavidin. In *Methods in Enzymology*, Wilchek, M.; Bayer, E. A., Eds. Academic Press: 1990; Vol. 184, pp 51-67.

30. Li, Z.; Li, M.; Li, F.; Zhang, M., Paper-based chemiluminescence enzyme-linked immunosorbent assay enhanced by biotin-streptavidin system for high-sensitivity C-reactive protein detection. *Analytical Biochemistry* **2018,** *559*, 86-90.

31. Park, J.; Park, J.-K., Pressed region integrated 3D paper-based microfluidic device that enables vertical flow multistep assays for the detection of C-reactive protein based on programmed reagent loading. *Sensors and Actuators B: Chemical* **2017,** *246*, 1049-1055.